Architecture Design and Analysis of Layered WDMA Wide-Area Networks

by

Xin Huang, B.A.Sc.

A thesis submitted to the
School of Graduate Studies and Research
in partial fulfillment of the requirements
for the degree of
Master of Applied Science

Ottawa-Carleton Institute for Electrical Engineering
Department of Electrical Engineering
Faculty of Engineering
University of Ottawa
December 1993

ISBN 0-612-00471-6

Canada

UNIVERSITÉ D'OTTAWA
UNIVERSITY OF OTTAWA

In Memory of

My Grandparents and My Mother

Abstract

Wavelength Division Multiple Access (WDMA) networks are likely to play a key role in future telecommunication infrastructure. In recent years, different aspects of these networks have been explored to address the challenge of utilizing the huge bandwidth capacity of optical fiber. This thesis focuses on the aspects of architecture design and interconnection of WDMA fiber ring local-area networks.

As a method of approach, the elements of network architecture and the system and device technology are integrated together in one study. Recently, as the field of optical network architectures has begun to evolve and interest has grown, it has become evident that the combination of emerging network architectures and the maturing photonic and optoelectronic device / system technologies will be necessary for continued progress. I hope, through this analysis, readers can have a clear picture of the component requirements for potential network architectures as well as the network impact of the new optical devices and integrated subsystems.

The research work is divided into two parts. In the first part, the design of WDMA ring ATM-based local-area network architectures and the photonic components, including optical Add-Drop Multiplexers for architectural implementation, are studied. Based on this, the physical constraints of these components on the overall network performance are explored. The emphasis is placed on gaining a theoretical understanding from the modeling of the random gain of cascaded optical amplifiers in WDMA ring ATM-based local-area networks with optical Add-Drop Multiplexers.

With the advent of fiber optic LAN research, a major issue that has surfaced is the interconnection of optical LANs using fiber optic technology. In the second part of this thesis, which focuses on this topic, the WDMA fiber ring ATM-based LANs proposed previously are taken as the basic building elements in the low layer of the proposed hierarchical three-layer all-optical wide-area network architecture. Several distributed wavelength routing topologies for interconnection of fiber ring LANs are proposed as the network intermediate layer architecture. They are implemented using the photonic component called Bragg Cell Cross-connect as the optical bridge. Concepts like wavelength reuse and network scalability are developed with this architecture. At the top layer, an ultra-high capacity photonic ATM switch based on ultra-short optical pulse time/frequency division and wavelength division multiplexing is proposed and studied as a part of the backbone wide-area lightwave network that interconnects the intermediate layer networks. Overall, this architecture should offer significant advantages in network capacity and connectivity.

Acknowledgments

My greatest thanks go to my advisor, Dr. Mohsen Kavehrad, for his supervision of my research work throughout the two years of Master's study in the Lightwave Communications Research Laboratory at the University of Ottawa. He has given me guidance since I started an undergraduate project on an optical communications system in his research group four years ago. Dr. Kavehrad helped me in every aspect of my engineering career. Without his strong hand it would not have been possible for me to start or continue this journey.

Special thanks to Professor Mahmoud Tabiani of Sharif University of Technology for many valuable discussions on the topics of optical switching and networking. Dr. Tabiani also helped me on other aspects of my work, and I enjoyed the time with him in the photonics lab during his sabbatical.

I would like to thank the PDFs in the photonics lab for their help. Wholehearted thanks go to Drs. Jiang, Yun and Simova, for they, with their excellent knowledge, helped me invaluably in my research work.

I cannot forget my teachers during my undergraduate years at the University of Ottawa , who helped me establish a solid background in the field of electrical engineering.

Warm thanks to a wonderful group of former and current members of this laboratory. I enjoyed working with them and many times had brain-storming sessions with them.

This thesis is dedicated to my grandaunt Margaret and my uncle Duncan. Without their financial and spiritual support for my undergraduate and graduate studies in Ottawa, no success would be possible. Great appreciation goes to my family for all the love and happiness they bring to me. They have always been understanding and supportive of my efforts.

Finally, I would like to thank the University of Ottawa and the NSERC for their financial support through a scholarship program over the past two years.

Contents

Acronyms

WDM	Wavelength Division Multiplexing
WDMA	Wavelength Division Multiple Access
FDMA	Frequency Division Multiple Access
CDMA	Code Division Multiple Access
TDMA	Time Division Multiple Access
DFB	Distributed FeedBack
DBR	Distributed Bragg Reflector
LAN	Local Area Network
MAN	Metropolitan Area Network
WAN	Wide Area Network
ASE	Amplified Spontaneous Emission
ATM	Asynchronous Transfer Mode
AOTF	Acousto-Optic Tunable Filter
ADM	Add-Drop Multiplexer
WSR	Wavelength Selective Router
EDFA	Erbium Doped Fiber Amplifier
RF	Radio Frequency
PIATOF	Polarization Independent Acoustical Tunable Filter
HIPIO-Circulator	High-Isolation Polarization Independent Optical Circulator
BER	Bit Error Rate
OOK	On-Off Key
FSK	Frequency Shift Key
DPSK	Differential Phase Shift Key
ISR	Interference to Signal Ratio

SNR	Signal to Noise Ratio
FET	Field Effect Transistor
TW	Traveling Wave
MQW	Multiple Quantum Wall
VSTEP	Vertical-to-Surface Transmission Electro-Photonic device
VPI	Virtual Path Identifier
VCI	Virtual Channel Identifier
CS	Cell Selector
CB	Cell Buffer
CD	Cell Decoder
WD	Wavelength Demultiplexer
OFS	Optical Frequency Selector
OD	Optical Decoder
LCSG	Logic Control Signal Generator
S-SEED	Symmetric Self-Electro-Optic Device

List of Publications

X. Huang, M. Tabiani, and M. Kavehrad "An All-Optical ATM Switch Using PFDM and WDM", in *Proceeding of International Conference of Application of Photonic Technology*, Toronto, June 1994..

X. Huang and M. Kavehrad" A WDMA Ring Network with Holographic Wavelength-Selective Partial Demultiplexers " in *Proceedings of Canadian Conference on Electrical and Computer Engineering*, pp. 1119-1121, Vancouver, September 1993

X. Huang, Q. Jiang and M. Kavehrad" A WDMA Ring Network using Fabry-Perot Add-Drop Multiplexers " in *Proceedings of Photonics'93* Atlanta, Georgia, September 1993

Chapter 1
Introduction

1.1. Background

In today's telecommunications field, the design and implementation of vast capacity optical system and network has become a widening avenue of research since its aggregate capacity is expected to create numerous applications to meet the needs of future customers. The great appeal of lightwave for such applications is the enormous bandwidth of tens of terahertz inherent in the optical medium. With the advancement in technology, the application of optical fiber in point-to-point transmission facilities is now being supplemented with the applications to multiuser local and metropolitan area networks, where many users couple onto and share the transmission capacity of a single fiber.

Since the processing speed of the opto-electronic components at network access nodes is only a tiny fraction of the usable optical spectrum (gigahertz versus terahertz), the approach of *optical multi-access network* is proposed in order to tap into this huge bandwidth reservoir. Indeed, it is only in such multi-user networks that we can begin to exploit the bandwidth potential of optical fiber, measured in tens of terahertz. Specifically, until the advent of true optical processing (i.e., optical gates, memories, etc.), end-user speeds will be limited to the gigabit-per-second performance of electronics that generate and sink traffic on the network. Therefore, the potential of sharing this tremendous bandwidth of optical medium among a multitude of relatively lower-speed users in a network is regarded as the major attraction of lightwave technology for multi-user applications.

Among the various techniques to exploit this tremendous bandwidth, *wavelength division multiplexing*(WDM) appears to be very promising. Such multiplexing enables many optical signals at different wavelengths to be transmitted concurrently on a single link through multi-wavelength technology. It takes advantage of the huge bandwidth of optical fiber to achieve high capacities, and of the orthogonality of different wavelengths to realize multi-channel operation.

Classification of WDMA Network Systems:

WDMA networks based on their channel spacing in the optical domain (i.e., the difference between two adjacent wavelengths) are categorized in three different classes.

1) ***Conventional WDMA:*** In these networks channels are separated by *10 nm* or more.

2) ***Dense WDMA:*** In these networks, channels are separated by *1 nm.*

3).***Optical FDMA:*** Channel spacing in these networks is in the order of signal bandwidth.

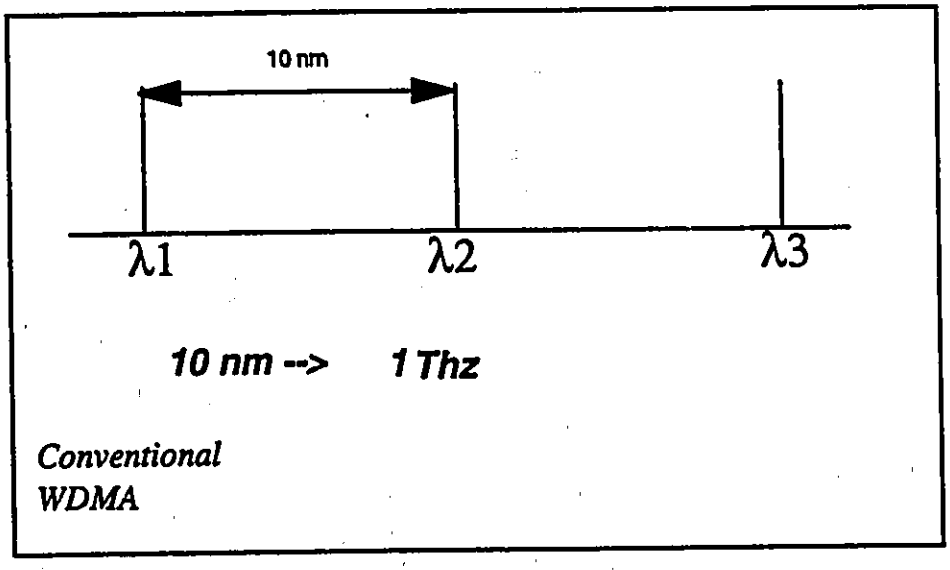

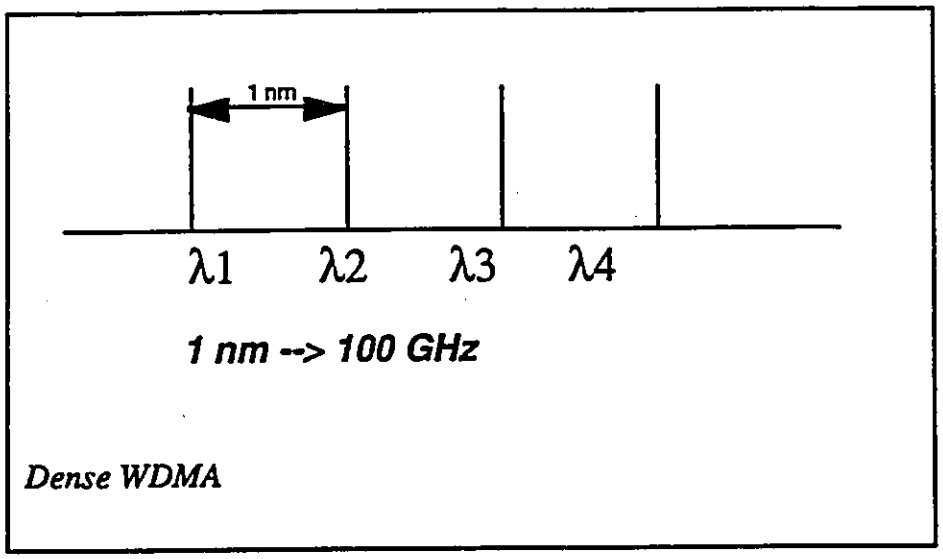

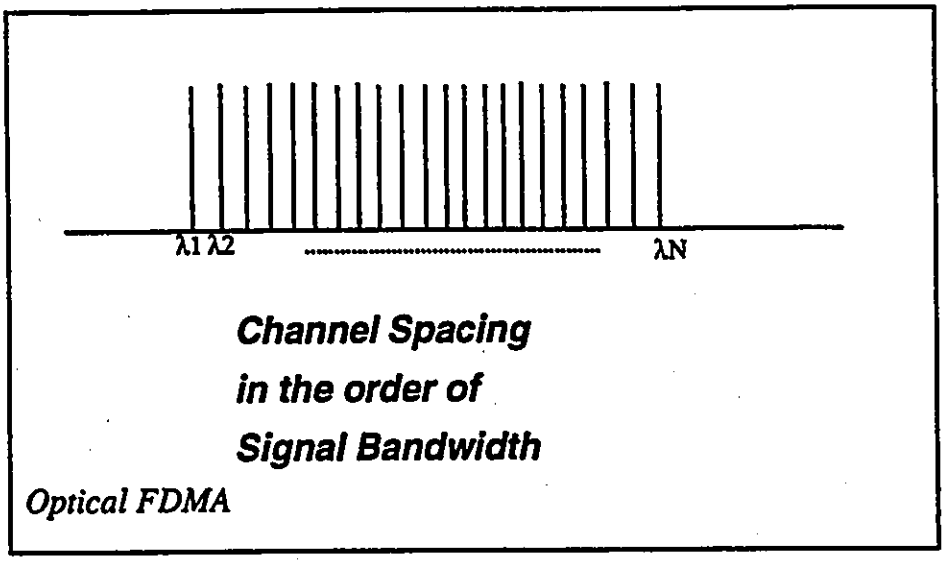

Fig. 1.1

As illustrated in Fig. 1.1, we can send several broadband signals concurrently on the fiber without their interfering with each other, by having several different carriers placed at different wavelengths. In a perfect system, with high-quality lasers capable of producing pure tones, we can have hundreds of these channels in one fiber (optical FDMA).

The minimum channel spacing is limited by crosstalk. By employing distributed feedback laser (DFB) or distributed Bragg Reflector (DBR) laser and other narrow linewidth lasers , a channel spacing of 1 nm or less can be achieved.

In order to develop an effective WDMA network, an end user must be able to transmit to multiple WDM channels, or receive from multiple WDM channels, or both. Accordingly, a great amount of effort is being devoted to the design of tunable transmitters (lasers), tunable receivers (filters), which can operate over a wide range of WDM channels, and channel-tuning (switching) operations of which can also be performed very fast, ideally in a few nanoseconds or less.

In the optical domain, one can build a multi-access network in which dynamically available connections between nodes are possible using different optical wavelengths. Since each node can transmit data at the rate of a few gigabits per second, in this electronic domain (namely the second level), different multiplexing schemes can be used to fit a very large number of simultaneous connections, by using different time slots (electronic time division multiplexing-TDMA), or different signal waveforms (code division multiplexing-CDMA), or different frequency carriers (electronic frequency division multiplexing-FDMA). Since electrical carriers compared to optical carriers are subcarriers, electronic FDMA is also called subcarrier multiplexing.

Classification of WDMA Network Architectures:

WDMA lightwave networks can be classified into two categories: broadcast-and-select networks, and wavelength-routing networks. In turn, each of these can be classified as either single-hop networks, or as multi-hop networks. This classification is shown in Fig. 2.2 and each of these categories will be discussed.

Broadcast-and-Select Networks:

In broadcast-and-select networks, the transmission from each station is broadcast to all of the network stations. At the receiver, the desired signal is then extracted from all the signals. For example, each station could transmit at an optical wavelength different from the other stations, and then at each receiver a tunable optical filter would be used to select the desired wavelength for reception. Alternatively, tunable transmitters and fixed tuned receivers, or both tunable receivers and transmitters could be used. This network architecture is suitable in LAN and MAN.

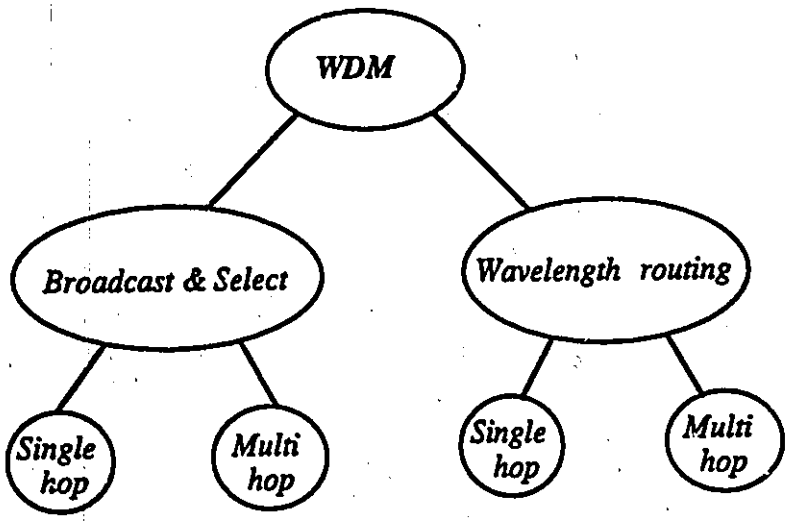

Fig. 1.2. Network Architecture Classification

Wavelength Routing:

In wavelength routing networks, wavelengths are routed along perhaps a limited number of optical switches so as to be able to reuse the wavelengths in the network. In

these networks, as long as the paths taken by any two connections do not overlap, they can be on the same wavelength. This results in a tremendous reduction in the number of required wavelengths. In addition, the power-splitting problem is no longer present. This network architecture is suitable for WAN applications.

Single-Hop Networks:

We use this term for the networks where information transmitted reaches its final destination directly, without being converted to electronic form in between. Single-hop networks are sometimes called all-optical networks.

Multi-hop Networks:

We use this term for the networks where information transmitted reaches its final destination after being converted to electronic form in the intermediate nodes.

Typical Network Topologies:

In broadcast-and-select networks, topologies such as star, bus and ring can be used for the purpose of broadcasting. In the following, a comparison between star and bus topologies is given. Ring as a topology for these kind of networks will be the focus of the research in this thesis.

Star and Bus Topologies:

The star topology shown in Fig.1.3 is preferred to the bus topology shown in Fig. 1.4, because it is more efficient in distributing the optical power. Both the star and the bus use passive 2x2 optical couplers. In the bus architecture, each station transmits into the bus through a coupler and receives from the bus via another coupler. Each 2x2 coupler distributes the power from the input ports to the output ports according to a specific splitting ratio. If this ratio is optimized, and if each station transmits with a power P , then, in a bus, only P/N^2 is received by another station, where N is the number of stations on the bus. A single-mode fiber NxN star coupler is made up of 2x2 couplers, each with a splitting ratio of 0.5. Thus, in the star architecture, each station receives a power of P/N. In practice, couplers are not ideal devices and they introduce an excess loss in addition to a splitting ratio .

In star, the power is distributed evenly among all the stations and the dynamic range required for the receivers is small, whereas in a bus, there are different power values, requiring a larger dynamic range for the receivers. Typically, a bus can support a few tens of stations. Wideband optical amplifiers can be used to increase this number .

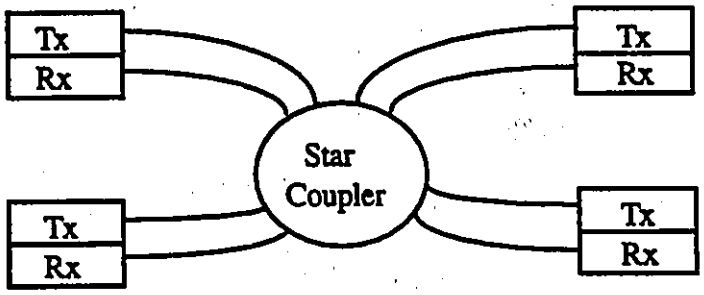

Fig. 1.3. Star Topology

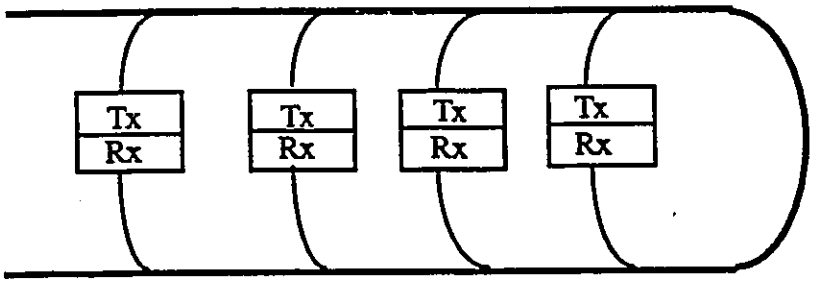

Fig. 1.4. Bus Topology

Impacts of Optical Amplifiers in WDMA Networks

The main physical limitations for high-speed transmission systems in WDMA networks result from the transport properties of optical fibers, namely, attenuation and dispersion characteristics. To overcome the attenuation and eliminate the optical budget restrictions, optical amplifiers have been used in these networks to replace regenerators, because the WDM approach increases the regenerator complexity significantly if the separate wavelength channels must be demultiplexed, separately regenerated, and multiplexed again. Obviously, amplified WDM systems expand transmission capacity in long-distance lightwave telecommunications.

Although optical amplifiers are of great value in WDM networks, they can degrade signal quality, primarily through noise added to the output signal, and nonlinearities caused by dynamic saturation of the optical gain. In a chain of repeat amplifiers, amplified spontaneous emission (ASE) generated in each amplifier accumulates and is further amplified by the succeeding amplifiers. The accumulated ASE noise is proportional to the gain of each amplifier and the number of amplifiers. It has effects on both the detected

noise and the gain saturation. The detected noise at the receiver due to ASE consists of both a spontaneous-spontaneous component which is the self-beat noise of the ASE power within the optical band of the receiver, and a signal-spontaneous component from the beats between the signal and the ASE. Its degradation will be studied in some sections of Chapter 2. Chapter 3 is focused on the saturation effect of optical amplifiers in WDMA ring networks.

1.2. Organization of Thesis

The thesis is focused on architecture design and analysis of layered WDMA wide-area networks. My original contribution in this thesis is as follows:

Chapter 2 is focused on the study of WDM fiber ring Local-Area Networks, in which two architectures are proposed and their system and component building blocks, as well as performance, are studied. In Chapter 3, the model of random gain due to non-linear effect (saturation) of optical amplifiers in WDMA ring networks is proposed. These two chapters are focused on the architecture design of WDMA ring LANs, which is considered as the element (or the low layer) in the design of layered WDMA wide-area network architecture. Chapter 4 is focused on the intermediate layer and the top layer, in which the hierarchy of layered wide-area networks is proposed systematically first; then using Bragg cell cross-connect to interconnect WDMA ring LANs is proposed as the distributed approach for internetworking in the intermediate layer; and in the top layer, an ultra-high capacity photonic ATM switch based on optical pulse FDM and WDM is proposed to interconnect the Intermediate Layer Networks. Finally, a conclusion is provided in Chapter 5.

Chapter 2
Architectures for WDMA Fiber Ring Local-Area Networks

With the development of fiber-optic transport systems, the demand for high throughput in interoffice communications grows. In [1], a TDM fiber ring is proposed for this application. As the need for the transmission capacity at Central Offices increases in the network, the limitation of electro-optic process speed becomes more pronounced. The best solution to this problem is to employ Wavelength Division Multiplexing (WDM) technology. WDM allows expansion of network traffic volume simply by adding more wavelengths, as opposed to expensive system upgrades in electronics and fiber transmission systems. In [2][3], passive WDM ring networks are proposed using acousto-optic tunable filters (AOTFs) as optical add-drop multiplexers (ADM). Compared with the TDM fiber ring network, the aggregate throughput of the network is increased substantially.

In this thesis, a transparent dense WDM ring network using a four-port Fabry-Perot etalon as ADM is proposed and studied in Section 2.1. This novel ADM achieves a much better resolution bandwidth than an AOTF ADM (1 *nm*). Therefore the conventional WDM can be replaced by dense WDM technology, in which the channel spacing is in the order of 1 *nm* and the crosstalk between channels is minor. By inserting optical amplifiers on the ring network, the network capacity and the distance between Central Offices can be increased significantly. In Section 2.2, an alternative approach is proposed, in which an Add-Drop Multiplexer is replaced by a Wavelength-Selective Router. Although this architecture is theoretically less flexible than the first one proposed in Section 2.1, it is a better solution in terms of power divisioning.

2.1. WDMA Architecture I: A Transparent Dense WDMA Ring Network using Fabry-Perot Add-Drop Multiplexer

2.1.1 Introduction

With the continuing advances in photonic devices, the design of novel network architectures that exploit these devices becomes desirable. Particularly, the invention of optical amplifier creates the exciting possibility to push fiber LANs into the realm of large-scale, high-capacity, all-optical networks. The expansion raises the demand on the network growth, flexibility and other issues that are considered secondary in today's photonic network design. From this point of view, the power-division problem is no longer the dominant factor among the troublesome limitations in photonic network design, and the advantages of the star topology are not obvious. Alternative architectures need be explored in order to to best exploit the emerging technologies.

In general, throughput, delay and power budget are taken as the figures of merit in comparing different optical network architectures. With recent dramatic advances in fiber-optic technologies, attention has been drawn to those network architectures that are viable for the next technology generation. In other words, consideration should be given to the architecture in which the network structure and connectivity can be reconfigured easily, in order to enhance network function without significant physical modifications; thus services may be added or removed over time to accommodate diverse requirements sparked by the new technologies. Besides, as the evolution of photonic network architecture becomes more and more sensitive to the rapid advancement of photonic technology, the network topology should accommodate the novel photonic devices easily and cost-effectively, and utilize them efficiently. As newly invented photonic devices like fiber amplifiers make it a reality to build the fiber network covering a large geographic area, it will eventually become important to achieve full network connectivity with a minimum number of

single-mode fibers. Among various topologies, the fully transparent fiber ring shows promise in fulfilling these requirements, and can be envisioned as a suitable candidate to meet the changing traffic and service needs of the future.

The fully transparent fiber ring provides a single data path which is shared by all the attachments; compared with star, it is usually fairly easy to add (or remove) one more access node. Therefore, the fiber ring, a purely broadcast network, can be used as a common physical medium, and its access nodes are taken as multiple subscriber premises (e.g., B-ISDN, circuit-switched service) integrated onto this fiber ring. Thus reconfiguration can be achieved fairly easily. Unlike bus, it possesses the geometric feature that provides it with at least double the area-coverage efficiency. Therefore, taking ring as a physical topology, the network can be expanded to a large scale in geographic span. Also, it can support a large number of users by placing optical amplifiers economically in the "common single data path", and the benefit of optical amplifier can be shared by more than one access node. Optical amplifiers, in conjunction with WDM technology, could therefore dramatically increase the network capacity and offer a significant performance advantage in all-optical networks. Thus, with a fairly reasonable power budget, the network capacity can be increased. Also, for large-scale optical networks, unlike star topology, ring topology does not require a large number of fibers, and the network implementation cost is lowered.

2.1.2. Network Architecture

The proposed network configuration is shown in Fig.2.1.1. Four nodes are used for illustration. The network is composed of N communication nodes which are interconnected passively by a single-mode fiber forming a ring. The single-mode fiber serves as a unidirectional communication link, allowing the information transmission in a fixed direction along the

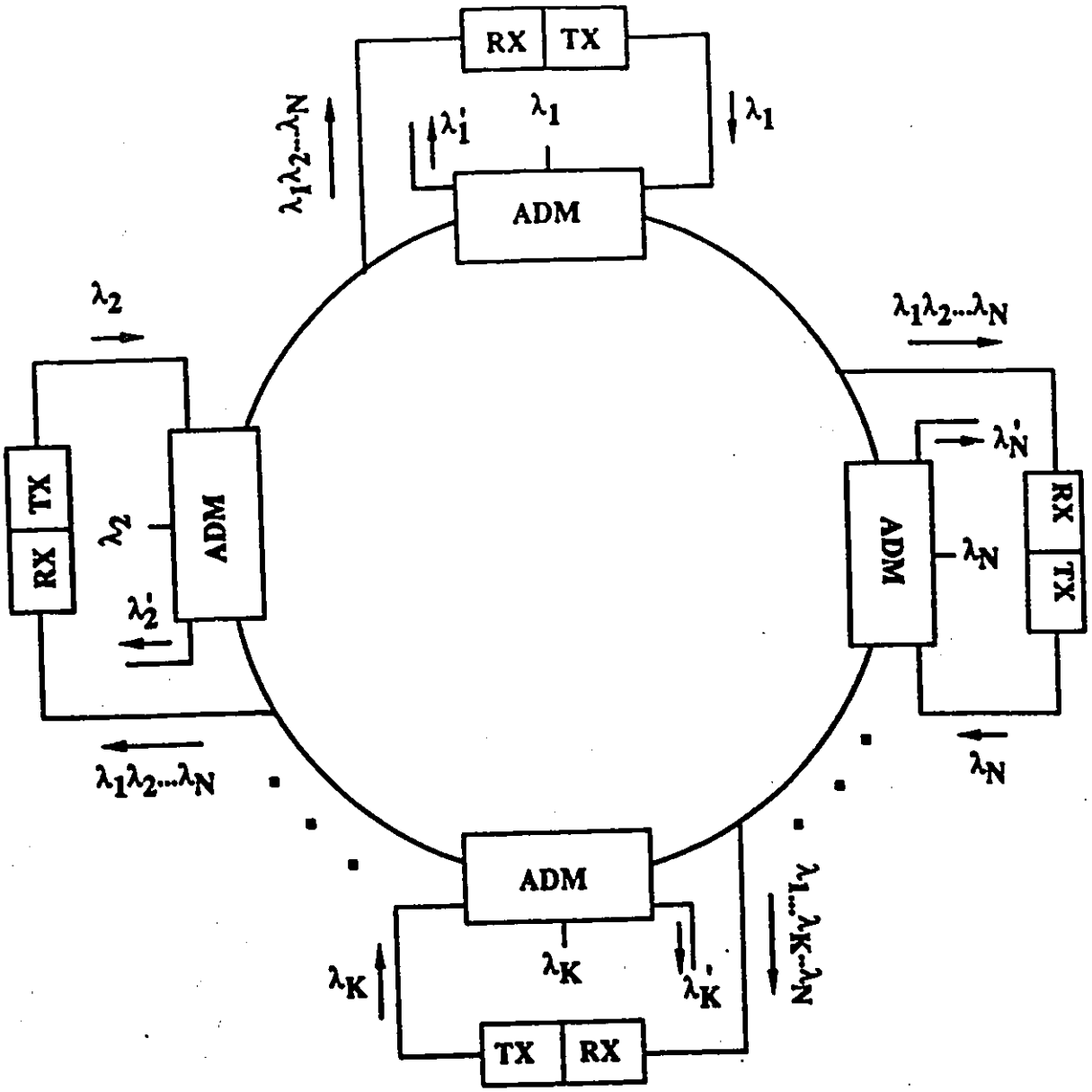

Fig.2.1.1 WDMA Ring Network Architecture

ring, which it is defined to be counter-clockwise here without loss of generality. Therefore, each node has both incoming and outgoing links. In the fiber ring, an EDFA is placed in the incoming link of each node, adjacent to each receiver system in order to compensate for the power loss. The ring is a fully passive medium by being "all-optical" in nature, in the sense that once the information enters the ring network, the information may remain in optical domain until it is delivered to its destination; accordingly, the ring provides full connectivity among communication nodes, perfectly transparent to bit rate and signal format.

Each network access node comprises an Add-Drop Multiplexer (ADM) and an optical receiver system. The function of ADM is three-fold. First, to inject the optical information signal on the pre-defined wavelength for this node into the optical fiber ring so that it can propagate through the other communication nodes. Second, to extract the residual of the same wavelength light previously injected out of the ring after it passes through all the receivers of the other access nodes on the ring exactly once. This is done in order to prevent the light from circulating around the ring indefinitely and interfering with later transmissions on the same wavelength through the same ADM. Third, to direct the optical signals of other wavelengths back into the fiber ring for further circulation. Therefore, each of them has virtually four ports corresponding to the incoming link, the outgoing link, the port to which the optical information on selected wavelength is injected from the transmitter, and the port where the removed residue is extracted. Optical signals are injected/removed to/from the fully transparent fiber-optic ring at different pre-defined wavelengths on each node. A single-longitudinal-mode laser diode operating at the pre-defined wavelength is linked to the individual ADM as a transmitter. Therefore, the ADM plays the role of the source node in this architecture. On a predefined wavelength, each user transmits its information onto the optical fiber ring through the ADM. The injected signals are allowed to circulate counter-clockwise for one complete round and offer a fraction of their power to any node along the path.

The remaining power will be filtered out by the ADM at the network access nodes where they originate.

The receiver system at each node consists of a wavelength de-multiplexer using cascaded Mach-Zehnder periodic filters, and an array of as many as *N* electro-optic receivers containing PIN photodiodes. The de-multiplexer separates different carrier wavelengths before photodetection of the individual signal. The receiver system can receive and process transmissions simultaneously and asynchronously from the source of any of the other nodes.

With this architecture and these system components, N different users transmit information at N different wavelengths concurrently through the fully transparent fiber ring. All the information on the ring is received by each node, selected by a multitude of receivers. Therefore, WDMA scheme is realized via ring.

2.1.3. Optical Add-Drop Multiplexers

The realization of Wavelength Division Multiple Access (WDMA) optical networking via ring topology is contingent upon the development of its key component, namely, optical Add-Drop Multiplexer(ADM). In this subsection, implementation of optical ADM is studied systematically. In 2.1.3.1, mode-coupling effect ADM is described; 2.1.3.2 explains the proposal of implementing optical ADM using high-isolation polarization-independent optical circulators and Fabry-Perot etalon; finally, the two approaches are compared in 2.1.3.3.

2.1.3.1. Overview of Mode Coupling Effect ADM

The mode-coupling approach attempts to exploit the advantage of some special features in structures and properties from the acousto-optic and electro-optic family of tunable passive filters. The functions of these filters are solely based on the wavelength dependence of mode coupling induced by external perturbations.

Among these mode-coupling effect filters, the acousto-optic tunable filter[4] is more attractive because it can cover the entire spectrum of low-loss region in the single-mode fiber in terms of tunability. The electro-optic filter covers a typical band of only 16 nm, although it has faster tuning speed. This discrepancy arises because the period of the acoustooptic grating is equal to the acoustic wavelength, which can be adjusted easily; for the electro-optic filter, the periodicity is fixed during fabrication. Also, acousto-optic devices can exhibit very precise frequency tuning using electronic RF oscillators, with drive voltage as low as a few mW for guided wave interaction. Because of the large electric field within the electro-optic device, its modulation voltage is generally much higher. Although both acousto-optic devices and electro-optic devices are not mature, it is more efficient to realize ADM by employing acousto-optic filters with state-of-the-art technologies.

The operating principle of acousto-optic filters is as follows: An acoustic transducer generates acoustic waves in the acousto-optic medium. The waves cause a periodic perturbation in the refractive index. Under the phase matching conditions, this perturbation allows only a narrow range of optical wavelength to be filtered. The acousto-optic filter is set to different wavelengths by changing the acoustic drive frequency.

A typical example of acousto-optic device for ADM function is the four-port polarization-independent acoustical tunable optical filter (PIATOF) [5]. The most remarkable feature of this device is its ability to interchange any one or more of the wavelengths in one input with the same subset of wavelengths on the other input. The selection of wavelength is controlled by the acoustic drive frequency. This mechanism together with its four-port structure and polarization-independent property makes it available in realizing ADD-DROP function in WDM ring network[2].

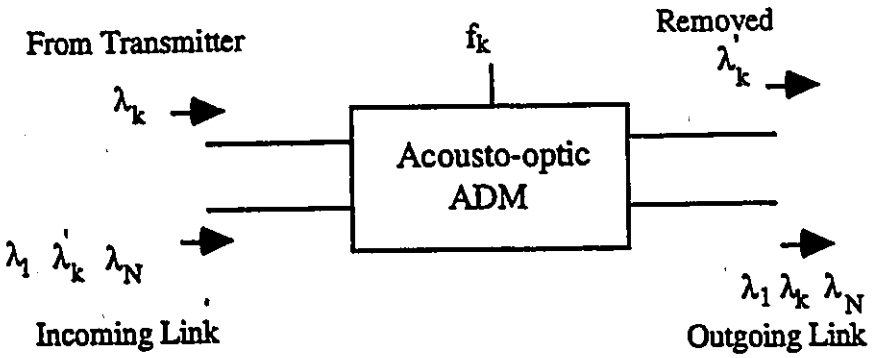

Fig.2.1.2. Block Diagram of Acousto-optic ADM

As shown in Fig.2.1.2, the network access nodes are interconnected so that the lower input port of the PIATOF-ADM of one node is connected to the lower output port of the PIATOF-ADM of the preceding node by a section of single-mode fiber; and the lower output port is connected to the fiber going to the succeeding node. This process is repeated for the rest of the adjacent nodes to form a complete closed optical path. For the other two upper nodes which are not connected in the ring, the upper input node serves as the link to the transmitter, while the upper output node is used as the export for the removed signal of the previous transmission.

2.1.3.2. Four-Port Fabry-Perot ADM

The mechanism of four-port Fabry-Perot ADM is wavelength correlation with transmissions and reflections from beams interference by multiple reflections in a Fabry-Perot etalon[4]. Fig.2.1.3 (a) shows an ideal model, with the selected wavelength of the Fabry-Perot etalon defined as λ_k. The light from the fiber ring containing the whole spectrum of WDM wavelengths enters the Fabry-Perot etalon from Port 1. An infinite number of partial waves is produced by the reflections and transmissions on Mirror 1 and Mirror 2, and the light that is trapped in the etalon gradually leaks out through these two mirrors. The light containing the selected wavelength λ_k, namely the transmitted wave, exits the etalon at Port 3. The light containing the other wavelengths, namely the reflected wave, exits at Port 2 into the fiber ring. Therefore, the DROP function is exercised. At Port 4, the transmitter injects the light containing the selected wavelength λ_k. By the principle of reversibility, this light beam transmits through these two mirrors without reflection, and is combined with the light beam of the other wavelengths at Port 2 into the fiber ring. Therefore, the ADD function is exercised.

Fig. 2.1.3 (b) illustrates the configuration of practical implementation of Fabry-Perot ADM. It consists of one Fabry-Perot etalon and two High-Isolation Polarization-Independent Optical Circulators [6] [7] coupled with single-mode fibers.

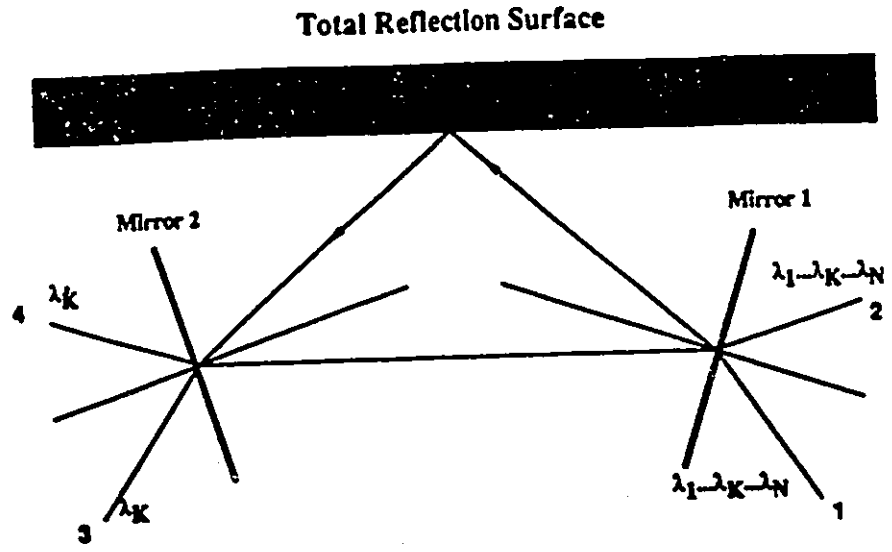

Fig. 2.1.3 (a) Ideal Model of Fabry-Perot ADM

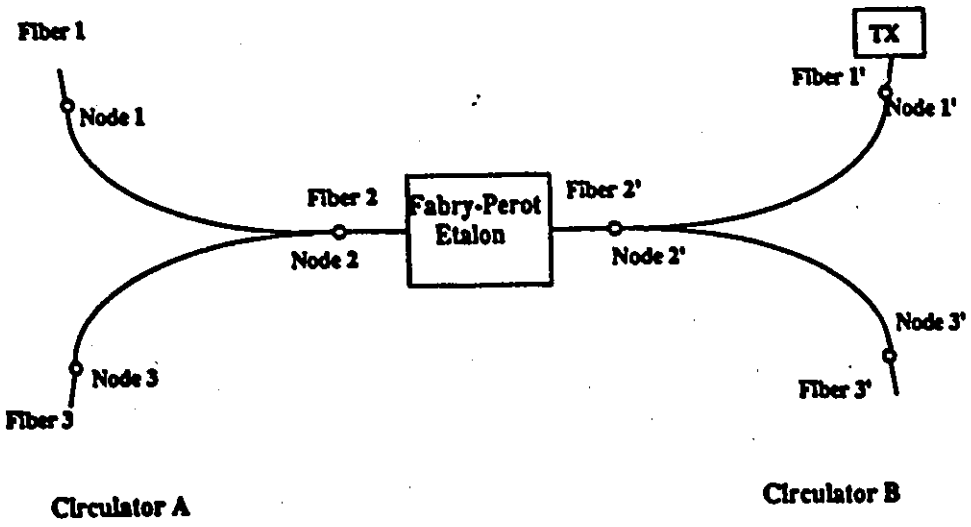

Fig. 2.1.3(b) Implementation of Fabry-Perot ADM

The optical circulator is a non-reciprocal functional device exhibiting the distinct feature of directing light emerging in one circulator port in its unique direction to another predefined port. With this device, the functionality of communication systems can be greatly enhanced. Applications of circulators combined with optical amplifiers have already been studied and experimentally confirmed [8] [9] [10].

In general, the optical circulator has N ports (typically, four) coupled with single-mode fibers which can be connected into the lightwave communication systems and networks. The light emerging from fiber i and entering the circulator at port i ($1 \le i \le N-1$, integer) proceeds through the circulator and exits only at port i+1, and is injected into fiber i+1; and that from port N couples only to port 1.

Consider the beam propagation from i to j in a 4-port circulator, where i and j are integers from 1 to 4, and j=i+k(mod 4). The propagation mode k=0 means the return by reflection, called "return loss", k=1 is the forward mode termed "insertion loss", and k=2 and 3 are backward modes or "isolation". In [6], the prototype high-isolation polarization-independent optical circulator (HIPIO-Circulator) is reported to possess isolation over 30 dB and insertion loss at 1 dB or less at wavelength 1.299um. In [7], the prototype HIPIO-Circulator using birefringent crystals is reported to exhibit over 60 dB of isolation and insertion loss under 1.5 dB in the wavelength range of 70 nm around 1550 nm. In [11], a high-isolation polarization-independent quasi-Optical Circulator is reported to be fabricated. This circulator has a much simpler structure than those previous reported, and preserves the same level of isolation, insertion loss and return loss as shown in [11].

With the desirable feature of the optical circulator, the ADD-DROP function is demonstrated as follows: at node k, Fiber 1 and Fiber 3 coupled with Optical Circulator A are connected into the

fully transparent fiber-optic ring, with Fiber 1 to the incoming link and Fiber 3 to the outgoing one. The light with the entire spectrum of WDM wavelengths λ_i, $i=1,...k,...N$, travels into the circulator through Fiber 1 at Port 1. Because of the unique feature of an optical circulator, the light beam exits at Port 2 of the circulator, passes through Fiber 2, and is incident on the reflector surface of the Fabry-Perot etalon, whose selected wavelength is λ_k. According to the effect of beam interference by multiple reflections, the incident light of wavelength λ_k, which is injected previously into the fiber ring and has circulated for one round in the ring, passes through the etalon and enters the Optical Circulator B at Port 2'. This light is exported by the circulator at Port 3'; in the meantime, the effect of beam interference by multiple reflections also causes the incident light containing other wavelengths λ_i, $i=1....,k-1,\ k+1,...N$, to reverse its propagation direction and re-enter Optical Circulator A at Port 2. According to the unique feature of the optical circulator, this light beam leaves the circulator at Port 3, connected to the outgoing link, goes back into the fully transparent fiber optic ring and propagates to the next access node.

A transmitter is linked to Port 1' of Optical Circulator B, and injects light at wavelength λ_k. The injected light proceeds through Optical Circulator B, emerges at its Port 2', and enters Fiber 2' toward the etalon of selected wavelength λ_k. Then the light transmits through this " band-pass filter" of its own wavelength and is combined with the returning light of the remaining wavelengths propagating through Optical Circulator A into the fiber optic ring.

With Fabry-Perot etalon, as follows, we take the typical parameters used in commercial industry for the performance analysis in the next section: for the selected wavelength, the insertion loss is 3 dB, and the reflection loss is 15 dB; for the non-selected wavelength, the insertion loss is 30 dB, and the reflection loss is 0.1 dB; for one circulator, the insertion Loss is 1 dB, and isolation is greater than 29.9 dB.

When the light containing non-selected wavelength, λ_i, $i=1...,k-1, k+1,...N$, passes through one interference ADM, it loses 2.1 dB power. When the injected light at wavelength λ_k, travels through the ADM into the fiber ring, it loses 5 dB power. The filtered light at wavelength λ_k, which has circulated in the ring for one complete round, has a small fraction of power reflecting back into the ring. The degradation of this power from ADM is 17 dB. In other words, the residue of the previous transmission wavelength λ_k decreases by 17 dB.

2.1.3.3. Comparison of an Acousto-optic ADM and a Fabry-Perot ADM

Obviously, considering the structure, a Fabry-Perot ADM with two physical ports exhibits the same system function as the acousto-optic ADM with four physical ports. In combination with the optical circulators, the virtual four-port Fabry-Perot ADM has four physical ports.

Besides the structural difference, there is an inherent difference in the overall performance of the two types of ADM because of the different physical mechanisms. For the ADM using acousto-optic filter, for example, PIATOF, there is a wider tuning range (-400 nm), but a poorer resolution (-1 nm), so it is suitable for conventional WDM all-optical networks with a wide channel spacing.

The Fabry-Perot ADM, on the other hand, provides a much better resolution bandwidth (< 0.01 nm) but a narrower tuning range (around 50 nm). Thus, this ADM is suitable for dense WDM ring networks with an ultra-fine channel spacing.

The unique features of simple structure and the very fine resolution bandwidth of Fabry-Perot ADM, coupled with the advantage of high gain (-30 dB) of Er+3-Doped fiber amplifier

(with an operating bandwidth of 30 nm) make the idea of WDMA on ring topology attractive when utilizing dense WDM technology.

2.1.4. A Limiting Network Performance Analysis

The following symbols and values are used in the performance evaluation of the dense WDMA fiber ring network using Fabry-Perot ADM:

L_{fiber} : Loss factor of the fiber (including splicing losses) : 0.3 dB / Km, or $10^{\frac{-0.3d}{10}}$, where d is the distance between two nodes in the ring. Assume nodes are equally spaced over the ring.

L_{tap}: Excess loss factor of the tap : 0.2 dB or $10^{\frac{-0.2}{10}}$.

G: EDFA equivalent gain. Typically, EDFA gain is taken as 30 to 35 dB. Taking coupling efficiency η_{in} as 0.31 and η_{out} as 0.26 into account, the equivalent gain is assumed to be 20 dB, or $10^{\frac{20}{10}}$. EDFA gain is wavelength-dependent, and gain equalizers have been proposed to obtain a flat gain [12]. In the following calculations, we assume an equalized gain EDFA. Therefore, the result obtained is an upper bound on the performance of a WDMA ring network using unequalized gain EDFAs.

P_{LASER}: Power injected from the laser: 1 mW.

$L_{F-P-Trans}$: Loss factor of the transmitted power passing through the Fabry-Perot ADM, 5 dB as calculated in the previous section.

$L_{F-P-Pass}$: Loss factor of the reflected wavelength power as passing through Fabry-Perot ADM, 2.1 dB as calculated in the previous section.

β : Tap fraction of each node towards the Mach-Zehnder de-multiplexer.

L_{M-Z}: Loss factor of the Mach-Zehnder demultiplexer, 10 dB assuming it has five stages and 32 channels.

α: Loss between amplifier and receiver,

$$\alpha = \beta \, L_{tap} \, L_{M-Z} \qquad (2.1.)$$

N : The number of nodes in the ring network, where N = 32.

Then. the resulting loss factor between nodes is

$$K_{p-n} = L_{fiber}\ G\ L_{tap}\ (1-\beta)\ L_{F-P-Pass} \qquad (2.2.)$$

Direct detection scheme is used in the receiver system. A worst case uncoded bit error rate (BER) of 10^{-9} is used as the minimum required performance. Here, the worst case is considered as the case when the power from node #1 reaches the receiver at the node # N.

The output power from the Nth optical amplifier is

$$p_{amp-out-N} = P_{LASER}\ L_{F-P-Trans}\ K^{N-1}{}_{p-n}\ [L_{F-P-Pass}\ (1-\beta)\ L_{tap}\ ]^{-1} \qquad (2.3.)$$

so the power into the PIN receiver is

$$P_r = p_{amp-out-N}\ \alpha \qquad (2.4.)$$

After opto-electronic processing, the electrical signal power is: $S = (\frac{e\lambda}{hc}\eta P_r)^2$ (2.5.)

where e is the electron quantity, $e = 1.6 \times 10^{-19}$, h is the Plank constant, $h = 6.63 \times 10^{-34}$, c is the speed of light $c = 3 \times 10^8$ m/sec, λ is the optical wavelength taken as 1.55 μm, η is the quantum-efficiency taken as 1 for the ideal case.

The interference-to-signal ratio is,

$$ISR = K_{p-n}{}^{N} L' / L_{F-P-pass} \qquad (2.6.)$$

Where L' is the loss factor of the selected wavelength reflecting back into the ring through the Fabry-Perot. Here L' is 17 dB as calculated in the previous section.

The parameters and formula for noise calculation are the following:

N_{sp}: EDFA spontaneous emission factor. $N_{sp} = 1.4$.

Rb: Transmission bit rate per channel, assuming all the channels have equal bit rates.

Be: the electrical bandwidth of the receiver , here $Be = 0.7$ Rb.

Bo: The optical bandwidth of the receiver. With 30 nm bandwidth of EDFAs (1 nm is equivalent to 133 GHz at 1.55 μm), for each of the 32 channels, $Bo = 62$ GHz.

I_{th}: The peak thermal noise equivalent current density is taken to be 12 $pA/\sqrt{Hz}$ according to [13].

Since there are N fiber amplifiers distributed in the ring, for the amplifier-related noises at the Nth receiver, we have the effective spontaneous emission factor as:

$$N_{sp-eff} = \eta_{out}(N_{sp} + K_{p-n}N_{sp} + K^2{}_{p-n}N_{sp} + \ldots + K^{N-1}{}_{p-n}N_{sp}) = \eta_{out}N_{sp}\frac{1-K^N{}_{p-n}}{1-K_{p-n}} \quad (2.7.)$$

Then, the thermal noise is [13]:

$$N_{th} = I_{th}{}^2 Be \quad (2.8.)$$

The shot noise is:

$$N_{shot} = 2\frac{\eta e^2}{h\nu}Be(P_r + \alpha N_{sp-eff}(G-1)h\nu Bo) \quad (2.9.)$$

The signal and spontaneous beat noise is:

$$N_{s-sp} = 4\frac{\eta^2 e^2}{h\nu}BeP_r\alpha(G-1)N_{sp-eff} \quad (2.10.)$$

The spontaneous-to-spontaneous beat noise is:

$$N_{sp-sp} = \eta^2 e^2 \alpha^2 [N_{sp-eff}(G-1)]^2(2BoBe - Be^2) \quad (2.11.)$$

Most gigabit applications have a BER requirement between 10^{-9} and 10^{-15}. Among them, *Visualization* and *Conferencing* have a BER requirement of 10^{-9}, while *Medical Image* and *CPU Interconnect* require a BER of 10^{-15}. Assume γ is the electrical signal-to-noise ratio at the receiver; then according to the communications theory, to obtain a BER of 10^{-9}, γ is assigned the following values: 72 for OOK; 20 for DPSK; 36 for FSK; to obtain a BER of 10^{-12}, γ is assigned the following values: 99.1232 for OOK; 26.631 for DPSK; 49.5616 for FSK; to obtain a BER of 10^{-15}, γ is assigned the following values: 123.874 for OOK; 33.874 for DPSK; 61.937 for FSK.

Solving the following nonlinear equation by computer with β equal to 0.02,

$S/N = f(R_b, d) = \gamma$ (2.12.).

The performance can be achieved as shown in Table 1. The results in Table 1 are the attenuation-limited transmission distances. Here, we assume the laser linewidth is sufficiently small so that the material dispersion-limited distance is sufficiently long, and also the modal dispersion is negligible. Besides, the total system rise time is small enough to support the assumed range of bit rates.

Note that these calculations are obtained assuming there is no interference on the network. The real case is slightly worse. To determine the impact of the interference on the system performance, we relate the ISR to the interference power penalty (i.e., the degradation of the required optical signal power at the detector's input, relative to the case of no interference). We assume that the effects of the interference can be recovered, by restoring the original eye opening (i.e., without the interference) at the decision circuit of the receiver. The increase in the minimum-detectable received power required for the same error rate is defined as the power penalty. The computation of power penalty involves a worst-case assumption that a logic ZERO in the signal coincides with interference logic ONEs, and vice versa.

Based on these assumptions, the eye opening with interference is smaller than the eye opening without interference by the factor (1-ISR)[14]. Consequently, the power penalty is

$$10\log_{10}\left(\frac{1}{1-ISR}\right)dB \qquad (2.13.)$$

The result of interference-to-signal ratio versus bit rate is shown in Table 2, and the corresponding power penalty versus bit rate is shown in Table 3.

Table 1.(a) Bit Rate Versus Distance Between Nodes (BER=10^{-9})

Bit Rate (Gbit/s)	Distance (km)(OOK)	Distance (km)(FSK)	Distance (Km)(DPSK)
1	60.39	60.76	61.06
2	60.01	60.39	60.70
3	59.78	60.17	60.49
4	59.61	60.01	60.33
5	59.47	59.88	60.21
6	59.36	59.78	60.11
7	59.26	59.69	60.03
8	59.17	59.61	59.95
9	59.09	59.54	59.88
10	59.01	59.47	59.82

Table 1.(b) Bit Rate Versus Distance Between Nodes (BER=10^{-12})

Bit Rate (Gbit/s)	Distance (km)(OOK)	Distance (km)(FSK)	Distance (Km)(DPSK)
1	60.217	60.589	60.912
2	59.828	60.217	60.551
3	59.588	59.992	60.334
4	59.410	59.828	60.178
5	59.267	59.697	60.054
6	59.146	59.588	59.951
7	59.039	59.494	59.863
8	58.944	59.410	59.768
9	58.858	59.335	59.717
10	58.778	59.267	59.645

Table 1.(c) Bit Rate Versus Distance Between Nodes (BER=10^{-15})

Bit Rate (Gbit/s)	Distance (km)(OOK)	Distance (km)(FSK)	Distance (Km)(DPSK)
1	60.094	60.471	60.793
2	59.697	60.094	60.428
3	59.451	59.865	60.209
4	59.267	59.697	60.050
5	59.118	59.563	59.924
6	58.991	59.451	59.819
7	58.879	59.353	59.729
8	58.779	59.267	59.650
9	58.687	59.189	59.579
10	58.601	59.118	59.514

Table 2. (a) Bit Rate Versus Interference-to-Signal Ratio (dB) (BER=10^{-9})

Bit Rate (Gbit/s)	Inter-to-Signal (OOK)	Inter-to-Signal (FSK)	Inter-to-Signal (DPSK)
1	-31.017	-34.531	-37.437
2	-27.366	-31.018	-34.004
3	-25.138	-28.903	-31.952
4	-23.500	-27.366	-30.473
5	-22.189	-26.151	-29.308
6	-21.086	-25.138	-28.344
7	-20.127	-24.266	-27.519
8	-19.275	-23.500	-26.795
9	-18.505	-22.813	-26.150
10	-17.799	-22.189	-25.567

Table 2.(b) Bit Rate Versus Interference-to-Signal Ratio (dB) (BER=10^{-12})

Bit Rate (Gbit/s)	Inter-to-Signal (OOK)	Inter-to-Signal (FSK)	Inter-to-Signal (DPSK)
1	-29.355	-32.925	-36.028
2	-25.617	-29.355	-32.560
3	-23.314	-27.193	-30.480
4	-21.609	-25.617	-28.976
5	-20.233	-24.362	-27.788
6	-19.068	-23.314	-26.802
7	-18.049	-22.409	-25.957
8	-17.137	-21.609	-25.214
9	-16.308	-20.888	-24.552
10	-15.542	-20.233	-23.952

Table 2.(c) Bit Rate Versus Interference-to-Signal Ratio (dB) (BER=10^{-15})

Bit Rate (Gbit/s)	Inter-to-Signal (OOK)	Inter-to-Signal (FSK)	Inter-to-Signal (DPSK)
1	-28.174	-31.791	-34.884
2	-24.364	-28.174	-31.382
3	-21.999	-25.975	-29.276
4	-20.234	-24.364	-27.748
5	-18.803	-23.077	-26.539
6	-17.583	-21.999	-25.533
7	-16.510	-21.064	-24.668
8	-15.544	-20.234	-23.908
9	-14.661	-19.486	-23.227
10	-13.841	-18.803	-22.609

Table 3.(a) Bit Rate Versus Power Penalty due to Interference (dB)(BER=10^{-9})

Bit Rate (Gbit/s)	Power Penalty (OOK)	Power Penalty (FSK)	Power Penalty (DPSK)
1	0.003473	0.001737	0.000869
2	0.007810	0.003473	0.001737
3	0.013442	0.005642	0.002605
4	0.019499	0.007810	0.003907
5	0.026411	0.010411	0.005208
6	0.033744	0.013442	0.006510
7	0.042354	0.016472	0.007810
8	0.051805	0.019499	0.009111
9	0.061664	0.022957	0.010411
10	0.072782	0.026411	0.012143

Table 3.(b) Bit Rate Versus Power Penalty due to Interference (dB)(BER=10^{-12})

Bit Rate (Gbit/s)	Power Penalty (OOK)	Power Penalty (FSK)	Power Penalty (DPSK)
1	0.00521	0.00217	0.0008685
2	0.01214	0.00521	0.002605
3	0.02036	0.00824	0.003907
4	0.03029	0.01214	0.005642
5	0.04149	0.01604	0.007377
6	0.05395	0.02036	0.009111
7	0.06950	0.02512	0.016844
8	0.08472	0.03029	0.013009
9	0.10300	0.03547	0.01517
10	0.12289	0.04149	0.01734

Table 3.(c) Bit Rate Versus Power Penalty due to Interference (dB)(BER=10^{-15})

Bit Rate (Gbit/s)	Power Penalty (OOK)	Power Penalty (FSK)	Power Penalty (DPSK)
1	0.0065	0.00304	0.001303
2	0.01604	0.00651	0.003039
3	0.02771	0.01084	0.005208
4	0.04149	0.01604	0.007377
5	0.05738	0.02123	0.009544
6	0.07662	0.02771	0.0121433
7	0.09791	0.03417	0.014741
8	0.12289	0.04149	0.017770
9	0.1511	0.04923	0.020792
10	0.18326	0.05738	0.023821

2.1.5. Conclusions

A transparent WDMA ring network architecture using a Fabry-Perot etalon as an ADM has been proposed in this subsection. This ADM achieves a much better bandwidth resolution than the ADM using acousto-optic tunable filter (--1 nm) proposed previously. Therefore, dense WDM technology can be employed. In addition, the unique feature of ring topology makes it easy to incorporate optical amplifiers in the network. The network capacity and its geographic span can be increased significantly. However, the gain of the optical amplifier is wavelength-dependent. Research on the study of gain equalizer has been carried out. In this subsection, the limiting performance of the network capacity and geographic span was analyzed numerically under the ideal assumption of the optical amplifiers having a wavelength-independent gain. Meanwhile, the residual interference was also studied, numerically.

2.2. WDMA LAN Architecture II: A WDMA Ring Network With Holographic Wavelength-Selective Routers

2.2.1. Motivations

For WDMA fiber ring networks, there are two types of scenario for the noise power level at the receiver systems. One occurs where there are no optical amplifiers placed on the fiber ring, usually the case with small-sized Local Area Networks(LAN). The other occurs where optical amplifiers are placed on the ring, usually the case with large-sized LAN or Metropolitan Area Networks(MAN). With no amplifiers on the ring, two types of noise are present in the receiver system, namely thermal noise and signal shot noise. Both are linearly proportional to the transmission bit rate. Therefore, as the signal carried on one specific wavelength, say λ_1, propagates and is tapped by the remaining nodes on the fiber ring, the amount of power required to combat noise in the receiver is the same. In other words, the power sensitivity for the signal on this particular wavelength is the same for the receivers on the remaining nodes. If the optical amplifiers are placed on the optic fiber ring, the receiver noises consist of five elements: receiver thermal noise, signal shot noise, accumulated optical amplifier spontaneous shot noise, accumulated optical amplifier signal-spontaneous beat noise, and accumulated optical amplifier spontaneous-spontaneous beat noise. The greater the number of optical amplifiers the signal on this specific wavelength needs to pass before reaching the destination node, the larger the power sensitivity for the receiver at this wavelength at the node. In the case of the signal at wavelength λ_1 injected at node 1, the receiver of wavelength λ_1 at node N has the largest receiver power sensitivity.

On the other hand, the propagation power of the injected signal decreases as it propagates through more nodes. Take Prop i as the propagation power at node i for λ_1, then

Prop 1 > Prop 2 >... > Prop N.

In the previous scheme with optical ADMs, the same fraction of power β is tapped from the fiber ring to the receiver for all the wavelengths and in all the nodes. Therefore, the power appearing at the receiver nodes decreases from node 2 to node N along the ring. Because of the monotonously increasing power sensitivity and the monotonously decreasing propagating power along the path, this uniform tap causes a certain amount of power to be wasted, thus limiting the network performance from its potential capacity. In addition, residual power exists in the ring, and ADM is needed at the transmission node to remove this residual signal and prevent its interfering with the later transmitted signal.

2.2.2. Proposed new network architecture

In a network with ADMs, the following network components are present for each Network Interface Unit (NIU) as shown in Fig.2.2.1 (a):

(1). A gain equalized optical amplifier .[12]

(2). Wavelength Demultiplexer with a low crosstalk and a low insertion loss.

(3). Uniform tap which is insensitive to wavelengths and has a very low excess loss.

(4). ADM using optical filter with low crosstalk and low insertion loss.

(5). High-performance transmitters and receivers.

In order to avoid the problem discussed in the previous section, we propose a new network component, namely, Wavelength Selective Router (WSR), to replace items #2, #3 and #4 above. See Fig.2.2.1.(b).

The function of WSR is to non-uniformly tap the optical power from different wavelengths on the ring. This is done according to the prescribed power-tapping fractions pre-assigned to each node. The purpose is twofold: (1) to bring the optical power received at each node on the ring closer to its power sensitivity than with uniform tapping; therefore the transmission power is used more efficiently; (2) to make the optical power of the wavelength carrying the information, circulated exactly once, to be fully tapped and to be sent to the receiver at the last exit node. Therefore, in theory, the interference of the residue of the injected signal is fully eliminated, and expensive ADMs are not needed in the network.

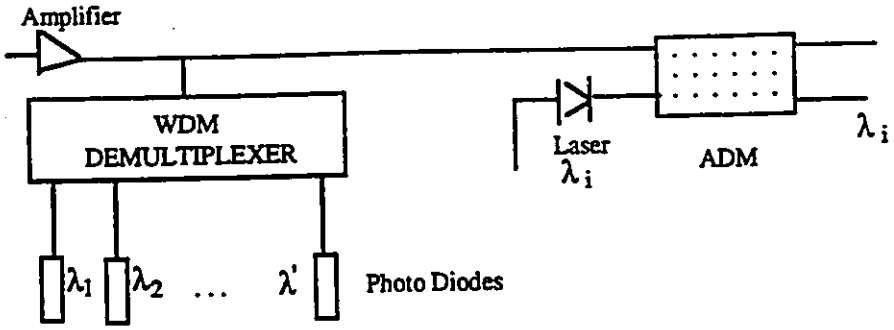

Fig. 2.2.1. (a). UNI in WDMA Ring Network with ADM

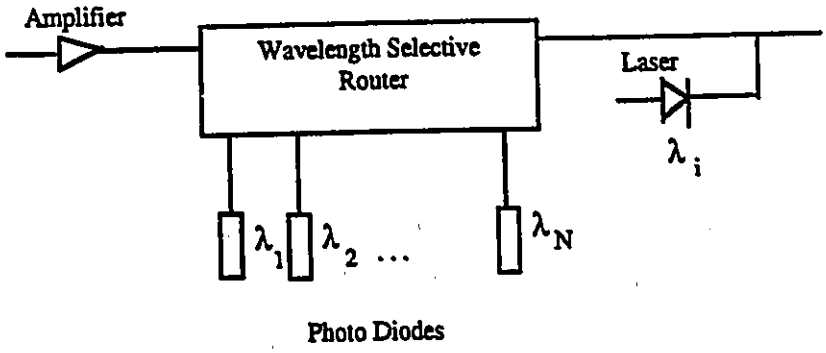

Fig. 2.2.1. (b) UNI in WDMA Ring Network with WSPD

Assuming that on the ring, node i injects signal on the pre-assigned wavelength λ_i; then the power-tapping fraction matrix for this network is:

| $wavelength$: ..... $\lambda_1 .. \lambda_2 .. \lambda_3 ..... \lambda_N$

| $Station\#1$ ..... $\beta_1 .. \beta_N . \beta_{N-1} ..... \beta_2$

| $Station\#2$ ..... $\beta_2 .. \beta_1 . \beta_N . \beta_{N-1} ..... \beta_3$

| .....

| .....

| $Station\#N$ ..... $\beta_N . \beta_{N-1} ..... \beta_2 . \beta_1$

define β_1=0, β_N=1. $\beta_1 < \beta_2 < .....< \beta_N$, then,

$wavelength: .....\lambda_1 ... \lambda_2 .. \lambda_3 ... \lambda_4 ..... \lambda_N$

$|Station\#\ 1 .....0 ... 1 .... \beta_{N-1} ..... \beta_2$

$|Station\#\ 2 ..... \beta_2 .. 0 .... 1 .... \beta_{N-1} ..... \beta_3$

$|Station\#\ 3 ..... \beta_3 .. \beta_2 .. 0 .... 1 .. \beta_{N-1} ..... \beta_4$

$|.....$

$|.....0 .... 1$

$|Station\#\ N ..... 1 .. \beta_{N-1} ..... \beta_2 .. 0$

The rows of this matrix are the parameters of WSR at each specific node, and the columns refer to the tapping fractions on the network nodes for each wavelength. This matrix indicates that no power on a specific wavelength is extracted from the transmission node, and all the power is removed from the last exit node. In order to make the amount of tapped power exactly equal to the power sensitivity of each node, the other elements on the matrix have to be expressed as functions of both static network parameters (i.e., distance between stations, loss factor of network components, amplifier gain) and network system transmission bit rate.

As in the analysis of the previous section, there are two factors contributing to the inefficient use of optical power: the degradation of signal level in propagation because of the amount of loss which is not compensated by the optical amplifiers, and the increase of power sensitivity at the receivers, which is due to the effect of accumulated optical amplifier spontaneous emission noise. Here, from a practical point of view, we propose a method to specify the other elements on the matrix only by static network parameters and to eliminate the effect of the first factor on the distribution of power.

2.2.3. Power Division Problem

In this subsection, the elements in the power-tapping fraction matrix are expressed as functions of static network parameters (i.e., distance between stations, loss factor of network components, amplifier gain). Based on this, the condition of minimum transmission power required at each node is derived.

2.2.3.1. Specification of the Matrix Elements

The matrix elements are specified according to the following criteria: for any one of the specific wavelengths, the amount of optical power which appears at the receiving nodes is the same, and the amount is chosen to be the power sensitivity of the last exit node. Since this value is the largest power required among all the receivers, the power received on the rest of the network nodes is beyond the power sensitivity of each node.

The following symbols are defined for the purpose of analysis:

L_{fiber} : loss factor of fiber (including splice) : 0.3 dB / Km, or $10^{\frac{-0.3d}{10}}$, where d is the average distance between any two nodes in the ring, assuming nodes are equally spaced in the ring.

G: amplifier equivalent gain. Assuming the carrier lifetime of the optical amplifier (i.e., EDFA) is much larger than the signal bit period, each node transmits continuous bit stream; then, during one carrier lifetime, average input power to each amplifier is the same, G is the same for all the amplifiers. Typically, EDFA gain is taken as 30 to 35 dB. Taking a coupling efficiency of η_{in} = 0.31 and η_{out} = 0.26 into account, the equivalent gain is assumed to be 20 dB.

P_{LASER}: the power value injected from the laser: 1 mW

L_{WSR}: loss of WSR

$L_{coupling}$: Coupling loss at the transmission node

Define P_{ri} as the power received at the ith node along the loop for a specific wavelength and the transmission node as the first node; in other words, P_{r1} =0. Then,

$$
\begin{aligned}
P_{r2} &= (P_{laser}L_{coupling})L_{fiber}GL_{WSR}\beta_2 \\
P_{r3} &= (P_{laser}L_{coupling})L^2_{fiber}G^2L^2_{WSR}(1-\beta_2)L_{coupling}\beta_3 \\
P_{r4} &= (P_{laser}L_{coupling})L^3_{fiber}G^3L^3_{WSR}(1-\beta_2)(1-\beta_3)L^2_{coupling}\beta_4 \\
&\cdot \\
&\cdot \\
P_{rn} &= (P_{laser}L_{coupling})L^{n-1}_{fiber}G^{n-1}L^{n-1}_{WSR} \\
&(1-\beta_2)(1-\beta_3)\ldots(1-\beta_{n-1})L^{n-2}_{coupling}\beta_n
\end{aligned}
\qquad (2.14)
$$

Define m=L_{fiber} L_{WSPD} $L_{coupling}$ G, by setting all the P_{ri} terms equal, the following relations are obtained:

$$\beta_n = \frac{m\beta_{n+1}}{1+m\beta_{n+1}}, \qquad (2.15)$$

where n=2,3,...N-1.

By mathematical induction, β_i can be expressed as a function of m, which contains only static network parameters.

$$\beta_N = 1$$

$$\beta_{N-1} = \frac{m}{1+m},$$

$$\beta_{N-2} = \frac{m^2}{1+m+m^2} = \frac{m^2}{\sum_{i=0}^{2} m^i},$$

$$\beta_{N-j} = \frac{m^j}{\sum_{i=0}^{j} m^i}$$

.

.

.

$$\beta_2 = \frac{m^{N-2}}{\sum_{j=0}^{N-2} m^j} = \frac{m^{N-2}(1-m)}{1-m^{N-1}}$$

In general,

$$\beta_k = \frac{m^{N-k}(1-m)}{1-m^{N-k+1}} \qquad (2.16)$$

2.2.3.2. Minimum Power Requirements

Define *Pr* as the power received at each of the photodiodes, then Pr is the same for each of the nodes, and we have

$$P_r = p_{r2} = P_{laser} m\beta_2 = P_{laser} m \frac{m^{N-2}(1-m)}{1-m^{N-1}} = p_{laser} \frac{m^{N-1}(1-m)}{1-m^{N-1}} \qquad (2.17)$$

After opto-electronic process, the electrical signal power is:

$$S = (\frac{e\lambda}{hc}\eta P_r)^2 \qquad (2.18)$$

where e is the electron quantity, $e = 1.6 \times 10^{-19}$c

h is the Plank constant, $h = 6.63 \times 10^{-34}$

c is the speed of light $c = 3 \times 10^8$m/sec

λ is the optical wavelength and taken as 1.55 μm

η is the quantum efficiency and is taken as 1 for the ideal case.

Since for a specific wavelength, the last exit node on the ring has the largest amount of noise on the receiver system, the minimum required power has to be large enough for the signal-to-noise ratio(SNR) to satisfy the prescribed value. In other words, given the static network parameters, the network can be implemented using the WSR with prescribed tapping matrix. In this network, there is an upper bound on the transmission bit rate such that all the SNR requirements of each node are satisfied.

The parameters and formula for noise calculation are:

N_{sp}: spontaneous emission factor. $N_{sp} = 1.4$

Rb: bit rate of transmission per channel, assuming all channels have equal bit rates

Be: the electrical bandwidth of the receiver; e.g., take $Be = 0.7$ Rb

Bo: the optical bandwidth of the receiver; e.g., for EDFA 's 30 nm bandwidth, and 1 nm equivalent to 133 GHz at 1.55 μm, for each of the 32 channels, $Bo = 62$ GHz

R_f: transimpedance resistance

g_m: transconductance of FET

R_E: input resistance

C_T: input capacity

We define the equivalent accumulated optical amplifier spontaneous noise factor as:

$$
\begin{aligned}
N_{sp-eff} &= \eta_{out} L_{WSPD} [\, N_{sp} m(1-\beta_{N-1}) + N_{sp} m^2 (1-\beta_{N-1})(1-\beta_{N-2}) + \cdots\cdots \\
&+ N_{sp} m^{N-2} (1-\beta_{N-1})(1-\beta_{N-2}) \cdots (1-\beta_2) \\
&+ N_{sp} m^{N-1} (1-\beta_{N-1})(1-\beta_{N-2}) \cdots (1-\beta_2)\,] \\
&= \eta_{out} L_{WSPD} N_{sp} \left(\frac{m}{1+m} + \frac{m^2}{1+m+m^2} + \cdots\cdots \right. \\
&\left. + \frac{m^{N-2}}{1+m+\ldots+m^{N-2}} + \frac{m^{N-1}}{1+m+\ldots+m^{N-2}} \right) \\
&= \eta_{out} L_{WSPD} N_{sp} \left(\sum_{i=1}^{N-2} \frac{m^i}{\sum_{j=0}^{i} m^j} + \frac{m^{N-1}}{1+m+\ldots+m^{N-2}} \right)
\end{aligned}
\qquad (2.19)
$$

The sensitivity of an optical PIN-FET receiver is mainly determined by the following noise sources:

Thermal noise of the transimpedance resistance:

$$N_{th} = \frac{4kT}{R_f} Be = I_{th}^2 Be \qquad (2.20)$$

Noise of the FET-transistor:

$$N_{FET} = \frac{4.4kT}{g_m}\left[\frac{1}{R_E}Be + (2\pi C_T)^2 \frac{1}{3}Be^3\right] \quad (2.21)$$

Shot noise :

$$N_{shot} = 2\frac{\eta e^2}{h\nu}Be(P_r + N_{sp-eff}(G-1)h\nu Bo) \quad (2.22)$$

Signal and spontaneous beat noise:

$$N_{s-sp} = 4\frac{\eta^2 e^2}{h\nu}BeP_r(G-1)N_{sp-eff} \quad (2.23)$$

Spontaneous-to-spontaneous beat noise:

$$N_{sp-sp} = \eta^2 e^2 [N_{sp-eff}(G-1)]^2 (2BoBe - Be^2) \quad (2.24)$$

Defining γ as the electrical signal-to-noise ratio at the receiver, then the minimum power transmitted must satisfy the following equation:

$$\frac{S}{N_{th} + N_{FET} + N_{shot} + N_{s-sp} + N_{sp-sp}} \geq \gamma \quad (2.25)$$

For the given static network parameters and transmission power, the transmission bit rate which satisfies the above equation is an upper bound on the bit rate for each transmission node in the network.

2.2.4. Integrated Waveguide Holographic Multiple Phase Grating: A Proposed Approach to build Wavelength Selective Router

Physically, the function of Wavelength Selective Router can be realized by using multiple gratings to diffract different wavelengths from one multiple wavelength optical input into many different directions[15] [16]. Each pre-recorded grating deflects one and only one wavelength

with pre-determined diffraction efficiency to a pre-determined angle into the receiver system. For a perfectly phase-matched, lossless, unslanted transmission grating, the diffraction efficiency is:

$$\eta_i = \sin^2\left[\frac{\pi \Delta n d}{\lambda_i (\cos\theta)^{\frac{1}{2}}}\right] \qquad (2.26)$$

where Δn and d are the associated index modulation and interaction length, respectively. By adjusting Δn and d, as well as θ, we can get the desired tapping efficiency (which is equal to the diffraction efficiency) for wavelength λ_i. Notice that the long interaction length (>1cm) coupled with the large index modulation depth (Δn >0.1) will dramatically increase the wavelength selection resolution and deflection angle resolution. However, they will also increase the absorption loss and spread the beam. Trade-off exists between these factors. Parameter d is controlled by the lithographic process and Δn is manipulated through exposure dosage and wet and dry processing parameters.

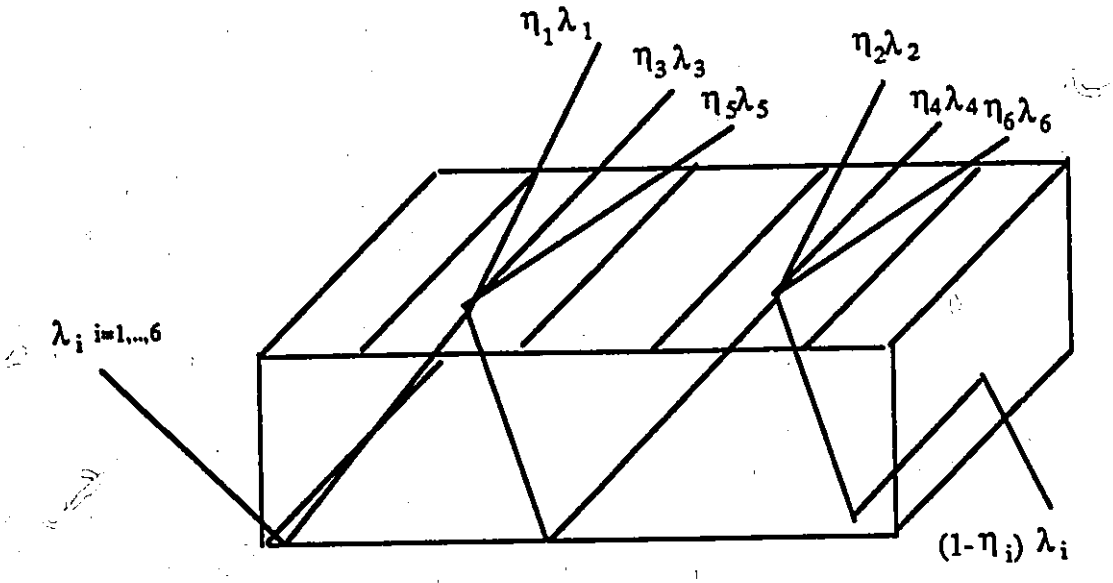

Fig.2.2.2. Structure of Multiple Grating WSPD

As shown in Fig.2.2.2 above, the planar optical waveguide with a holographic grating can be fabricated monolithically through the standard ion-exchange process. The multiple wavelength light beam is launched into the planar waveguide through a prism coupler. The light propagates down the planar waveguide until it encounters the phase grating on the top of it. Because of the evanescent field interaction, the light will be deflected, according to the pre-defined diffraction efficiency, by the phase grating recorded in the applied photosensitive material.

Multiple grating has additional advantage of being more economical to mass produce as a product to fit different tapping matrix specifications.

2.2.5. Conclusions

In this section, an alternative approach to realize WDMA via a ring topology has been proposed. Theoretically, it is a better solution to the power-divisioning problem than WDMA ring network with ADMs. However, it is less flexible in modifying the network parameters. Since holographic grating is easy to duplicate once it is recorded, this architecture can be an option in standardization for WDMA ring network.

Chapter 3
Modeling of the Optical Amplifiers' Random Gain in WDMA Ring Networks with Add-Drop Multiplexers

3.1. Introduction

In the analysis of the previous chapter, the optical amplifiers are modeled to possess a constant wavelength-independent gain. With this ideal model, the results obtained in the previous chapter are considered to be a limit on the performance of the WDMA ring networks. In reality, many problems arising from the intrinsic physical property of optical amplifiers degrade the network system performance.[17]

In WDMA ring network, optical amplifiers amplify several channels at different wavelengths at the same time; therefore the network link budget improves. However, many problems related to the optical amplifiers (i.e., induced crosstalk and noises) can reduce the amount of link budget improvement actually obtained. Typical problems are as follows:

-Wavelength-dependent gain of optical amplifiers can cause serious problems in cascaded optical amplifier systems. Gain equalizers have been proposed to solve this problem. Further study has also been carried out.[18]
-Inter-modulation distortion can become significant if the optical carriers are spaced too closely such that the carrier density can respond at the beat frequency. This problem can be solved by arrangement of relatively large channel intervals, e.g., greater than 10 GHz.[19]-[23]

In this chapter, the focus is on the modeling of the amplifier nonlinearity (or gain saturation) induced channel crosstalk problem in WDMA ring network with ADMs. The problems of unequal gain and intermodulation distortion are assumed to have been solved. The

amplifier here can be a doped fiber amplifier or a semiconductor laser amplifier.[17] Here, we assume the typical problems related to each of these two types of amplifiers have been solved, i.e., for semiconductor laser amplifiers, assume that the problems of polarization dependence and Fabry-Perot ripple in the gain have been solved so that the available gain is limited by noise and saturation rather than by the facet reflectivity or polarization dependence of the gain.

3.2. Statement of the Problem

In the optical amplifier stimulated emission model, the dynamics of the carrier density in the active region are described by a carrier rate equation assuming the spontaneous emission intensity is much smaller than the signal intensity in the gain region[24]:

$$\frac{dn(t)}{dt} = \frac{n_c}{t_c} - \frac{n(t)}{t_c} - \frac{I_{in}(t)}{I_{sat}} \frac{[G(t)-1]}{\alpha L t_c} \qquad (3.1)$$

Where t_c is the carrier recombination lifetime, L is the length of the active region, α is the gain coefficient, n_c is the pumping intensity, I_{sat} and I_{in} are the saturation and the input optical intensity, respectively.

When the input intensity is varying at a rate much smaller than $\frac{1}{t_c}$, the carrier density in the optical amplifier responds rapidly to the changes in the input intensity. In other words, with an intensity-modulated data stream (i.e., OOK) coming into the amplifier at a bit rate much smaller than $\frac{1}{t_c}$, the steady state conditions are reached quickly within a fraction of the bit period, and the left-hand of Equation (3.1.) can be set to zero. Therefore,

$$I_{in}(t) = \frac{I_{sat}}{G(t)-1} \alpha L [n_c - n(t)] \qquad (3.2.)$$

and by setting

$$G_o = exp[\alpha L [n_c - n_T]] \qquad (3.3.), (3.4)$$

$$G(t) = exp[\alpha L [n(t) - n_T]]$$

where n_T is the transparency density corresponding to the onset of population inversion, we get [24]:

$$I_{in}(t) = \frac{I_{sat}}{G(t)-1} In \frac{G_o}{G(t)} \qquad (3.5.)$$

or

$$p_{in} = \frac{P_{sat}}{G-1} In \frac{G_o}{G} \qquad (3.6.)$$

Here, $P_{in} = I_{in}A$ and $P_{sat} = I_{sat}A$, A being the cross-sectional area. In this equation, G_o is the small signal gain of the amplifier (i.e., the gain when $P_{in} = 0$).

From this equation, we see that as the input intensity increases, carriers are depleted from the active region, resulting in a reduction in the gain.

From the above analysis, the following conclusions are reached:

(1) Gain is a function of the total input power to the amplifier. In other words, the gain seen by a particular channel is affected by the intensity level on other channels.

(2) At data rates much larger than the inverse of the carrier lifetime, the amplifier gain remains almost constant at a value corresponding to the average input power. In terms of effect on the signal power level of a particular channel (on a particular wavelength), only saturation component exists, that is, the steady-state reduction in the gain resulting from the existing signals' power on the other channels.

(3) At a data rate much smaller than the inverse of the carrier lifetime, the amplifier gain varies as the input power intensity changes. Both saturation component and crosstalk component exist. The crosstalk component refers to the variation in the gain resulting from the randomness of the total input power around the mean.

The crosstalk impact of gain saturation on the system performance is a strong function of the lifetime in the optical amplifier. The carrier recombination lifetime in the semiconductor laser amplifier is around 1 ns; the fluorescence life of ions within a Doped-Fiber Amplifier is around 10 ms. Therefore, two types of amplifier gain models are proposed in the WDMA ring network with ADMs:

(1) *Constant Gain Model*

This corresponds to the doped fiber amplifiers with regularly varying input intensities. In this case, the amplifier gain cannot respond to the fluctuations in the input power level, and the ion density within the amplifier will remain a constant.

(2) *Random Gain Model*

This corresponds to the doped fiber amplifiers with randomly varying input intensity or semiconductor laser amplifiers (TW, MQW) with any sources.

In the following section, emphasis is placed on the random gain model in WDMA ring networks with Add-Drop Multiplexers. The problem related to this proposed model is referred to as the Two-Dimensional Crosstalk issue.

3.3. Closed-Loop Markov Chain Model for Optical Amplifiers' Random Gain in WDMA Ring Networks

Consider the process for a signal injected into the fiber loop of WDMA ring networks towards the last exit node. The signal passes through n optical amplifiers. When the condition for Constant Gain Model is satisfied, the amplifier gain is considered to be a constant, and the model and analysis in the previous chapter are valid. However, if the condition for Constant Gain Model is not satisfied, a stochastic model needs to be established to simulate the random gains, determined by the total random input power of OOK optical signals, provided the parameters of the optical amplifiers are given. This model is referred to as a Closed-Loop Markov Chain Model. In it two types of probabilities are involved, namely the probability distribution of the number of channels at "ON" state for a specific optical amplifier (referred to as the amplifier stage) in the signal route, and the transition probability of the signal path from one optical amplifier to the optical amplifier in the next stage. In Subsection 3.3.1., expressions for these two probabilities are derived from different sorts of sources. In Subsection 3.3.2., the transition probabilities of the case when multiple ADMs are placed between a pair of optical amplifiers are derived. In Subsection 3.3.3., a Closed-Loop Markov Chain Model is formulated. Subsection 3.3.4. is devoted to a brief description of the effect of two-dimensional crosstalk based on the Closed-Loop Markov Chain model.

3.3.1. Probability Distribution and Transition Probability for Different On-Off Key Source Models

In this subsection, the two types of probabilities for different On-Off Key source models are derived. Starting with the general continuous bit stream source model, the regular ATM source model and bursty ATM source model are derived. These will be used as the fundamental models in the following study of optical amplifiers' random gain.

3.3.1.1. General Continuous Bit Stream Source Model

Assume coding is applied to the source and as a simple model, the bits in continuous stream x_n=1,2,... are dependent and satisfy the following property, i.e.,

$$P(x_{n+1}=1|x_n=0)=a$$
$$P(x_{n+1}=0|x_n=1)=b \qquad \text{(3.7.)-(3.8.)}$$

where $0<a<1, 0<b<1$. Then the transition matrix is[25]:

$$p=\begin{array}{c|cc} & 0 & 1 \\ 0 & 1\text{-}a & a \\ 1 & b & 1\text{-}b \end{array} \qquad (3.9)$$

$$p^n=\frac{1}{a+b}\begin{vmatrix} b & a \\ b & a \end{vmatrix}+\frac{(1\text{-}a\text{-}b)^n}{a+b}\begin{vmatrix} a & -a \\ -b & b \end{vmatrix} \qquad (3.10)$$

and the stationary distribution is,

$$(\pi_0,\pi_1)=(\frac{b}{a+b},\frac{a}{a+b}) \qquad (3.11)$$

Define T as the length of a bit, τ as the round trip delay on the fiber ring, then $\tau = Nn'd/c$, where N is the number of channels in the WDMA ring network, d is the equal distance between stations, c is the speed of light, n' is the refractive index of single-mode dispersion-flat fiber. Therefore, when $nT < \tau < (n+1)T$,

$$Probability\{n.new.pulses.generated.in.(0,\tau)\} = \frac{(n+1)T-\tau}{T}$$
$$Probability\{n+1.new.pulses.generated.in.(0,\tau)\} = \frac{\tau-nT}{T} \qquad (3.12)\text{-}(3.13)$$

thus,

$$P_{1,1} = p[x(t)=1, x(t+\tau)=1] = p[x(t)=1]p[x(t+\tau)=1 | x(t)=1]$$
$$= \frac{a}{a+b} Prob[(n.new.pulses.generated.given.above)] \bigcup (n+1.new.pulses.generated.given.above)]$$
$$= \frac{a}{a+b}\{[\frac{(n+1)T-\tau}{T}]P_{1,1}^{n} + [\frac{\tau-nT}{T}]P_{1,1}^{n+1}\}$$
$$= \frac{a}{a+b}\{[\frac{(n+1)T-\tau}{T}](\frac{a}{a+b} + \frac{(1-a-b)^n b}{a+b}) + [\frac{\tau-nT}{T}](\frac{a}{a+b} + \frac{(1-a-b)^{n+1} b}{a+b})\}$$
$$= \frac{a^2}{(a+b)^2} + [1-(a+b)(\frac{\tau-nT}{T})]\frac{(1-a-b)^n ab}{(a+b)^2}$$

Similarly,

$$P_{0,0} = P[x(t)=0, x(t+\tau)=0] = \frac{b^2}{(a+b)^2} + \frac{(1-a-b)^n ab}{(a+b)^2}[1-(a+b)(\frac{\tau-nT}{T})]$$
$$P_{0,1} = P[x(t)=0, x(t+\tau)=1] = \frac{ab}{(a+b)^2} - \frac{(1-a-b)^n ab}{(a+b)^2}[1-(a+b)(\frac{\tau-nT}{T})]$$
$$P_{1,0} = P[x(t)=1, x(t+\tau)=0] = \frac{ab}{(a+b)^2} - \frac{(1-a-b)^n ab}{(a+b)^2}[1-(a+b)(\frac{\tau-nT}{T})]$$

(3.14)-(3.17)

so for a continuous bit stream, the probability that out of $N-1$ channels, K of them are ON is,

$$P_r(x=K) = \frac{(N-1)!}{K![(N-1)-K]!}\pi_1^K \pi_0^{N-K-1} \qquad (3.18)$$

Let $P_0^{'}$, $P_1^{'}$ and $P_{-1}^{'}$ denote the probabilities that the number of ON channels remains the same, increases by one, and decreases by one when the signal passes through an ADM, respectively. Then we have,

$$\begin{aligned} P_0^{'} &= P_{1,1} + P_{0,0} \\ P_1^{'} &= P_{0,1} \\ P_{-1}^{'} &= P_{1,0} \end{aligned} \qquad (3.19)\text{-}(3.21)$$

3.3.1.2. Regular ATM Bit Stream Source Model

Assume the ATM cells for the N channels are synchronized in each cell slot, and the probability of sending a cell for a particular channel at time t is q, which is the same as that at any other time $t+\tau$. In each cell, for each bit period T, the probability that the bit is ON or OFF is $(\pi_0, \pi_1) = (\frac{b}{a+b}, \frac{a}{a+b})$ as derived before. Let x denote the number of ON channels in the input of an optical amplifier, then

$$\begin{aligned} P_r\{x = K'\} &= \sum_{n=0}^{N} P_{x|N}(K'|n) P_N(n) \\ &= \sum_{n=K'}^{N} \frac{n!}{K'!(n-K')!} \pi_1^{K'} \pi_0^{n-K'} \frac{N!}{n!(N-n)!} q^n (1-q)^{N-n} \\ &= \frac{N!}{K'!(N-K')!} (\pi_1 q)^{K'} (1-\pi_1 q)^{N-K'} \end{aligned} \qquad (3.22)$$

Where $K'=0,1,2,...,N$.

When a specific channel is assigned to be in ON state, for $N-1$ other channels, with K of them in ON state, the probability is given by

$$P_r\{x = K\} = \frac{(N-1)!}{K!(N-1-K)!}(\pi_1 q)^K (1-\pi_1 q)^{N-1-K} \qquad (3.23)$$

where $K=0,1,2,...,N-1$.

Let $P_0^{'}$, $P_1^{'}$ and $P_{-1}^{'}$ denote the probabilities that the number of ON channels remains the same, increases by one, and decreases by one when the signal passes through an ADM, respectively. Then we have,

$$P_1^{'} = q^2\pi_0\pi_1 + (1-q)q\pi_1$$
$$P_{-1}^{'} = q^2\pi_1\pi_0 + q\pi_1(1-q) \qquad (3.24)\text{-}(3.26)$$
$$P_0^{'} = q^2(\pi_0\pi_0 + \pi_1\pi_1) + q\pi_0(1-q) + (1-q)q\pi_0 + (1-q)^2$$

3.3.1.3. Bursty ATM Bit Stream Source Model

Assume time is divided into two periods, Period I and Period II, and the periods alternate, the transition probability between these two periods is,

	Period I	Period II
Period I	γ_1	$1-\gamma_1$
Period II	$1-\gamma_2$	γ_2

(3.27)

Then, the distributions of Periods I and II are geometric with parameters γ_1 and γ_2, respectively.

Model A: Assume Period I is an active period, and each slot contains a cell with a probability α, independently. Period II is assumed to be a silent period. The average arrival rate of a cell is then

$$q = \frac{\alpha(1-\gamma_2)}{1-\gamma_1+1-\gamma_2} \qquad (3.28)$$

Model B: Assume Period I is an active period, and each slot contains an ATM cell with probability α_1, independently; Period II is also an active period, and each slot contains an ATM cell with probability α_2, independently. Then the average arrival rate of an ATM cell is,

$$q = \frac{\alpha_1(1-\gamma_2)}{1-\gamma_1+1-\gamma_2} + \frac{\alpha_2(1-\gamma_1)}{1-\gamma_1+1-\gamma_2} \qquad (3.29)$$

With these expressions, the other probability distributions are the same as the regular ATM bit stream source model as detailed in the previous section.

3.3.2. Transition Probability for Multiple Add-Drop Multiplexers Between Optical Amplifiers

Assuming there are M ADM's between two optical amplifiers, then the transition probability is,

$$P_x = \sum_{\left\{\begin{matrix}(n_1,n_2,n_3) \\ n_1+n_2+n_3=M \\ n_1-n_3=x\end{matrix}\right\}} \frac{M!}{n_1!\,n_2!\,n_3!} p_1^{n_1}\, p_0^{n_2}\, p_{-1}^{n_3} \qquad (3.30)$$

where p_x's denote the probability that the number of ON channels increases by x, if x is positive; decreases by x if x is negative as the signal passes through M Add-Drop Multiplexers, respectively. Variable x can be any integer from $-M$ to M. More specifically,

for $x > 0$,

$$p_x = \sum_{n_1=x}^{M} \frac{M!}{n_1!(M-2n_1+x)!(n_1-x)!} p_1'^{n_1} p_0'^{M-2n_1+x} p_{-1}'^{n_1-x} \qquad (3.31)$$

for $x < 0$,

$$p_x = \sum_{n_3=-x}^{M} \frac{M!}{(n_3+x)!(M-2n_3-x)!n_3!} p_1'^{n_3-x} p_0'^{M-2n_3-x} p_{-1}'^{n_3} \qquad (3.32)$$

Example 1. For two ADMs between optical amplifiers, the transition probabilities are

$$\begin{aligned}
p_0 &= P_0'^2 + 2P_1' P_{-1}' \\
p_1 &= 2P_1' P_0' \\
p_{-1} &= 2P_0' P_{-1}' \\
p_2 &= P_1'^2 \\
p_{-2} &= P_{-1}'^2
\end{aligned} \qquad (3.33)$$

Example 2. For three ADMs between optical amplifiers, the transition probabilities are

$$\begin{aligned}
p_0 &= 6P_1' P_0' P_{-1}' + P_0'^3 \\
p_1 &= 3P_1' P_0'^2 + 3P_1'^2 P_{-1}' \\
p_{-1} &= 3P_{-1}' P_0'^2 + 3P_{-1}'^2 P_1' \\
p_2 &= 3P_1'^2 P_0 \\
p_{-2} &= 3P_{-1}'^2 P_0 \\
p_3 &= P_1'^3 \\
p_{-3} &= P_{-1}'^3
\end{aligned} \qquad (3.34)$$

3.3.3. Closed-Loop Markov Chain Model: An Approximation of Optical Amplifier Random Gain

To model the different random gain levels of a signal on a specific wavelength on the ring, a model for approximation is proposed in this subsection. As shown in Equation (3.6), for signals on a particular wavelength of a particular channel, the only external parameter related to the optical amplifier gain G is the input power level, P_{in}, consisting of three terms:

P_i: power level of the ON signal in the specific channel to be traced.

P_{N-1}: total power of the other $N-1$ channels, which is a random variable depending on how many actual number of the $N-1$ other channels are ON.

P_{ASE}: accumulated spontaneous emission noise introduced by all the amplifiers in the ring at the input of one particular optical amplifier. Since no single amplifier is treated any differently than any other amplifier in the ring, on an ensemble and statistical average basis, P_{ASE} is a constant for all the amplifiers. Its formula will be derived below.

Assume L as the total loss per section between two optical amplifiers, g as the equivalent gain per section based on statistical average, taking into account the external factor P_{in} and the internal factor G_0 (G_0 is different for different wavelengths in reality). Based on this, define the section coefficient δ as the product of L and g. Therefore, the non-lasing condition for the loop is $\delta \leq 1$. The stable condition for the loop is $\delta < 1$

In the following derivations, assume the stable condition is satisfied.

3.3.3.1. Derivation for P_{ASE}:

Assume there are N channels, N_{amp} optical amplifiers on the ring. The optical bandwidth of each channel is B_0. For each channel, the spontaneous emission noise power at the output of the inducing amplifier is given by:

$$P_N = 2N_{sp}h\nu B_0(g-1) \qquad (3.35)$$

where N_{sp} is the spontaneous emission factor, $h\upsilon$ is the photon energy.

In the following derivation, take $N=N_{amp}$. Each amplifier is followed by a user node, including a receiver and an ADM. Therefore, the amplifiers can be denoted as Amp1, ..., AmpN corresponding to the user nodes of wavelengths λ_1 to λ_N. Since the total input noise to each of the amplifiers is the same, an arbitrary amplifier, say Amp1, can be taken for analysis; the result obtained is the same for the rest. The total accumulated spontaneous emission noise at the input of Amp1 can be derived as follows:

$$P_{ASE} = P_{ASE,\lambda_1} + P_{ASE,\lambda_2} + \ldots + P_{ASE,\lambda_N} \qquad (3.36)$$

where $P_{ASE,\lambda_1},\ldots,P_{ASE,\lambda_N}$ are the accumulated spontaneous emission noise powers on wavelengths λ_1 ,...., λ_N., respectively.

For P_{ASE,λ_1}, since only the spontaneous emission noise generated by Amp1 is filtered out by the ADM at Node 1 tuned to λ_1 adjacent to it, so

$$\begin{aligned} P_{ASE,\lambda_1} &= (\delta + \delta^2 + \ldots + \delta^{N-1})2N_{sp}h\nu B_0 \\ &= \delta\frac{1-\delta^{N-1}}{1-\delta}2N_{sp}h\nu B_0 \end{aligned} \qquad (3.37)$$

For P_{ASE,λ_2}, the spontaneous emission noise on this wavelength generated by Amp1 and Amp2 is filtered by the ADM at Node 2 tuned to λ_2, so

$$P_{ASE,\lambda_2} = (\delta + \delta^2 + \ldots + \delta^{N-2}) 2N_{sp} h\nu B_0$$
$$= \delta \frac{1-\delta^{N-2}}{1-\delta} 2N_{sp} h\nu B_0 \qquad (3.38)$$

Similarly, for spontaneous emission noise power at wavelength λ_{N-1},

$$P_{ASE,\lambda_{N-1}} = \delta \frac{1-\delta^{N-(N-1)}}{1-\delta} 2N_{sp} h\nu B_0 \qquad (3.39)$$

For spontaneous emission noise power at wavelength λ_N, all the noise power generated by N amplifiers is filtered by the ADM tuned to λ_N before reaching Amp1, so,

$$P_{ASE,\lambda_N} = 0 \qquad (3.40)$$

so the total spontaneous emission noise power at the input of Amp1 is,

$$P_{ASE} = \frac{\delta}{1-\delta}[(N-1) - (\delta + \delta^2 + \ldots + \delta^{N-1})] 2N_{sp} h\nu B_0$$
$$= \frac{\delta}{1-\delta}[(N-1) - \delta \frac{1-\delta^{N-1}}{1-\delta}] 2N_{sp} h\nu B_0 \qquad (3.41)$$

3.3.3.2. Closed-Loop Markov Chain Model

As seen from the previous discussion, when the internal parameter of the optical amplifier is given, the gain level of the amplifier is determined by the total input power level, P_{in}, which is a combination of three terms: P_i, the power level of the ON signal in the specific channel which is to be examined; P_{N-1}, the total power of the other N-1 channels, which depends on the actual number of the remaining ON channels; and P_{ASE}, the accumulated spontaneous emission noise induced by all the amplifiers in the ring at the input of one particular optical amplifier. Among them, only P_{N-1} is a random variable, making P_{in} a random variable. Thus the gain level becomes a random variable. The distribution of the number of ON channels is given by Equation (3.23). Therefore, the number of remaining ON channels is distributed according to (3.23) for each stage of amplifier input. Taking these numbers as states between consecutive stages of amplifiers, we see they form a Markov chain, as shown in Fig.3.1. The transition probabilities are derived in the previous section. Note that this Markov chain is closed-loop in the sense that Amp N is directed to Amp1 with the same transition probabilities.

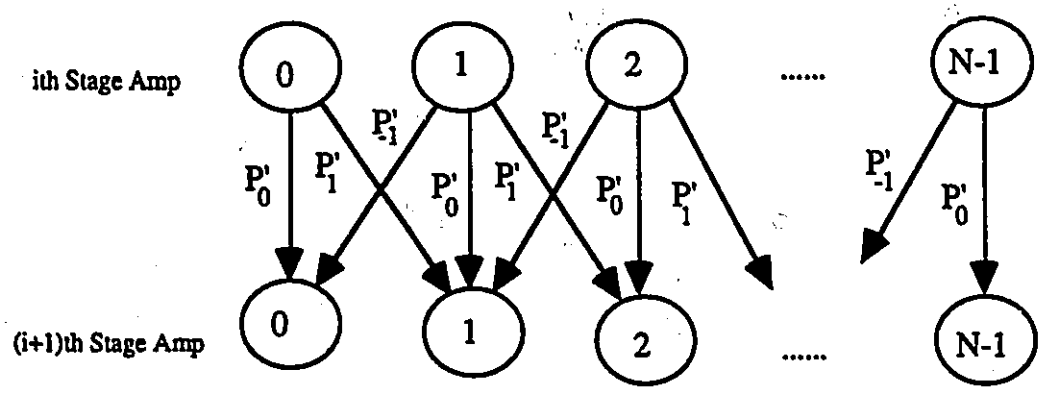

Fig.3.1. Markov Chain for Number of ON Channels

Denote $P_{i,j}$ as the total power of the *N-1* channels of Stage *i* amplifier with *j* channels ON, then $P_{i,j}$s form a Markov chain with the same transition probabilities as shown in Fig.3.2.

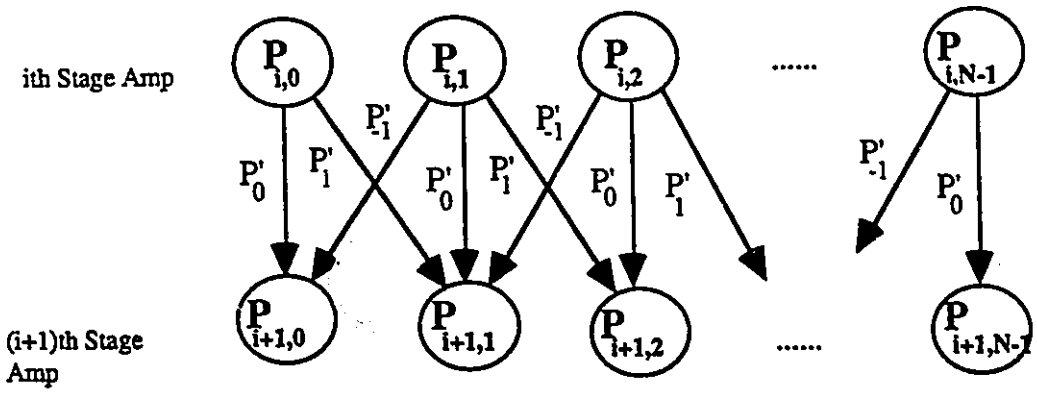

Fig.3.2. Markov Chain for Total Power of N-1 Channels

The gain levels of optical amplifiers as seen by a particular signal also form the closed-loop Markov chain with the same transition probabilities. With these random gains, the signal levels at the receiver have multiple amplitudes. This will cause a power penalty in the system, as discussed briefly in the next section.

As an approximation, for the *i*th stage amplifier that a signal propagates through, if there are *n* out of *N-1* ON channels at the amplifier input, the total input power of the *N-1* amplifiers can be approximated as,

$$P_{i,n} = \frac{n}{N-1}\frac{1-\delta^{i-1}+\delta^{i}-\delta^{N}}{1-\delta}p' \qquad (3.42)$$

where $P' = P_{Laser} L_{ADM} L_{fiber}$, while L_{ADM} and L_{fiber} are the loss of ADM and the loss of fiber, respectively. Note that there is a one-to-one mapping of $P_{i,n}$ with P_{in} at the ith stage amplifier, and P_{in} has a one-to-one mapping with G_i, the gain of ith stage amplifier. The input signal power to be examined at the ith stage amplifier is

$$P_{ith.stage} = L^{i-1} G_1 \ldots G_{i-1} P' \qquad (3.43)$$

Proof of (3.42) is as follows:

(1) At the input of Stage 1 amplifier of a particular channel, if all the other channels are ON, on the average, the power of each channel is

$$\frac{1}{N-1} P'(\delta + \delta^2 + \ldots + \delta^{N-1}) = \frac{P'}{N-1} \delta \frac{1-\delta^{N-1}}{1-\delta} \qquad (3.44)$$

so the total input power from the interfering channels to the first stage amplifier when n of the $N-1$ interfering channels are ON is

$$P_{1,n} = \frac{n}{N-1} P' \frac{\delta - \delta^N}{1-\delta} \qquad (3.45)$$

Setting $i=1$ in equation (3.42), the same result can be obtained.

(2) At the input of Stage 2 amplifier of a particular channel, if all the other channels are ON, on the average, the power of each channel is

$$P_{2,n} = \frac{1}{N-1} P'(1+\delta^2+\delta^3+\ldots+\delta^{N-1})$$
$$= \frac{P'}{N-1}(1+\delta^2\frac{1-\delta^{N-2}}{1-\delta}) \qquad (3.46)$$
$$= \frac{P'}{N-1}(\frac{1-\delta+\delta^2-\delta^N}{1-\delta})$$

Setting $i=2$ in equation (3.42), the same result can be obtained.

(3) Assume Equation (3.42) holds for the ith Stage amplifier, that is,

$$P_{i,n} = \frac{n}{N-1}\frac{1-\delta^{i-1}+\delta^i-\delta^N}{1-\delta} p' \qquad (3.47)$$

then, for $i+1$ Stage amplifier, the total input power level is

$$P_{i,n} = \frac{n}{N-1}(\frac{1-\delta^{i-1}+\delta^i-\delta^N}{1-\delta} + \delta^{i-1} - \delta^i)P'$$
$$= \frac{n}{N-1}P'(\frac{1-\delta^i+\delta^{i+1}-\delta^N}{1-\delta}) \qquad (3.48)$$

Thus, the proof is complete by mathematical induction.

3.3.4. Two-Dimensional Crosstalk Issue

Saturation-induced crosstalk is a potential problem in WDMA networks. In [26],[27], this problem has been analyzed for WDMA networks with one optical amplifier. It occurs because of the dependence of the amplifier gain level on the total input intensity. Increase of the input intensity results in a reduction in the gain. Thus, the gain seen by a particular channel is affected by the intensity level of other channels.

Two components from the interference of other channels contribute to the power penalty of an optical link, namely the saturation component arising from the steady-state reduction in

the amplifier gain resulting from the increase in the average input power, and the crosstalk component arising from the variation in the gain resulting from the randomness of the total input power around the average input power. The saturation component is proportional to the total number of channels in the network and the probability of one particular channel being ON at any given instant. The crosstalk component appears when the data rate is much smaller than the carrier lifetime.

When only one optical amplifier is placed in the optical link, the amplifier gain level follows the same Binomial distribution $P(x,N)$ as that for when x number of N independent channels are ON. Therefore, the signal level at the receiver end is a random variable with the same probability distribution $P(x,N)$. The spread of signal level causes a crosstalk power penalty in addition to the power penalty caused by saturation.

When N optical amplifiers are placed in the optical link, with M optical ADMs between each pair of optical amplifiers, the multiplexed amplifier gain level of the link is distributed with probabilities $P(x,N)P_a'P_b'\ldots P_{c'}'$, where a', b', c' are integers from $-M$ to M, P_i's are transition probabilities in the Markov Chain, and there are a total of $N-1$ such terms in a single product. Therefore, the crosstalk penalty is determined not only by the Binomial distribution of the ON channels at the input of the first optical amplifier in the link, but also by the randomness of the "add" and "drop" bits of the optical ADMs. In this thesis, this phenomenon is referred to as two-dimensional crosstalk in which the degree of randomness is larger and the spread of signal is more severe than the one-dimensional crosstalk[27]. Much work has been reported on one-dimensional crosstalk[27]. In further research, the closed-loop Markov chain model of optical amplifier gain proposed in the previous section can be used as one model for the investigation of the power penalty resulting from two-dimensional crosstalk in different WDMA ring networks.

Chapter 4
Towards Layered Wide-Area Networks

4.1. Introduction

In the previous chapters, architecture and performance analysis of Wavelength Division Multiple Access (WDMA) fiber ring local-area networks were presented. In addition, physical constraints of photonic and opto-electronic components (e.g., optical amplifiers, optical ADM) employed in WDMA fiber ring local-area networks were studied. All these studies focus on one objective: the design of a WDMA fiber ring local-area network (LAN) that possesses a high performance, while at the same time preserving the possibility that the network evolves in time, not only in terms of size, but also in terms of technological and architectural improvements. This is taken as the first step and considered to be fundamental to the rest of the work in this thesis.

When several WDMA fiber ring LANs exist, the natural question of how to interconnect them arises. Interest in this question has grown as research in optical wide-area networks draws more and more attention. Hence, in this chapter, the topics of interconnecting WDMA fiber ring LANs and the logical structure and physical implementation of WDMA wide-area networks are addressed.

4.1.1. The hierarchy of photonic Wide-Area Networks

In this thesis, the logical structure of proposed WDMA wide-area networks employs a three-layer hierarchy, with WDMA fiber ring LANs studied previously as their elementary

building blocks. The layers are defined from bottom to top to be **Broadcast-and-Select Layer, Distributed Wavelength Routing Layer**, and **Centralized Switching Layer**, as shown in Table 4.1.

Table 4.1. Functions of Layers in WDMA wide-area Networks

Top Layer	Massive Interconnection of a finite set of Intermediate Layer optical networks with a centralized ultra-high capacity all-optical switch
Intermediate Layer	Pairwise interconnection of a finite set of ring LANs using Bragg Cell cross-connect with distributed wavelength routing scheme
Low Layer	WDMA ring LANs with broadcast-and-select scheme

The low layer of the hierarchy, namely the Broadcast-and-Select Layer, is a set, or a collection of WDMA fiber ring LANs using optical Add-Drop Multiplexers (ADM) proposed previously. Each of them is all-optical in nature. In other words, all the optical ring LANs in the low layer are single-hop networks with broadcast-and-select scheme. Obviously, they can support not only the sessions of point-to-multipoints broadcast, but also those of point-to-point and conferencing. Improved with advanced technology, these WDMA fiber ring LANs are considered as the elementary building blocks in the wide-area global high-speed communications infrastructure.

The technology and architecture for interconnection of these networks is the main theme in the design of the intermediate and top layers. In this thesis, the distributed routing approach is applied to the intermediate layer, and the centralized switching approach is proposed for the top layer.

4.1.2. Wavelength Reuse and Network Scalability in the Intermediate Layer

The intermediate layer is also called the Distributed Wavelength Routing Layer. The techniques here focus on one idea: **wavelength reuse**, which, theoretically, is the principle of using each available wavelength many times throughout the network, either in different times, or in different spatial locations, or over different routing paths, in such a way that the signals at the same wavelength never interfere with each other on the same transmission path, except for the crosstalk from the wavelengths nearby.

In this approach, the total number of wavelengths, W, available from the two low-loss wavelength windows of single-mode optical fiber in the spectrum around 1.3 μm and 1.5 μm is divided into two categories, namely **the intra-LAN wavelength (or local wavelength)** λi, $i = 1,2,..., N$, and **inter-LAN wavelength (or communicating wavelength)** $\lambda' k$, $k = 1, 2, ..., K$. Therefore, $W = N+K$. This total number, W and the number of N and K are functions of the technologies used in the network of this intermediate layer and information bandwidth of the signal to be transported. As shown in Fig. 4.1, each WDMA fiber ring LAN shares local wavelengths λi, $i = 1,2,..., N$, internally, and there is reuse of this subset of wavelengths among different WDMA fiber ring LANs in the same layer logically, but different geographic locations spacially. In this thesis, this is defined as **Level One Wavelength Reuse**. In fact, in each of the WDMA fiber ring LANs with optical ADM, different information signals carried on the same wavelength injected through the same optical ADM on a specific node propagate through the ring loop at different times. The interference of the residual signals on the newly transmitted one is minimized through the optical ADM pre-tuned on this wavelength. This is also a phenomenon of wavelength reuse temporally, defined as **Level Zero Wavelength Reuse**. As a consequence, **Level Two Wavelength Reuse** refers to the reuse of the subset

of inter-LAN wavelengths, or the communicating wavelengths, $\lambda'k$, $k = 1, 2, ..., K$, between different pairs of WDMA fiber ring LANs.

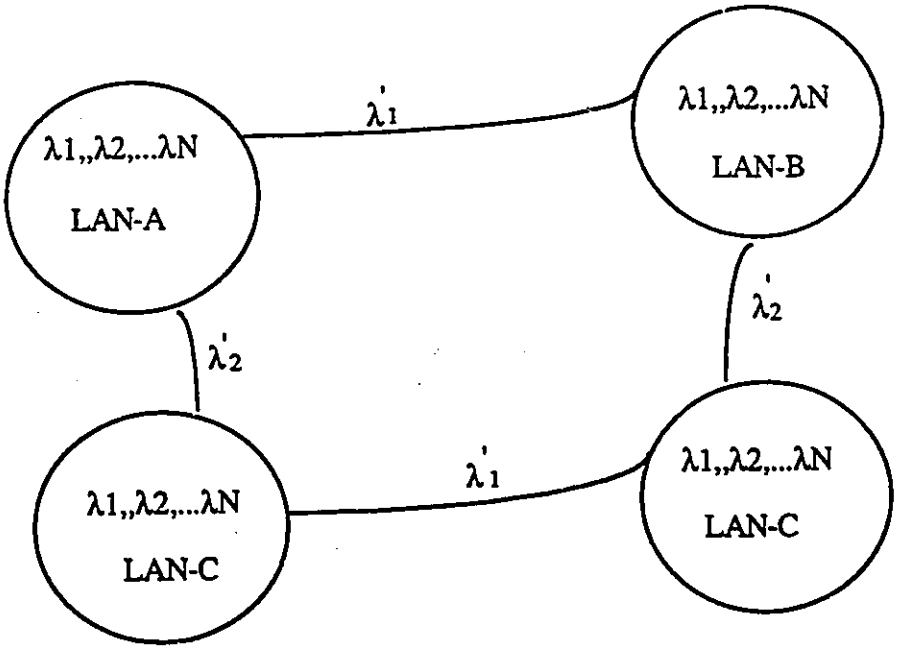

Fig.4.1 Wavelength Reuse in the Intermediate Layer Network

The larger the number K is, the more routing paths the network provides. In this thesis, K is assigned integer values between 2 and 4 in the proposed topologies. The wavelength reuse at this level is achieved by carefully designing the connection patterns of WDMA fiber ring LANs so that the signal on the reused communicating wavelength does not overlap the signals on the same wavelength over different routing paths, and by selecting or implementing suitable photonic or opto-electronic devices so that the pre-defined function of communicating wavelength reuse can be realized. In Section 4.2, several architectures are proposed and corresponding performance is analyzed and compared.

The wavelength reuse techniques create the possibility for the architecture of the intermediate layer network to be scalable in all the dimensions. In this thesis, the "dimension" refers to the number of users and the transmission data rates of each user. In the intermediate layer with distributed wavelength routing, the network is defined to be **scalable** if and only if all of the *Level Zero, Level One* and *Level Two Wavelength Reuse* are achievable. Physically, scalability implies one more access node may always be added to a network in the intermediate layer; therefore, the intermediate layer network user nodes can grow to an arbitrary large population spreading over an arbitrary large service domain. With this definition of scalability, the number of nodes in the intermediate layer network is independent of the total number of wavelengths available, which is limited by the state-of-art technology practically, and is a finite value theoretically. Therefore, the intermediate layer network architecture can achieve an outstanding performance with a finite number of independent wavelengths. In this intermediate layer network, the only obstacle to the network expansion is the signal routing delay in the process of wavelength translation, as discussed later.

When the total number of wavelengths W and the number of communicating wavelengths K are given, the number of available local wavelengths N of each WDMA fiber ring LAN is fixed. These three numbers are technology-dependent. For example, using *Fabry-Perot etalons* as ADMs results in a larger number of local wavelengths compared to that using *polarization independent tunable acousto-optic filters* as ADMs. As a consequence, the total number of wavelengths in the intermediate network, W, will be larger. In other words, each WDMA fiber ring LAN in the low layer has a maximum number of nodes N. When a new node is added to a WDMA fiber ring LAN with $N-1$ users and the LAN reaches its maximum number of nodes, the LAN becomes a **module** in the intermediate layer network and further newly added nodes to this intermediate layer network topology form a new WDMA fiber ring LAN, which eventually evolves into a module.

Besides the feature of network scalability and modularity in the intermediate layer network resulting from wavelength reuse, there exists another mechanism for realizing dynamic wavelength routing, namely wavelength translation. With this feature, the intermediate layer network is in nature considered to be a multi-hop wavelength routing network.

Wavelength translation is defined here to be the process of moving a signal from one wavelength to another wavelength through the optical-to-electronic and electronic-to-optical transformations in the process of wavelength routing. At the device level, a wavelength translation function is performed by receiving and detecting a signal at one wavelength and then switching the detected signal to the proper transmission node containing a laser diode tuned to the desired wavelength through an electronic space-division cross-connect switch, and then retransmitting it on another wavelength. Practically, a detector array, a transmitter array, and a digital cross-connect chip can be integrated into a single module which serves as an intermediate node (called the Exit Node of LAN in this thesis) in the wavelength routing path.

In order to have a clear picture of wavelength routing, two terms need be defined:

Wavelength Path: The term "wavelength path" is defined as the network path taken by an optical signal traversing on a specific communicating wavelength, λk, $k = 1, 2, ..., K$. A wavelength path can contain a passive or active device which neither converts the optical signal to electronic form or vice versa, nor changes its optical frequency. Thus, a wavelength path can have optical amplifiers, optical ADMs, optical taps and optical filters on it, but not electro-optic transducers.

Information Path: The term "Information Path" is defined as the path which an optical signal traverses from a source to a destination in the network. Therefore, an Information Path may be a simple wavelength path, or it may be composed of several wavelength paths interconnected by wavelength converters that perform wavelength translation. Through an Information Path, an inter-LAN optical signal can route from any node as a source to any other node as its destination in multi-hop connections by relaying through the **Exit Nodes**, defined to be the nodes between two different communicating wavelengths.

When the network is expanded to a certain large size, the number of Exit Nodes becomes large. Consequently, the accumulated queueing delay at each Exit Node, together with the electro-optic processing delay in the wavelength converters, becomes a serious issue. With this limitation in network expansion, a third layer needs be defined for wide-area optical networks. This layer is considered as the top layer in the proposed hierarchy, and in this thesis is named Centralized Switching Layer, in which an ultra-high capacity photonic ATM switch is designed as the backbone of the global wide-area optical network to handle the traffic among different intermediate layer optical networks.

4.1.3. Ultra-High Capacity Photonic Switching in the Top Layer

In the design of wide-area photonic network architecture in the intermediate layer, the distributed wavelength routing approach demonstrates its advantage in network scalability with a number of available wavelengths. However, communications between user nodes from distant WDMA fiber ring LANs suffer from a large delay from the multi-hop wavelength translation process. To address this problem, the proposed network architecture in the top layer possesses opposite features. In this layer, a centralized wavelength division all-optical ATM

switch fabric is employed. The input and output ports of this switch fabric are linked with the intermediate layer networks discussed previously.

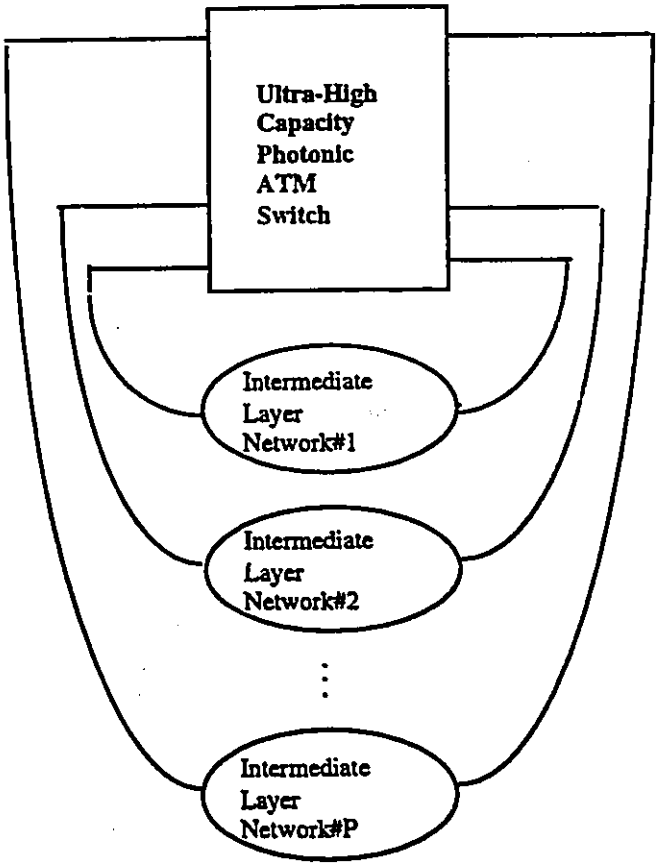

Fig. 4.2 Schematic Diagram of the Top Layer Network Architecture

Each of these intermediate layer networks takes full advantage of the wavelength reuse feature in its architecture; while the worst-case inter-LAN delay of information delivery within it is controlled to an acceptable level by limiting the network size at this layer. The proposed ultra-high capacity photonic ATM switch fabric is all-optical in natural, implying that the transport layer of the switch fabric is transparent, so that there is no optical-to-electronic or electronic-to-optical conversion during the switching process. This makes the delays of communications between the intermediate layer networks much smaller than those within each

intermediate layer network. However, the switching capacity (or the number of input and output nodes) is strongly correlated with the total number of available wavelengths. In other words, the ultra-high capacity photonic ATM switch fabric, which can be considered as the backbone of the optical network in the top layer, is not scalable in wavelength domain.

With the increasing demand on the network transport and process capacity, the future optical wide-area network needs to possess both a high capacity and a high flexibility to support services of various rates and nature. A similar requirement is imposed on the all-optical switch fabric in the top layer as its backbone.

To address the issue of high capacity, the large spectral. temporal, and spatial bandwidth offered by the state-of-the-art transparent photonic systems for switching function in optical domain needs to be fully exploited. By appropriate combination of space-, time-, and wavelength-division techniques, a multi-dimensional photonic switch with a high capacity can be formed. In this thesis, two techniques in optical domain are combined, namely the generation of ultra-short optical pulses through gain-switched distributed feedback laser diodes [28] or mode-locked laser diodes, and multiplexing over wavelength divisioning using tunable lasers with a wide tuning range combined with a narrow linewidth and a good frequency stability [29]. As solutions, the ultra high-capacity photonic ATM switch fabrics based on optical pulse time / frequency and wavelength division multiplexing are proposed.

To meet the demand of the high flexibility, the asynchronous transfer mode (ATM) [30], which is flexible to handle a multiplicity of rates and burstiness of traffic sources, is applied in the design of the photonic switch fabric. Thus, the implementation of the photonic switch fabric as a backbone of optical wide-area network can be realized through the integration of all these technologies.

4.2. Distributed Approach for Internetworking in the Intermediate Layer

In this section, the architecture for the intermediate layer network is studied. The work is divided into four parts. First, the design of the optical bridge for interconnection of WDMA fiber ring LANs is explored from the device level. Then, using this newly-proposed optical bridge as the interface between LANs, the intermediate layer network architecture with the advantage of wavelength reuse is proposed. Based on it, five topologies are proposed for the intermediate layer optical networks. Finally, the performance of these architectures in terms of inter-LAN routing throughput capacity is analyzed and compared.

4.2.1. Optical Bridge for Internetworking of WDMA Ring LANs Using Bragg Cell Cross-Connect

Three types of LAN interface are classified in communications networks, namely, bridge, router and gateway [31]. Only the design of a bridge using lightwave technology for interconnection of WDMA fiber ring LANs is studied in this thesis. In this subsection, starting with the physical mechanism, the design of the optical bridge and its function in WDMA fiber ring network interconnections are explored in detail.

4.2.1.1. Acousto-optic Interaction

The physical mechanism of the device named Bragg cell used in this proposed architecture is acousto-optic interaction [32]. Consider a light deflector cell as shown in Fig. 4.3.

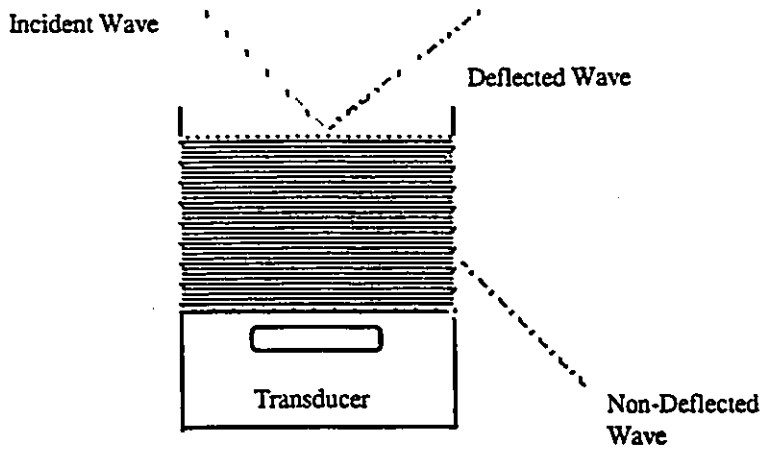

Fig.4.3 Light Deflection Through Acoustooptic Interaction in the Cell

Through the action of the transducer, the electrical signal is converted into the acoustic waves propagating in the acoustic medium. The pressure of the sound wave creates a travelling wave of compression and rarefraction in the medium. This results in a change in the density of the medium, which in turn causes a change in its index of refraction by[32]

$$\Delta n(z,t) = \Delta n \sin(w_s t - k_s z) \qquad (4.1)$$

where w_s and k_s are frequency and propagation vectors of the acoustic wave, whose velocity is

$$V = w_s / k_s. \qquad (4.2)$$

Thus, the cell acts as a thin (phase) grating with a grating line separation equal to the acoustic wavelength Λ, and the acoustic wave can be characterized as a series of partially reflecting mirrors separated by Λ, moving at acoustic wave velocity. Since the velocity of the

acoustic wave is much slower than that of the lightwaves, the medium can be treated as a stationary diffraction grating in the cell. Therefore, a light beam with a specific wavelength λ_0 incident on this acoustic wave with a specific angle is deflected through diffraction.

4.2.1.2. Bragg Diffraction

When the cell is thin, and the intensity of the acoustic wave is low, the change of direction of the ray during transmission through the cell is small. The emerging wave becomes a plane wave with its phase modulated spatially. This is the Raman-Nath diffraction pattern, in which a phase grating splits incident light into various orders with different scattered directions, and the angle θ_m (m=...-2,-1,0.1,2,...0) of the directions of the maxima of the emerging wave is governed by the grating equation[33]

$$\sin\theta_m - \sin\theta_i = m\frac{\lambda_0}{\Lambda}, \qquad \text{Where } m=\text{.....,-2,-1,0,1,2,.....} \quad (4.3)$$

and θ_i is the incident angle.

Thus, on both sides of the extending line from the direction of the incident ray, a number of maxima associated with m=.....,-2,-1,0,1,2,..... appear.

Obviously, this feature is not desired in the design of a photonic device which can act as a bridge in the distributed wavelength routing process of WDMA fiber ring LAN interconnection. The required feature in the design would be that only one order of the deflection beam is generated, so that the light power in this specific wavelength is guided in

only one spatial direction and routed on the predefined Information Path in the wavelength routing.

With a sufficiently wide transducer, the thickness of the cell and the intensity of the acoustic wave are increased. As a consequence, the cell becomes a stack of reflecting layers spaced by the acoustic wavelength Λ. When the difference in the optical paths between the adjacent layers equals an integral multiple of the light wavelength λ_0, the light rays reflected from each layer will be in phase and the reflected light intensity will display only one peak. This peak is the Bragg diffraction wave, which is in the direction where the diffraction angle is equal to the incident angle. This diffraction pattern is called Bragg diffraction, and a cell with this property is defined as a Bragg cell.

When the acoustic wavelength and the incident angle of the light beam containing a comb of wavelengths are given, only the power of one specific wavelength will satisfy the physical condition described above and be deflected. The power of the other wavelengths in the incident beam will pass through the Bragg cell without a change in the directions. The relation between this specific optical wavelength and other parameters, i.e., acoustic wavelength and incident angle, is derived by taking advantage of the dual particle-wave nature of light and of sound [33].

A light beam with a propagation vector k and (radian) frequency ω can be considered to consist of a stream of particles (photons) with momentum $\hbar k$ and energy $\hbar\omega$. The acoustic wave can likewise be considered to be made up of particles (phonons) with a momentum $\hbar k_s$ and energy $\hbar w_s$, where $\hbar = h/2\pi$, and $h = 6.63 \times 10^{-34}$ (J-S) denotes Planck's constant. The diffraction of light by an approaching sound beam becomes a series of collisions, each of which involves an annihilation of one incident photon at w_i, and one

phonon and a creation of a diffracted photon at w_d. The new photon propagates along the direction of scattered beam. The conservation of momentum requires that the momentum $\hbar(k_s + k_i)$ of the colliding particles be equal to the momentum $\hbar k_d$ of the scattered photon, so

$$k_d = k_s + k_i \qquad (4.4)$$

The conservation of energy principle gives the form

$$w_d = w_i + w_s \qquad (4.5)$$

If a new (diffracted) photon and a new phonon are generated while the incident photon is annihilated, the conservation of energy principle yields

$$w_d = w_i - w_s \qquad (4.6.)$$

Since the sound frequencies are below 10 GHz and the frequencies of the optical beam are above 10 THz, then

$$w_d \approx w_i \qquad (4.7)$$

So, $k_d \approx k_i$ (4.8)

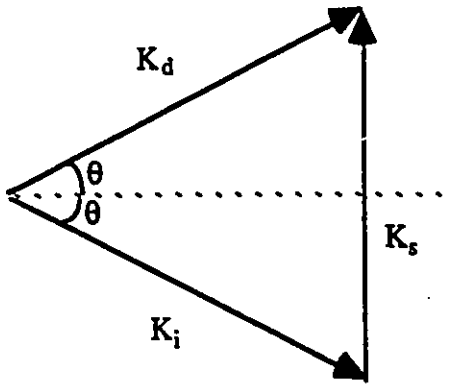

Fig.4.4 Momentum Conservation Relation of Propagation Vectors

As shown in Fig.4.4, take the magnitude of the two optical wave vectors as k. The magnitude of the sound vector is thus

$$k_s = 2k\sin\theta \qquad (4.9)$$

Using $k = 2\pi/\lambda_0, k_s = 2\pi/\Lambda$, the equation becomes,

$$\sin\theta = \frac{\lambda_0 / n}{2\Lambda} \qquad (4.10)$$

Therefore, if the cell thickness is large enough that the Bragg condition holds, that is,

$$L >> \frac{\Lambda^2}{\lambda_0} \qquad (4.11),$$

then the cell becomes a Bragg cell , and the power in wavelength λ_0 of the light beam incident at the angle θ, such as the above equation holds, will be deflected, and the power of the other wavelengths incident at this angle will pass through the cell directly.

4.2.1.3. Four-Port Bragg Cell with Micrograting

Micrograting refers to the grating in Bragg cell such that the grating period Λ becomes comparable with the optical wavelength λ_0.

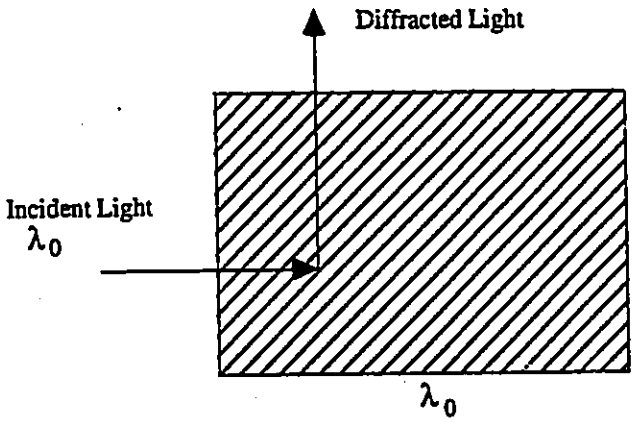

Fig 4.5 Bragg Cell with Micrograting Used in the Proposed Architecture

Consider the Bragg cell shown in Fig.4.5, in which $\Lambda = \frac{\lambda_0}{\sqrt{2}}$. Therefore, the light with wavelength λ_0 incident at 45^0 will be deflected by an angle 90^0. By changing the grating period slightly, the central wavelength of Bragg cell can be shifted in order to keep the Bragg condition satisfied. In terms of wavelength selectivity, a bandwidth of about 0.5 A^0 around the tuned wavelength can be achieved, and a wavelength separation of 10 A^0 can be obtained with very little crosstalk. Thus, by properly choosing the grating period Λ, only wavelength λ_0 from the coming input wave will be deflected by an angle 90^0, and all others, $\lambda_i \neq \lambda_0$ will remain on their original direction.

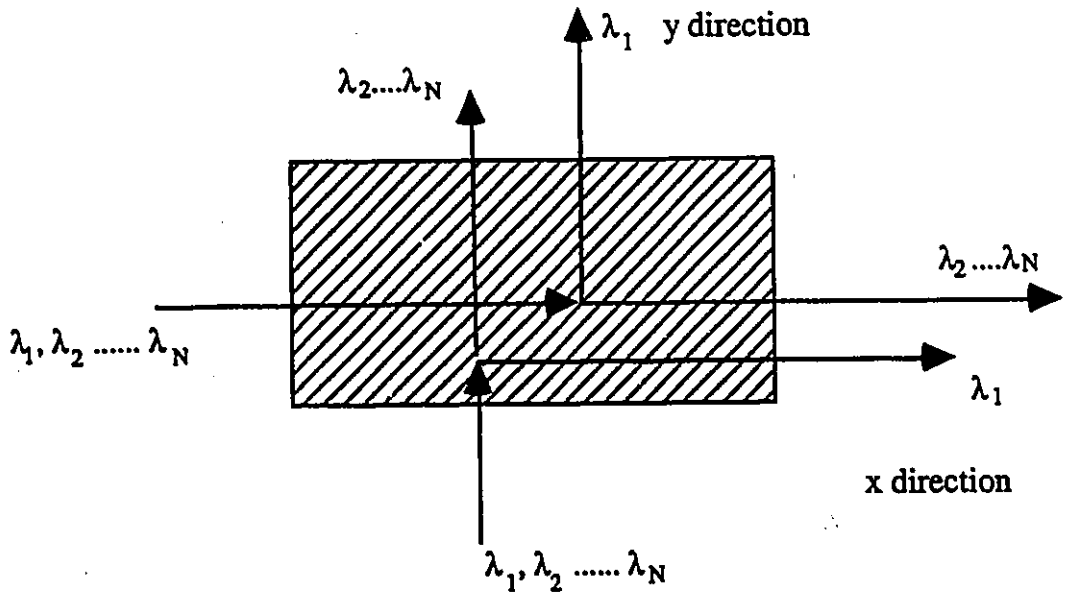

Fig. 4.6 (a) Four-Port Bragg Cell

Fig.4.6 (a) shows the four-port Bragg cell, which will become a basic building block for optical bridge in photonic network interconnection. Suppose an input in the *y* (or *x*) direction with *N* wavelengths $\lambda_1, \lambda_2, \ldots \lambda_N$ arrives at the single Bragg cell tuned to λ_1. Only λ_1 will be deflected by 90^0 and gets out in the *x* (or *y*) direction. All other wavelengths $\lambda_i \neq \lambda_1$ will propagate out in the original *y* (or *x*) direction.

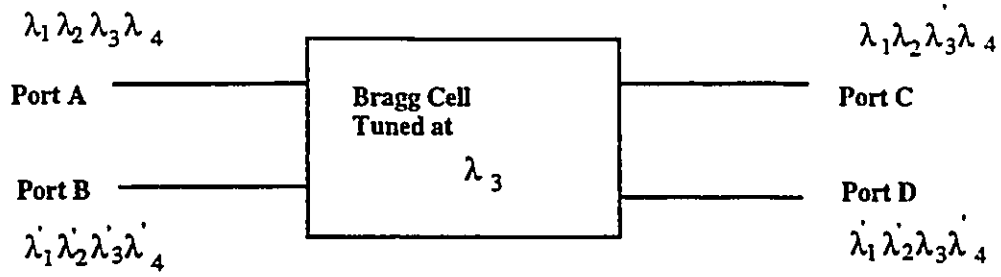

Fig 4.6 (b) Black Box Model of Four-Port Bragg Cell ($\lambda_i = \lambda_i', i = 1,..4$)

Fig 4.6 (b) shows the "blackbox" system model of it, in which deflection is represented by "port change" of the selected wavelength. The four ports are denoted as Port A, Port B, Port C and Port D.

4.2.1.4. An Optical Bridge Using Bragg Cells in Network Interconnection

Consider two WDMA fiber ring local-area networks using optical ADM, namely, LAN-A and LAN-B as shown in Fig.4.7 below. They are interconnected through an optical bridge consisting of four Bragg cells, namely, BC-A1, BC-A2, BC-B1, BC-B2. Each of them is a four-port Bragg cell with micrograting, as described in the previous subsection. BC-A1 and BC-A2 are linked in series in the ring loop of LAN-A using the same connection pattern as the optical ADMs in it. The same holds for BC-B1 and BC-B2 in LAN-B. Two ports of BC-A1 and two ports of BC-B1 are cross-connected with each other, respectively. With this architecture of interconnection, suitable for wavelength reuse, one communicating wavelength is sufficient for inter-LAN communications either from LAN-A to LAN-B, or from LAN-B to LAN-A, provided that the intra-LAN signal propagation along the loop is clockwise in one LAN and counter-clockwise in the other. Therefore, all the four Bragg cells are tuned to this

wavelength. Without loss of generality, define the information transmission along LAN-A to be counter-clockwise, and that of LAN-B to be clockwise.

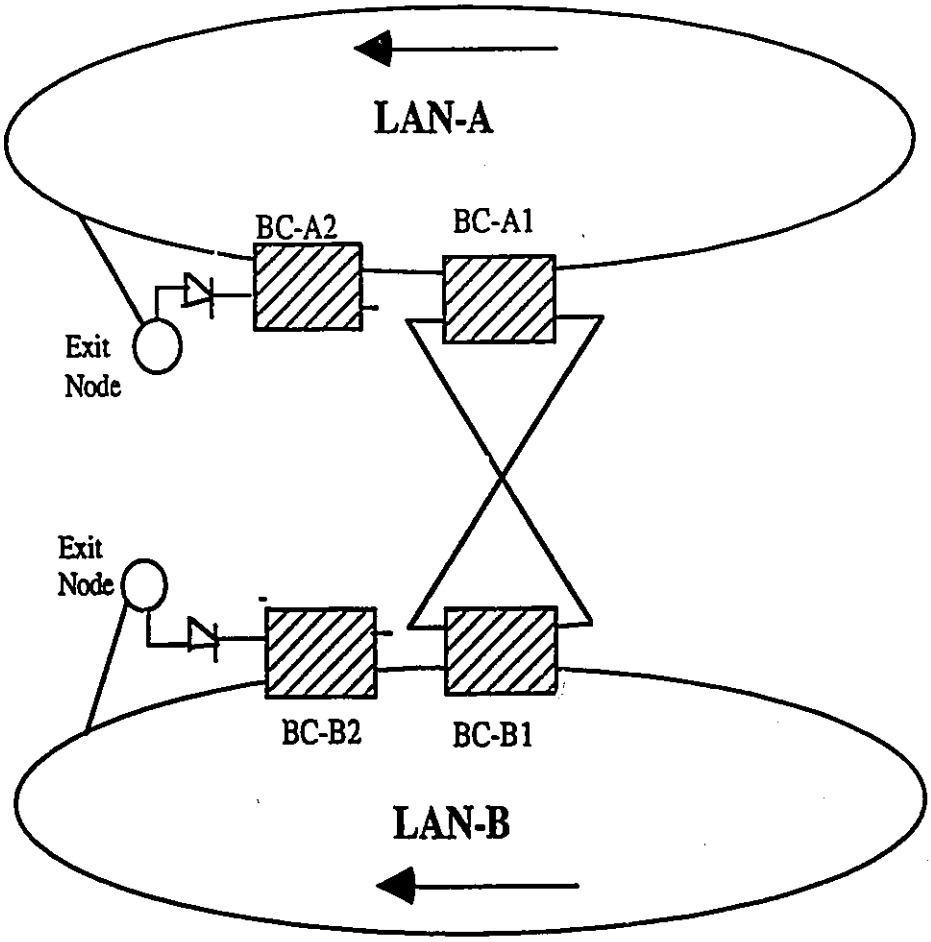

Fig.4.7. An Optical Bridge Using Bragg Cell Cross-Connect

The operation principle is as follows: Within each LAN, user nodes can send information to any other node on local wavelengths, $\lambda_1, \ldots \lambda_N$, defined previously, which are associated with the optical ADMs. When a node needs to send information to one or more nodes which are not located in the same LAN, say, for example, a node in LAN-A needs to send data to the nodes in LAN-B, as a first step, it broadcasts the information along the ring.

The information is tapped, and goes through WDM-de-multiplexer towards receivers at the Exit Node in addition to the N user nodes on the ring. BC-B2 is also located in this Exit Node shown in Fig.4.7. With ATM technology, the destination addresses are contained in the cell header. Through the electronic space-division switch as shown in Fig.4.8 below, the cells to be transmitted to LAN-B will be queued on the laser tuned on the communicating wavelength λ'. A laser diode is linked with Port B of the four-port Bragg cell BC-A2 of tuned wavelength λ', designed with certain grating period. According to the property described previously, this wavelength will be deflected, and exits the Bragg cell at Port C. It will then enter the BC-A1 at its Port A and be deflected at its Port D. Through the cross-connection, it will enter Bragg cell BC-B1 at Port A and be deflected at Port D. Then it will circulate around the ring in LAN-B clockwise, and deliver the signals to each node in one complete round. The remaining power will be filtered out through the deflection at Bragg cell BC-B2 at its Port D. This is done to prevent its circulating around the ring infinitely and interfering with later inter-LAN transmissions on the same communicating wavelength.

Similarly, for a user in LAN-B to transmit information to users in LAN-A, the ATM cells are converted from one local wavelength to a communicating wavelength through the wavelength translation at the Exit Node inside LAN-B. The communicating wavelength carrying the information will be deflected at Bragg cells BC-B2, BC-B1, go through the cross-connection, and be deflected at BC-A1. It will propagate clockwise inside LAN-A, delivering information to each node. After one complete round, the wavelength will be filtered out at BC-A2. Through these paths, wavelength reuse is achieved between mutual pairwise LANs inter-communications.

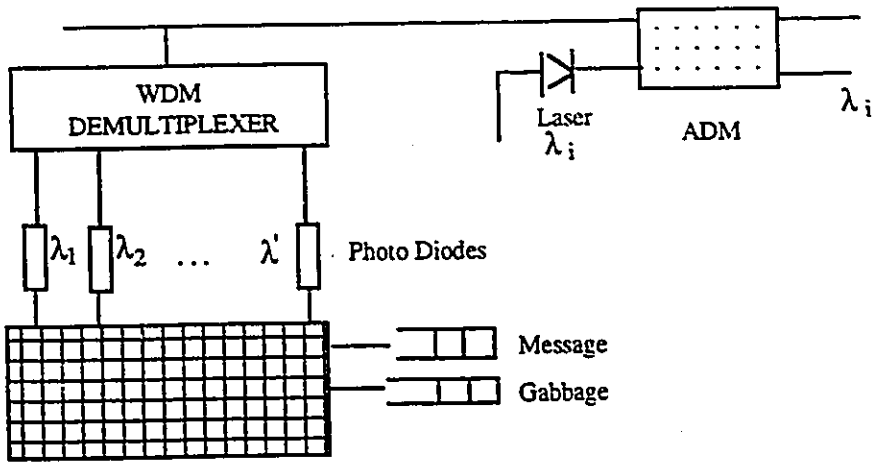

Local Node

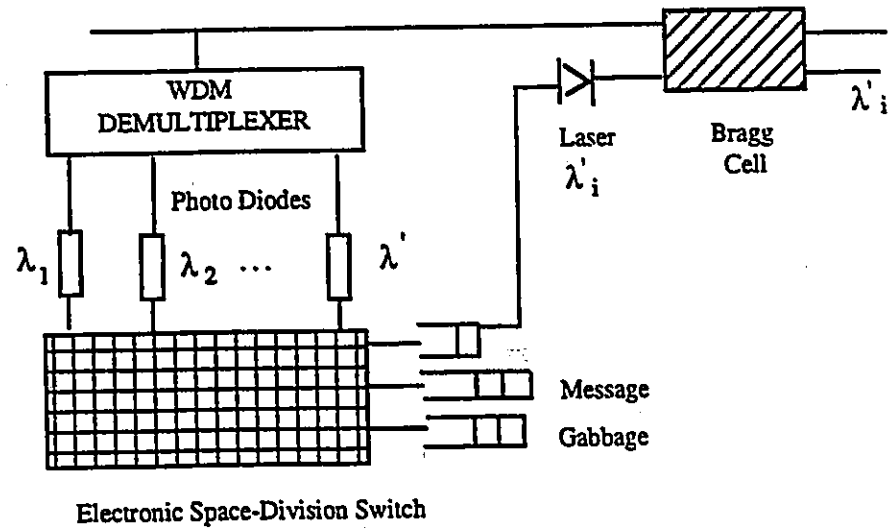

Exit Node

Fig. 4.8 Structures of Local Node and Exit Node in the WDMA Ring Network

4.2.2. Architecture for Wavelength Reuse through Bragg Cell Optical Bridge

Obviously, by using the Bragg cell optical bridge, intra-LAN wavelength ($\lambda_1, \ldots \lambda_N$) reuse is achieved inside each of the pairs of ring LANs, and one communicating wavelength is sufficient to achieve bi-directional inter-LAN communications. With a proper structure, inter-LAN wavelength $\lambda'_j, j=1,\ldots,k$, can also be reused among different pairs of LANs. Consider the structure shown in Fig. 4.9, in which each circle denotes a WDMA fiber ring LAN.

The LANs in this architecture are distributed according to the following criteria:

(1) Each LAN with its local information transmission direction in the loop clockwise is interconnected with those with their local information transmission direction counter-clockwise. Meanwhile, each LAN with its local information transmission direction counter-clockwise is likewise interconnected with those with their local information transmission direction clockwise.

(2) Each LAN needs to be connected with the same number of LANs. It is equal to the number of communicating wavelengths needed in the intermediate layer network, and also equal to the number of Exit Nodes on each LAN.

As shown in Fig. 4.9 below, by proper arrangement, the set of communicating wavelengths is reused properly for interconnection. With certain topology at the intermediate network layer, inter-LAN information transmission is achieved through routing of the communicating wavelengths. The information is first sent in the local wavelength, then goes through a finite number of wavelength translations. The routing Information Path is pre-

defined in the header of ATM cells, so that wavelength translations are only realized on the Exit Nodes of the pre-defined routing path.

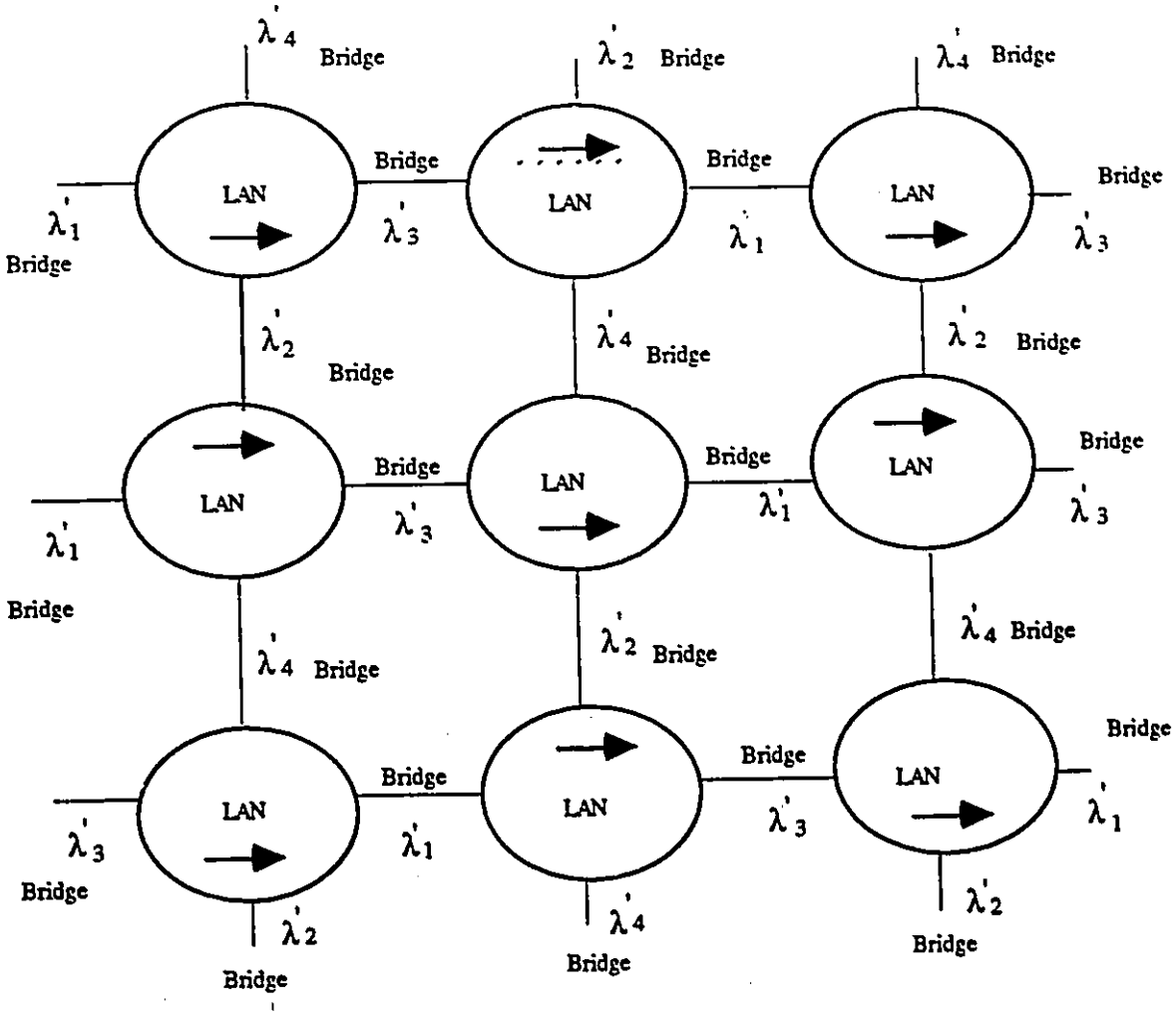

Fig.4.9 Architecture for the Intermediate Layer Network

4.2.3. Topologies for Distributed Approach in WDMA Ring LANs Interconnection

In this thesis, five types of topology interconnection of WDMA fiber ring LANs are proposed as shown in Fig.10 below, in which each circle represents a WDMA ring LAN. Among them, Type I is a spherical structure observed in a two-dimensional plane. It appears to be like a Manhattan Street network but, fundamentally, they are completely different. A Manhattan Street network is a logic structure with a uni-directional transmission, while Type I is a physical topology with each pair of LANs mutually communicating through the optical bridges. Each "link" represents a bi-directional cross-connection of Bragg cells. Four communicating wavelengths are required for this topology structure. In Type II, WDMA ring LANs are interconnected to form a loop, in which each "link" also represents a bi-directional cross-connection of Bragg cells. In this structure, two communicating wavelengths are required. Type III, Type IV and Type V have a similar structure. They are enhanced versions of Type II, in which three or four communicating wavelengths are required. Therefore, Type III, Type IV and Type V have a higher routing throughput than Type II. The following section will focus on the inter-LAN routing throughput analysis for the topologies of Type I, Type II and Type III, representing typical approaches in the proposed topology design. As a conclusion, their performances are compared after evaluation.

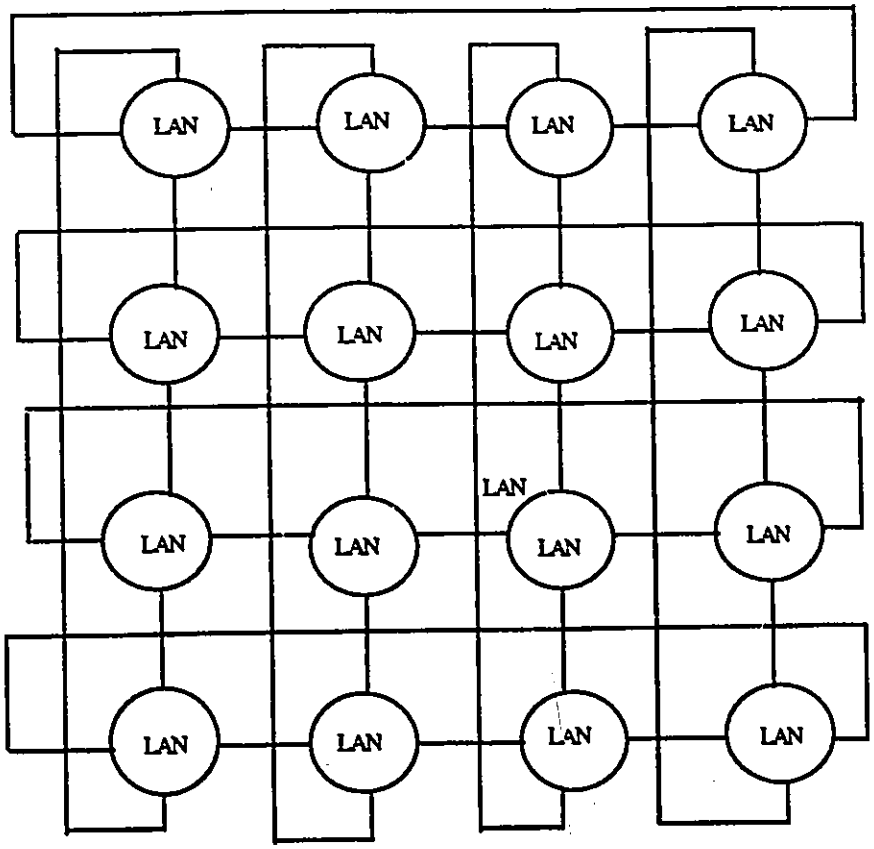

Fig.4.10 (a) Type I Topology

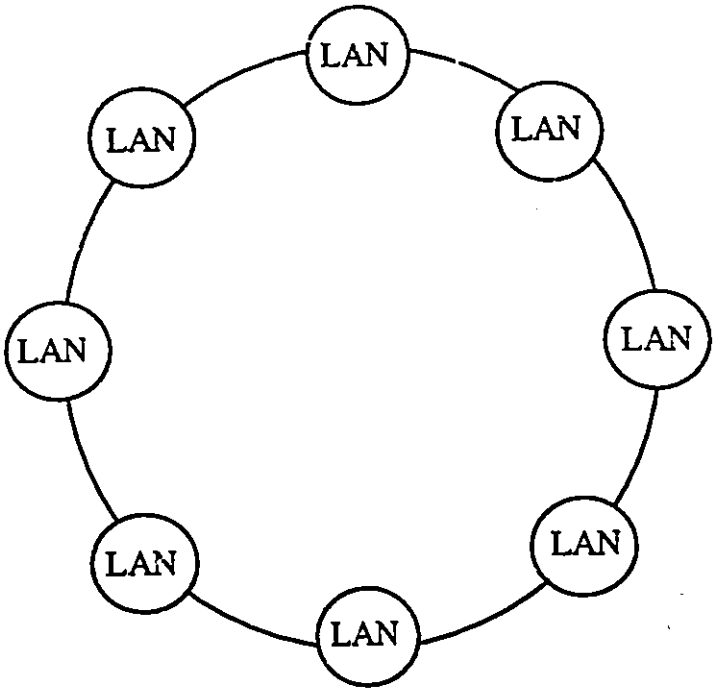

Fig. 4.10 (b) Type II Topology

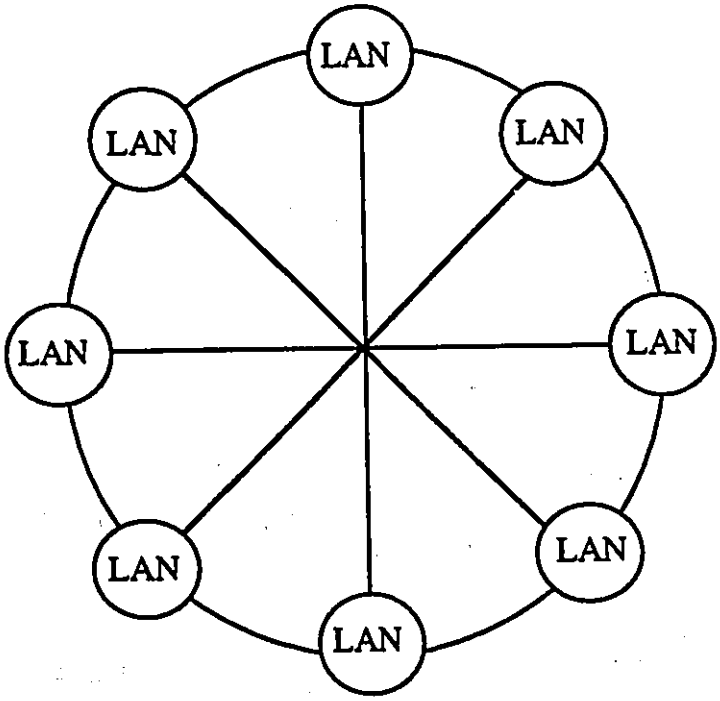

Fig. 4.10 (c) Type III Topology

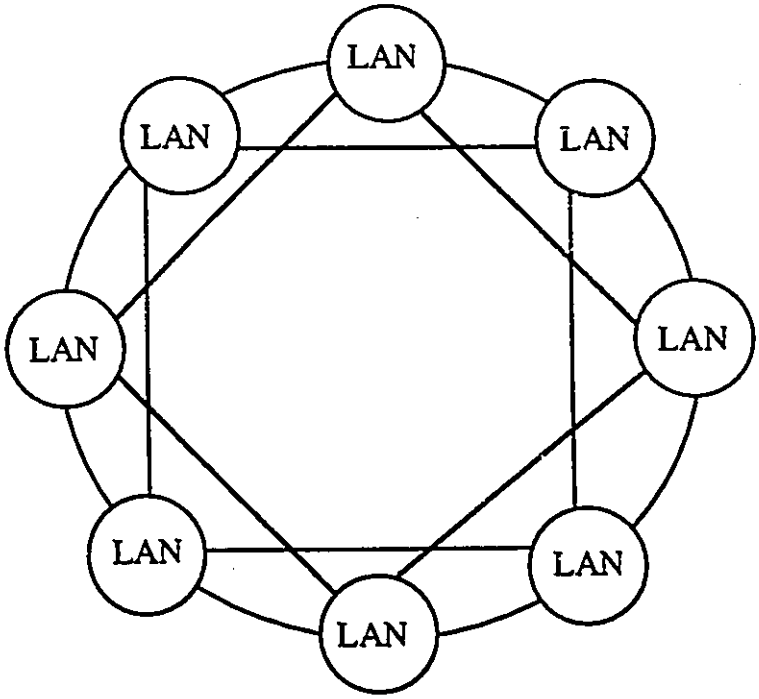

Fig 4.10 (d) Type IV Topology

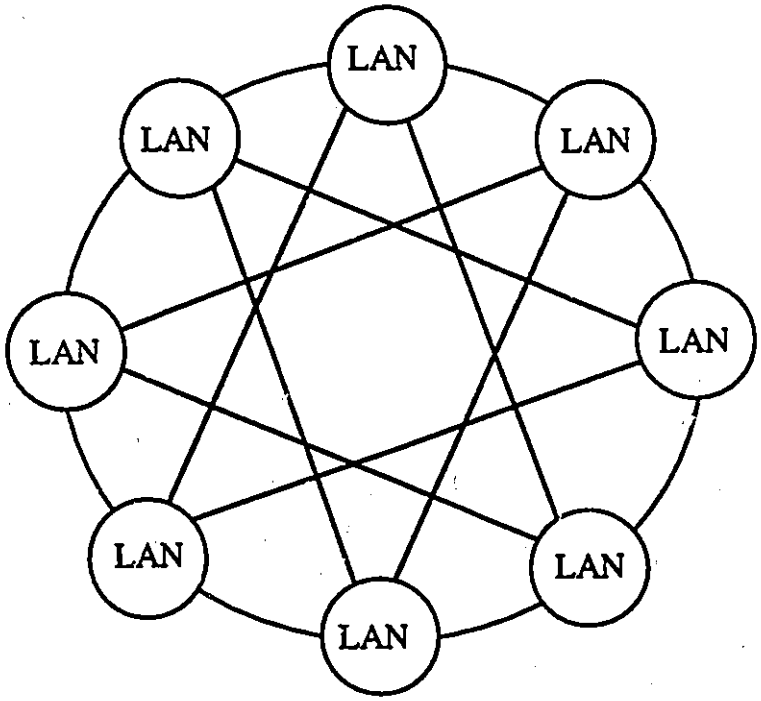

Fig 4.10 (e) Type V Topology

4.2.4. Throughput Analysis and Comparison

In this section, the performance of the three typical architecture topologies proposed above for the intermediate layer network are analyzed. At the intermediate layer, the main function of network is inter-LAN wavelength routing. Therefore, the figure of merit of the network performance will be the routing throughput between LANs. It is evaluated by the following criterion:

Assume the generated inter-LAN traffic is uniform throughout the networks in the intermediate layer. Define F as the statistical average of the number of wavelength translations required for a message from an arbitrary node to reach its destination in the other LAN.
By definition, F can be expressed as,

$$F = \sum_{i=1}^{w} i \times \{\text{number of destination nodes that need i wavelength translations}\} / \{\text{number of destination nodes}\}$$

where w is the maximum number of possible wavelength translations one node can have. The "node" in the above expression refers to the WDMA fiber ring LAN as an elementary unit in the intermediate layer network.
Thus, the throughput is defined to be

$$T = (N \times L) / F \qquad (4.12)$$

where N is the total number of LANs in the intermediate layer network and L is the number of communicating wavelengths available in this intermediate layer network.

4.2.4.1. Throughput Analysis of Type I Topology

In this closed spherical structure of LAN interconnection, each LAN has the same "surrounding" as any other LAN. In other words, no one LAN has a better position in the intermediate layer than the others in terms of receiving or transmitting information from or towards any other nodes located in the other LANs. Therefore, with the assumption of uniform traffic, the throughputs in terms of the transmission from one LAN to any other LANs are the same for each LAN, that is, L / F, where L=4 in this case. For the convenience of derivation, the number of nodes in the Type I interconnection can be written as $N = p^2$; then the number of destination nodes is $p^2 - 1$, where p is an integer, it can be even or odd.

case 1, when p is odd, then $w = 2 \times (p-1)/2$

number of destinations in *1* wavelength translation: *4*

number of destinations in *2* wavelength translation: *8*

.
.
.

number of destinations in *(p-1)/2* wavelength translation: *(p-1)/2 x4*

number of destinations in *(p+1)/2* wavelength translation: *(p-1)/2 x4*

number of destinations in *(p+3)/2* wavelength translation: *(p-3)/2 x4*

.
.
.

number of destinations in *2 x (p-1)/2* wavelength translation: *1 x4*

Then F can be expressed as follows:

$$F = \frac{1}{p^2-1}[\,1x4 + 2x(2x4) + 3x(3x4) + \ldots + \frac{p-1}{2}x(\frac{p-1}{2}x4)$$

$$+\frac{p+1}{2}x(\frac{p-1}{2}x4) + \frac{p+3}{2}x(\frac{p-3}{2}x4) + \ldots + (2x\frac{p-1}{2})x1x4\,]$$

(4.13)

By grouping terms, the following expression can be obtained,

$$F = \frac{4}{p^2-1}\{\sum_{h=1}^{\frac{p-1}{2}} h^2 + \sum_{h=1}^{\frac{p-1}{2}}[\frac{p+(2h-1)}{2}]^2 - \sum_{h=1}^{\frac{p-1}{2}}(2h-1)\frac{p+(2h-1)}{2}\}$$

$$= \frac{4}{p^2-1}\{\sum_{h=1}^{\frac{p-1}{2}} h^2 + \frac{1}{4}\sum_{h=1}^{\frac{p-1}{2}}[\,p^2 + 2p(2h-1) + (2h-1)^2\,]$$

$$-\frac{1}{2}\sum_{h=1}^{\frac{p-1}{2}} p(2h-1) - \frac{1}{2}\sum_{h=1}^{\frac{p-1}{2}}(2h-1)^2\}$$

$$= \frac{4}{p^2-1}\{\sum_{h=1}^{\frac{p-1}{2}} h^2 + \frac{p^2}{4}\frac{p-1}{2} + \frac{p}{2}\sum_{h=1}^{\frac{p-1}{2}}(2h-1) + \frac{1}{4}\sum_{h=1}^{\frac{p-1}{2}}(2h-1)^2$$

$$-\frac{p}{2}\sum_{h=1}^{\frac{p-1}{2}}(2h-1) - \frac{1}{2}\sum_{h=1}^{\frac{p-1}{2}}(2h-1)^2\}$$

$$= \frac{4}{p^2-1}\{\sum_{h=1}^{\frac{p-1}{2}} h^2 + \frac{p^2}{4}\frac{p-1}{2} - \frac{1}{4}(\sum_{h=1}^{\frac{p-1}{2}} 4h^2 - \sum_{h=1}^{\frac{p-1}{2}} 4h + \sum_{h=1}^{\frac{p-1}{2}} 1)\}$$

$$= \frac{4}{p^2-1}\{\sum_{h=1}^{\frac{p-1}{2}} h^2 + \frac{p^2(p-1)}{8} - \sum_{h=1}^{\frac{p-1}{2}} h^2 + \sum_{h=1}^{\frac{p-1}{2}} h - \frac{1}{4}\frac{p-1}{2}\}$$

$$= \frac{4}{p^2-1}\{\frac{p^2(p-1)}{8} + \frac{\frac{p-1}{2}(1+\frac{p-1}{2})}{2} - \frac{p-1}{8}\} \quad (4.14)$$

$$= \frac{1}{2(p^2-1)}(p^3-p) = \frac{p}{2}$$

case 2, when p is even, then $w = p$

number of destinations in *1* wavelength translation: *4*

number of destinations in *2* wavelength translation: *8*

.
.
.

number of destinations in *(p-2)/2* wavelength translation: *(p-2)/2 x4*

number of destinations in *p/2* wavelength translation: *p/2 x4-2*

number of destinations in *(p+2)/2* wavelength translation: *(p-2)/2 x4*

.
.
.

number of destinations in *p-1* wavelength translation: *4*

number of destinations in *p* wavelength translation: *1*

Then *F* can be expressed as follows:

$$F = \frac{1}{p^2-1}\{1x4 + 2x8 + \ldots + \frac{p-2}{2}x(\frac{p-2}{2}x4) + \frac{p}{2}x(\frac{p-2}{2}x4+2)$$

$$+\frac{p+2}{2}x(\frac{p-2}{2}x4) + \ldots + (p-1)x4 + px1\}$$

$$= \frac{1}{p^2-1}\{4x\sum_{h=1}^{\frac{p-2}{2}} h^2 + p^2 + 4\sum_{h=1}^{\frac{p-2}{2}} \frac{p^2-4h^2}{4}\}$$

$$= \frac{1}{p^2-1}\{4\sum_{h=1}^{\frac{p-2}{2}} h^2 + p^2 + \sum_{h=1}^{\frac{p-2}{2}} p^2 - 4\sum_{h=1}^{\frac{p-2}{2}} h^2\}$$

$$= \frac{1}{p^2-1}\{p^2 + p^2\frac{p-2}{2}\} \qquad (4.15)$$

$$= \frac{p^3}{2(p^2-1)}$$

So, for the Type I topology, the parameter F is:

$$F = \frac{1}{2}\cdot\frac{p^3}{2(p^2-1)} + \frac{1}{2}\frac{p}{2} = \frac{1}{4}(\frac{2p^3-p}{p^2-1}) = \frac{1}{4}(\frac{2N^{\frac{3}{2}}-N^{\frac{1}{2}}}{N-1}) \quad (4.16)$$

where N is the number of nodes representing LANs in the intermediate layer network.

Therefore, the routing throughput for Type I topology is

$$T = \frac{4N}{F} = \frac{16N(N-1)}{2N^{\frac{3}{2}}-N^{\frac{1}{2}}} = \frac{16\sqrt{N}(N-1)}{2N-1} \qquad (4.17)$$

4.2.4.2. Throughput Analysis of Type II Topology

In this loop structure of LAN interconnection, each LAN has the same "environment" as any other LAN. In the other words, no one LAN has a better position in the intermediate layer than the others in terms of receiving or transmitting information from or towards any other nodes located in the other LANs. Therefore, with the assumption of uniform traffic, the throughputs in terms of the transmission from one LAN to any other LAN are the same for each LAN, that is, L / F, where L =2 in this case. The number of LANs in this topology can be either even or odd.

case 1, when N is odd, then $w = (N-1)/2$

number of destinations in *1* wavelength translation: *2*

number of destinations in *2* wavelength translation: *2*

.
.
.

number of destinations in *(N-1)/2* wavelength translation: *2*

Then F can be expressed as follows:

$$F = \frac{1}{N-1}(1x2 + 2x2 + \ldots + \frac{N-1}{2}x2)$$

$$= \frac{2}{n-1}\frac{\frac{N-1}{2}(1+\frac{N-1}{2})}{2} = \frac{N+1}{4} \qquad (4.18)$$

case 2, when N is even, then $w = N/2$

number of destinations in *1* wavelength translation: *2*

number of destinations in *2* wavelength translation: *2*

.
.
.

number of destinations in $N/2 - 1$ wavelength translation: *2*

number of destinations in $N/2$ wavelength translation: *1*

Then F can be expressed as follows:

$$F = \frac{1}{N-1}[1x2 + 2x2 + \ldots + (\frac{N}{2} - 1)x2 + \frac{N}{2}]$$

$$= \frac{1}{N-1}[2\frac{(\frac{N}{2} - 1)\frac{N}{2}}{2} + \frac{N}{2}] = \frac{N^2}{4(N-1)} \qquad (4.19)$$

So for Type II topology, the parameter F is

$$F = \frac{1}{2}\frac{N+1}{4} + \frac{1}{2}\frac{N^2}{4(N-1)} = \frac{2N^2 - 1}{8(N-1)} \qquad (4.20)$$

where N is the number of nodes representing LANs in the intermediate layer network.

Therefore, the routing throughput for Type II topology is

$$T = \frac{2N}{F} = \frac{16N(N-1)}{2N^2 - 1} \qquad (4.21)$$

4.2.4.3. Throughput Analysis of Type III Topology

In this enhanced version of loop structure of LAN interconnection, each LAN has the same "environment" as any other LAN. In other words, no one LAN has a better position in the intermediate layer than the others in terms of receiving or transmitting information from or towards any other nodes located in other LANs. Therefore, with the assumption of uniform traffic, the throughputs in terms of the transmission from one LAN to any other LANs are the same for each LAN, that is, L / F, where L =3 in this case. The number of LANs in this topology must be even.

case 1, when N is a multiple of 4, then $w = 1+(N-4)/4$

number of destinations in *1* wavelength translation: *3*

number of destinations in *2* wavelength translation: *4*

.
.
.

number of destinations in $1+(N-4)/4$ wavelength translation: *4*

Then F can be expressed as follows:

$$F = \frac{1}{N-1}[1x3 + 2x4 + \ldots + (1 + \frac{N-4}{4})x4] \qquad (4.22)$$
$$= \frac{1}{N-1}\frac{N^2 + 4N - 8}{8}$$

case 2, when N is not a multiple of 4, then $w = 2+(N-6)/4$

number of destinations in *1* wavelength translation: *3*

number of destinations in *2* wavelength translation: *4*

.

.

.

number of destinations in *1+(N-6)/4* wavelength translation: *4*

number of destinations in *2+(N-6)/4* wavelength translation: *2*

Then *F* can be expressed as follows:

$$F = \frac{1}{N-1}[1x3 + 2x4 + \ldots + (1 + \frac{N-6}{4})x4 + (2 + \frac{N-6}{4})x2] \quad (4.23)$$
$$= \frac{1}{N-1}\frac{N^2+4N}{8}$$

So for Type III topology, the parameter *F* is

$$F = \frac{1}{2}\frac{1}{N-1}(\frac{N^2+4N-8}{8} + \frac{N^2+4N}{8}) \quad (4.24)$$
$$= \frac{N^2+4N-4}{8(N-1)}$$

where *N* is the number of nodes representing LANs in the intermediate layer network. Therefore, the routing throughput for Type III topology is

$$T = \frac{3N}{F} = \frac{24N(N-1)}{N^2+4N-4} \quad (4.25)$$

4.2.4.4. Comparison of Throughput Performance in Three Topologies

The throughput per node is defined as the total throughput in the network divided by the total number of nodes (or LANs) in the network. Table 4.2 below shows the computation results of the throughputs per node of Topology I, Topology II, and Topology III versus the total number of nodes (LANs) in the network. Since the total number of nodes in Topology I has to be the square of an integer, for the convenience of comparison the total number of nodes in Topology II and Topology III also have to take this form. From the results, we notice that the throughputs per node decrease as the total number of nodes in the network increases. This is because the more nodes in the intermediate layer network, the larger the span of the network is, and therefore the more destinations that need a large number of wavelength translations.

Topology I has the largest throughput per node of the three. Topology III the second largest. Meanwhile, Topology I has four communicating wavelengths, Topology III three, and Topology II two. This implies the larger the total number of communicating wavelengths available in the intermediate layer network, the larger the throughput is. Also, notice that larger throughput is associated with larger routing delay. The trade-off between them needs to be considered. On the other hand, the larger the total number of communicating wavelengths employed, the smaller the total number of local wavelengths is, and therefore the smaller the capacity that each LAN (module) possesses.

In Table 4.3 below, the total network throughputs in Topologies I, II and III are presented versus the total number of nodes in the network. These results can be used as an important parameter in the design of optical networks in the intermediate layer. In the design process, these two factors need to be taken into account: how many nodes (WDMA fiber ring LANs), in other words, the value of N, are needed in the photonic network at this layer; and

how large a capacity each LAN module should possess. In other words, what values of the total number of local wavelengths and the total number of communicating wavelengths should be assigned when the total number of wavelengths available, w, is constrained by the available photonic technology. Then, we find out from Table 4.3. whether the throughput (and the related queueing delay) is desirable.

As observed, Topology I has a significant change of throughput with the total number of nodes available in the network. On the other hand, the throughputs in Topologies II and III are quite stable as the total number of nodes increases.

Table 4.2. Throughputs Per Node in Topologies I, II, &III Versus the Total Number of Nodes

Total Number of Nodes [N]	Throughput per Node Topology I	Throughput per Node Topology II	Throughput per Node Topology III
16	1.9355	0.46967	1.1392
25	1.5673	0.30745	0.79889
36	1.3146	0.30745	0.58496
49	1.1311	0.15997	0.44427
64	0.99213	0.97553	0.34775
81	0.88337	0.79204	0.27903
100	0.79598	0.079204	0.22855
121	0.72425	0.065571	0.19046
144	0.66434	0.055171	0.16107
169	0.61356	0.047058	0.13793
196	0.56997	0.040609	0.11940
225	0.53215	0.035398	0.10435
256	0.49902	0.031128	0.091953
289	0.46977	0.027586	0.081632
324	0.44376	0.024615	0.072948
361	0.42047	0.022099	0.065573
400	0.39950	0.019950	0.059259
441	0.38052	0.018099	0.053811
484	0.36326	0.016495	0.049080
529	0.34750	0.015094	0.044944
576	0.33304	0.013865	0.041308
625	0.31974	0.011817	0.038095
676	0.30746	0.010959	0.035242
729	0.29609	0.010959	0.032697
784	0.28553	0.010191	0.030418
841	0.27570	0.009501	0.028369
900	0.26652	0.008879	0.026519

Table 4.3. Network Throughput in Topologies I, II, &III
Versus The Total Number of Nodes

Total Number of Nodes (N)	Throughput in Topology I	Throughput in Topology II	Throughput in Topology III
16	30.968	7.5147	18.228
25	39.184	7.6861	19.972
36	47.324	7.7808	21.058
49	55.423	7.8384	21.769
64	63.496	7.8760	22.256
81	71.553	7.9018	22.601
100	79.598	7.9204	22.855
121	87.635	7.9342	23.046
144	95.665	7.9446	23.194
169	103.69	7.9528	23.310
196	111.71	7.9593	23.402
225	119.73	7.9645	23.478
256	127.75	7.9688	23.540
289	135.76	7.9724	23.592
324	143.78	7.9753	23.635
361	151.79	7.9779	23.672
400	159.80	7.9800	23.704
441	167.81	7.9819	23.731
484	175.82	7.9835	23.754
529	183.83	7.9849	23.775
576	191.83	7.9861	23.793
625	199.84	7.9872	23.809
676	207.85	7.9882	23.824
729	215.85	7.9890	23.836
784	223.86	7.9898	23.848
841	231.86	7.9905	23.858
900	239.87	7.9911	23.867

4.3. Centralized Approach for Internetworking in the Top Layer

4.3.1. Overview of Photonic Switching

Because of the limits of the speed of electronic circuits, as well as the high power consumption and heat generation in high-speed electronic circuits, electronic ATM switching systems cannot achieve the desired future throughput level. The approach of photonic ATM switch should be considered in order to take full advantage of high optical bandwidth. Furthermore, the development of photonic ATM switching is essential to match the transmission bandwidth that fiber-optic links can provide.

At present, photonic ATM switching systems have been studied in order to exploit the broad spectral, temporal and spatial bandwidth of an optical medium [34]-[38]. One proposal has been made for large ATM switches based on memory switching and a passive optical star coupler [36]. This presents an example in which the system will achieve a switching capacity of 2.5 Tb/s. In [36], the authors have combined the strength of electronic switching with that of dynamic multiwavelength optical interconnection. Another ultra fast photonic ATM switch with optical output buffers is presented in [37]. Feasibility studies show that an 80 x 80 switch with a 1 Gb/s input/output can be constructed using the present technology. This ATM switch is based on a time-division broadcast and select network. In [39], the application of photonic space-division switching for fiber-optic subscriber network in B-ISDN is proposed. In [40], a photonic packet switching fabric, namely, HYPASS, is proposed. It combines space-division multiplexing (which can reconfigure itself rapidly to allow the sharing of space channel in time) with wavelength-division multiplexing. The space divisioning is controlled by another wavelength-division control network.

In general, the photonic ATM switch architectures proposed in [36]-[40] utilize separate electronic controllers for switching elements. With an increase in the number of input and output ports, the electronic control circuitry becomes quite complicated because of the rapidly growing number of high-speed electronic circuits. Investigations have been carried out to explore photonic ATM switches that use all-optical control inseparable from the switching element structure. In [41], a photonic ATM switch is proposed, which consists of the optical buffer memory and the optical header-driven self-routing circuit using the vertical-to-surface transmission electro-photonic devices (VSTEPs). This all-optical transport and control ATM switch is expected to reach a total throughput of Tb/s.

In this section, two photonic ATM switching architectures, namely (1) photonic ATM switching based on optical pulse time-division and wavelength-division multiplexing with separate electronic controllers, and (2) photonic ATM switching based on optical pulse frequency-division and wavelength-division multiplexing with integrated optic logical control, are proposed as the options for backbone in the top layer optical wide-area network. The idea of time divisioning comes from [37], and that of frequency divisioning is from [42]. The idea of wavelength divisioning comes from [43]. The combination of these ideas is explained for the design of ultra high-capacity photonic ATM switches in the following subsections.

4.3.2. Architecture I: Photonic ATM Switch Based on Optical Pulse TDM and WDM

4.3.2.1. Switching Architecture

The ATM switch fabric is an $N (= n \times k)$ inputs (k groups with n inputs per group as shown in Figure 4.11 below), $N (= n \times k)$ outputs based on an optical pulse time-division and wavelength-division "multiplexing and de-multiplexing" network with electronic control. All the cells of each group are time-multiplexed as ultrafast optical cells. They are compressed (in time) and they share the transparent devices with many other users. Each cell addresses a certain output according to the following high and low addresses:

1. A "high" address (Virtual Path Identifier [VPI] in the cell header) specifies the order of the output group that the input cell will be going to (at the output, we have k groups with n outputs in each group). This address tunes the tunable source to λ_i. The selected wavelength will be one of the available wavelengths $\lambda_1,..., \lambda_k$. With current technology, λ_i is in the order of nm [43]. The wavelength allocation is shown in Figure 4.12 below. On each λ_i we have an available bandwidth around $0.3nm$ (≈ 40 GHz).

2. A "low" address (Virtual Channel Identifier [VCI] in the cell header) specifies the address of the input cell within the pre-specified group of outputs. This address will be specified by λ_{add_i}.

We talk about input/output groups. On the input side, we have k groups, each with n cells, where each cell depends on one input. Each cell consists of a series of binary optical pulses with wavelengths chosen from λ_1 to λ_k, depending on the receiver group address. On the output side, the wavelengths $\lambda_1 ... \lambda_k$ are ordered by wavelength de-multiplexer in order to

route the signal to its appropriate group on the output side; on each wavelength (output group) there will be n cells in each frame which will be de-multiplexed in time in order to finalize the switching operation by the cell selector (CS), cell buffer (CB) and cell decoder (CD).

The last three blocks perform the address selection function. When the optical signal arrives through wavelength de-multiplexer at its appropriate output group, the cell selector's filter will separate the data from the low address and will convert it to an electrical signal in order to route the cell to the correct output via the cell buffer. The cell buffer controls the throughput of the selected data cells in order to have an output cell in one frame duration T. Therefore, between two successive cells, there is T second separation, and the cell decoder converts the optical cells to the electrical cells with duration T, at a rate V.

Cell time multiplexing is done by the coder and by k (n x 1) coupler as shown in Figure 4.11 for time multiplexing. Electrical cells with a duration T arrive at the inputs from various transmission links at a rate V [37]. Since in time multiplexing the signal synchronization is very important, when input cells arrive on different lines, they must be synchronized by the system clock again and will be formed within $[0,T]$ time frame in order to enter the cell coder. Simultaneously, according to the high addresses (VPI) on the cells, ultra-short optical pulses are generated, having a selected wavelength $\lambda_1...\lambda_i,...\lambda_k$ (based on wavelength allocation shown in Figure 4.12) and with a very narrow width $\Delta\tau$ at a repetition rate of V. As can be seen in Figure 4.11, the electrical cells from the input are first stored in a register and their data fields in the payload and address fields in the cell header are read separately. Then, an external modulator modulates the optical pulses on wavelength λ_i, on the basis of the cell data fields, and sends them to the compressor. Using the optical pulses, the cell coder converts the electrical data cells to ultra-fast optical data cells with a duration T/n, as shown in Figure 4.13.

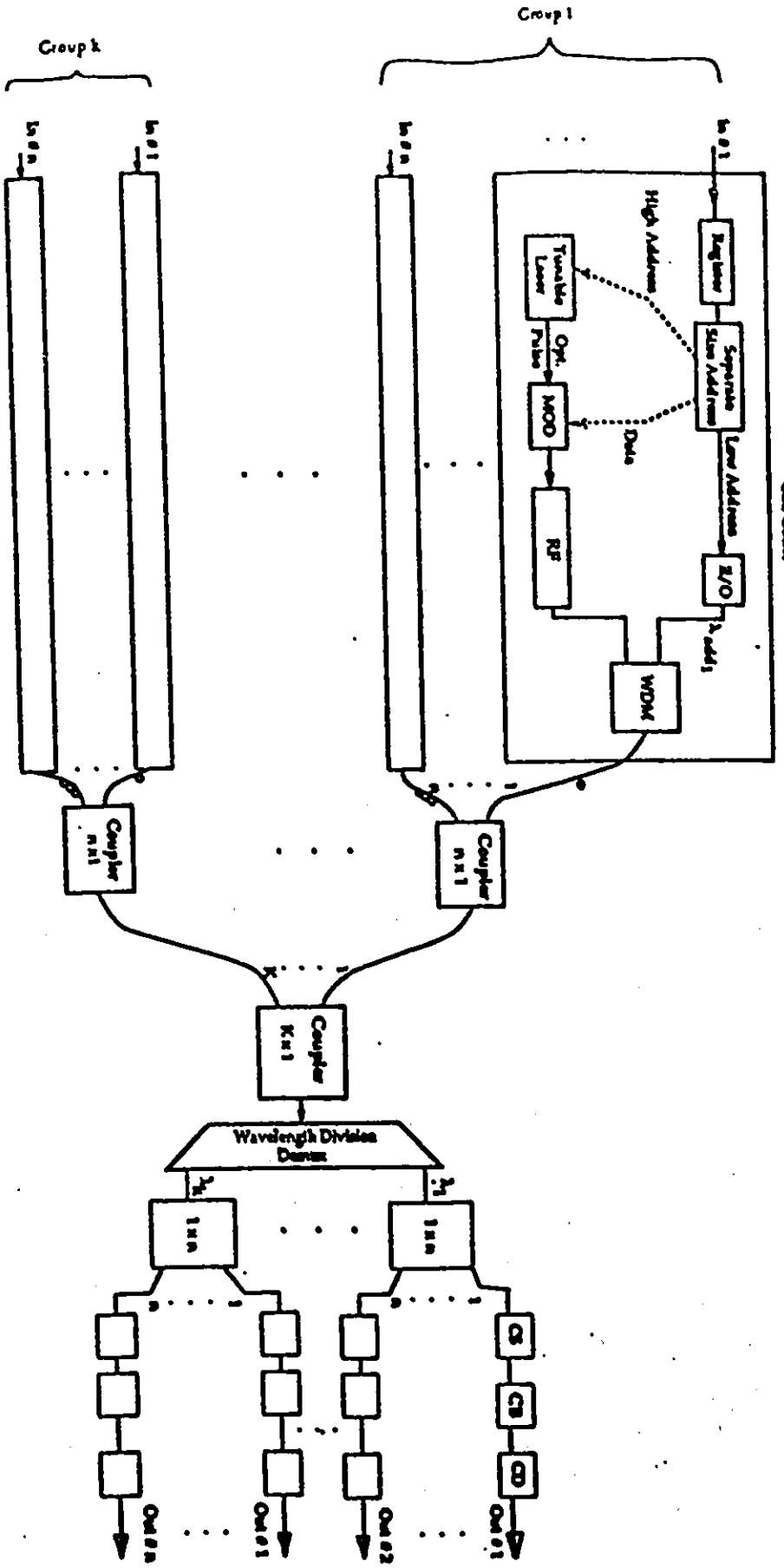

Fig.4.11. Block Diagram of the Proposed Photonic ATM Switch#1

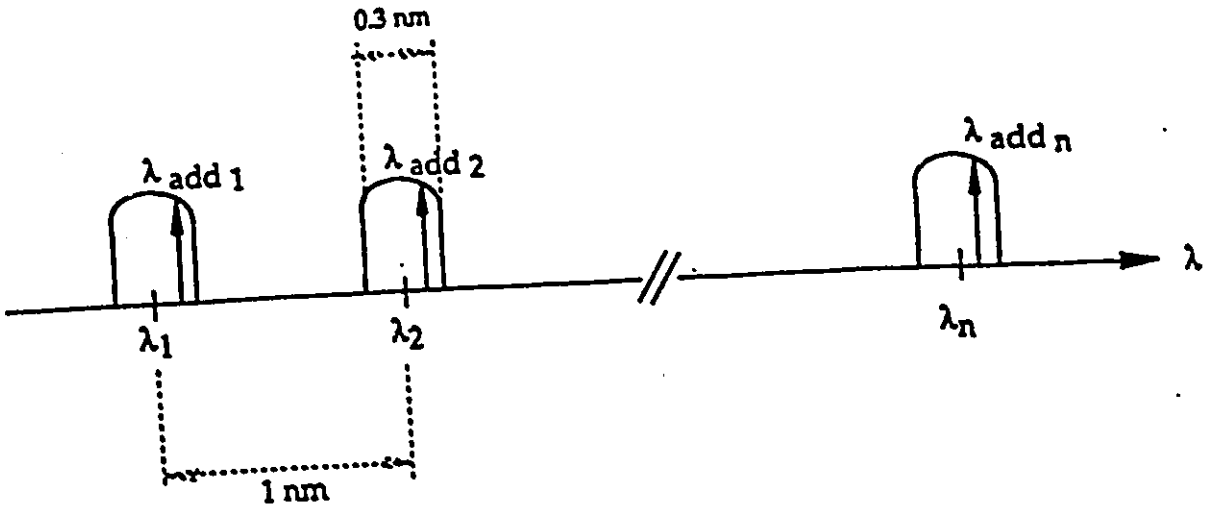

Fig. 4.12. Wavelength allocation using n wavelengths, each with ~ 0.3 nm bandwidth. On each λ_i we choose one λ_{add_i} as low address cells.

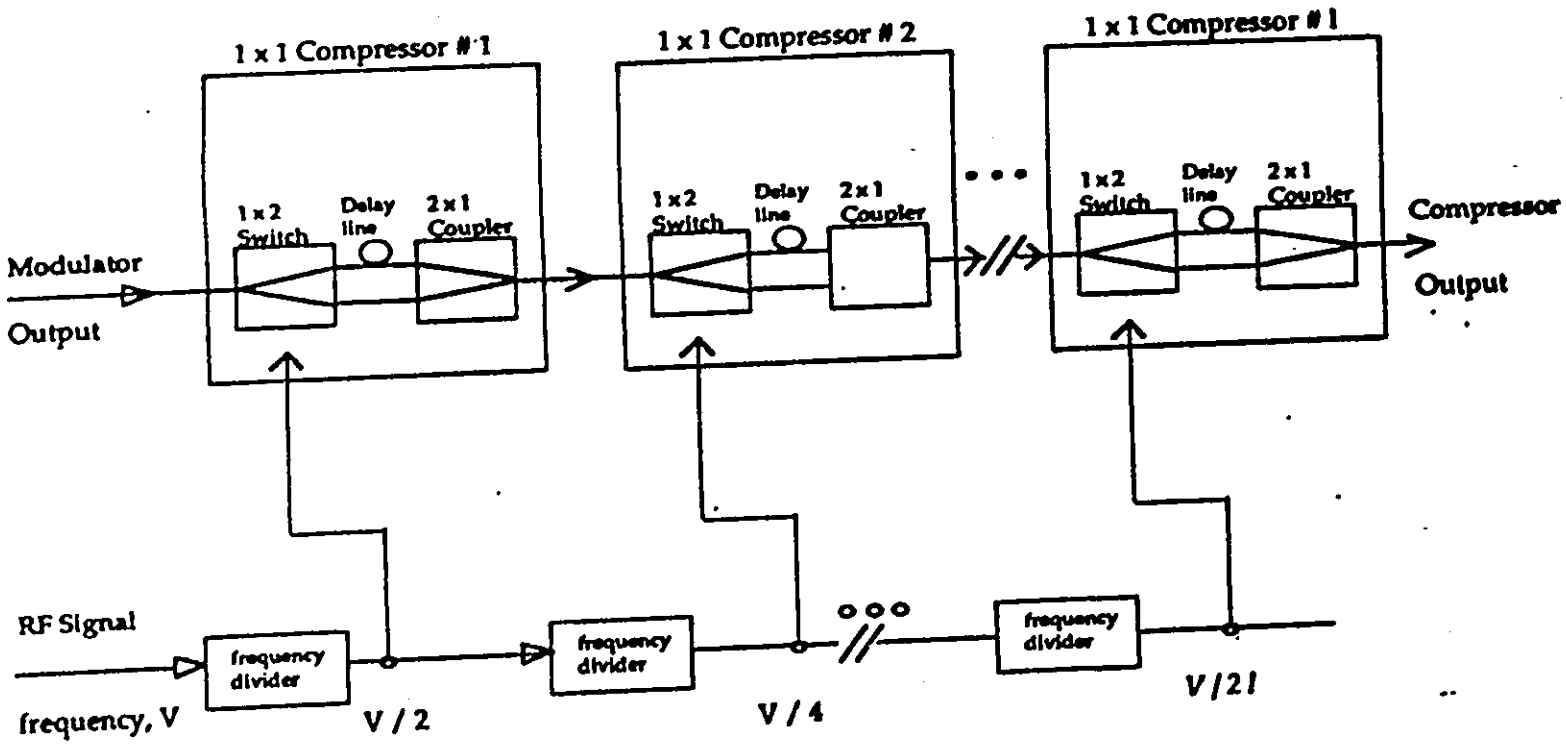

Fig.4.13. Configuration of the Compressor

Figure 4.13 shows the detailed structure of the compressor. Each sub-compressor consists of one 1 x 2 switch, two delay lines, and one 2 x 1 coupler. In 1 x 1 compressor #1, the 1 x 2 switch transmits pulses to high and low port alternately, with RF frequency V divided by 2, i.e., $V/2$. Other switches do the same job with different frequencies as shown. Therefore, by having $\ell(1 \times 1)$ compressors, we will put $L=2^{\ell}$ pulses besides one another. Of course, the output of the RF signal dividers is used for all compressors of each input cell, and for each input group, as well.

The compressor output and the address signal are wavelength multiplexed on each cell coder. An $n \times 1$ coupler combined with appropriately selected delay lines time-multiplexes each cell into a time slot. Finally, the outputs of all input groups are coupled together by a $k \times 1$ combiner, and the coupler distributes the cells over the optical highway (with signal multiplexed in time and wavelength domain). λ_{add_i} is a wavelength within the bandwidth of group wavelength λ_i, as shown in Figure 4.12. The bandwidth around each λ_i can be about 0.3 *nm* in order to carry ≡ 40 Gb/S around 1.3 μm [43].

Time division and wavelength division multiplexed signal arrives at the wavelength de-multiplexer (WD). The block diagram of the wavelength de-multiplexer is shown in Figure 4.14 below. In this figure there are k Bragg elements, and each is tuned to one of the k wavelengths $\lambda_1 \ldots \lambda_k$, as illustrated in Figure 4.12. Therefore, if wavelengths $\lambda_1, \lambda_2 \ldots \lambda_k$ arrive together, λ_1 will be deflected by 90^0 by the 1-th element, since it is tuned to λ_1, and $\lambda_2, \ldots \lambda_k$ will go through straight. Similar actions take place in the other elements, i.e., in the i-th element only λ_i will be deflected, and so on.

Each deflected wavelength, say λ_i, will go to the $1 \times n$ coupler and go through cell selector (CS), cell buffer (CB) and cell decoder (CD). Based on wavelength allocation shown

in Figure 4.12, each group wavelength of λ_i has the low address wavelength λ_{add_i} within the bandwidth of the *i*-th group wavelength.

Therefore, on the input side, there are *k* groups such that in each group there are *n* input modules. For each group, the compressor and the coupler provide time-multiplexing of *n* signals together. The wavelength multiplexing is done by a tunable laser on each cell coder depending on the output group address to which the signal has to be routed. This function is repeated for all the *k* groups and all the cell coders for each group; the time-multiplexed signals of all *k* groups (each group with *n* input modules) will then be coupled together to go through the *n* x *1* coupler with an appropriate delay element. The output cells of *k* (*n* x *1*) couplers are combined to bring the signal to the optical highway.

On the receive side, the received signal is first wavelength de-multiplexed, as shown in Figure 4.14. Then an appropriate group wavelength is sent to its *1*x *n* coupler, which guides the optical signal to *n* outputs on each group. The functions of cell selector (CS), cell buffer (CB) and cell decoder (CD) are explained in [37]. We will discuss their functions briefly, and modify them for wavelength de-multiplexing as well.

When a cell arrives at the output via the *1* x *n* coupler, its address is separated and is translated to an electric one. Then it is analyzed by the decoder to find out whether or not the low address matches a specific output. High address is specified by wavelength de-multiplexer as mentioned earlier and as shown in Figure 4.15. Therefore, the cell leaving the buffer during *T* is the only one cell.

The cell decoder function is shown in Figure 4.16 [37]. Optical information at a bit rate *n* x *V* will be converted to electrical cells at a rate *V*. In CD, first the narrow optical pulses are

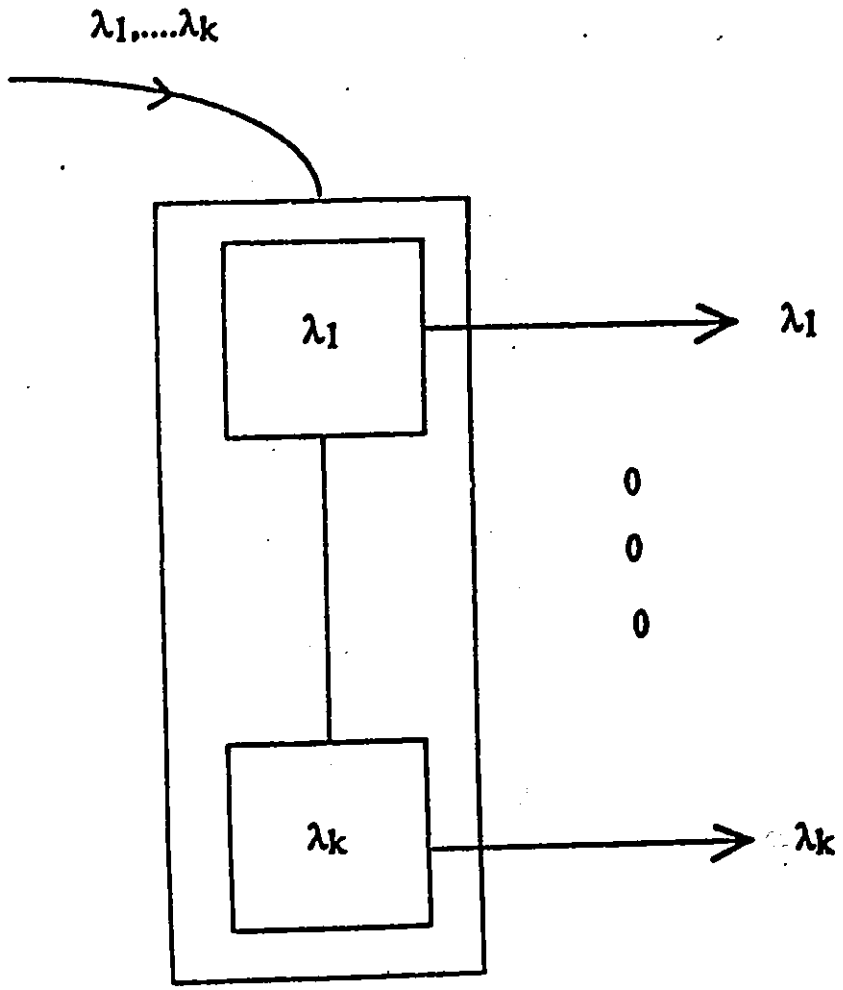

Fig. 4.14. Wavelength Demultiplexer

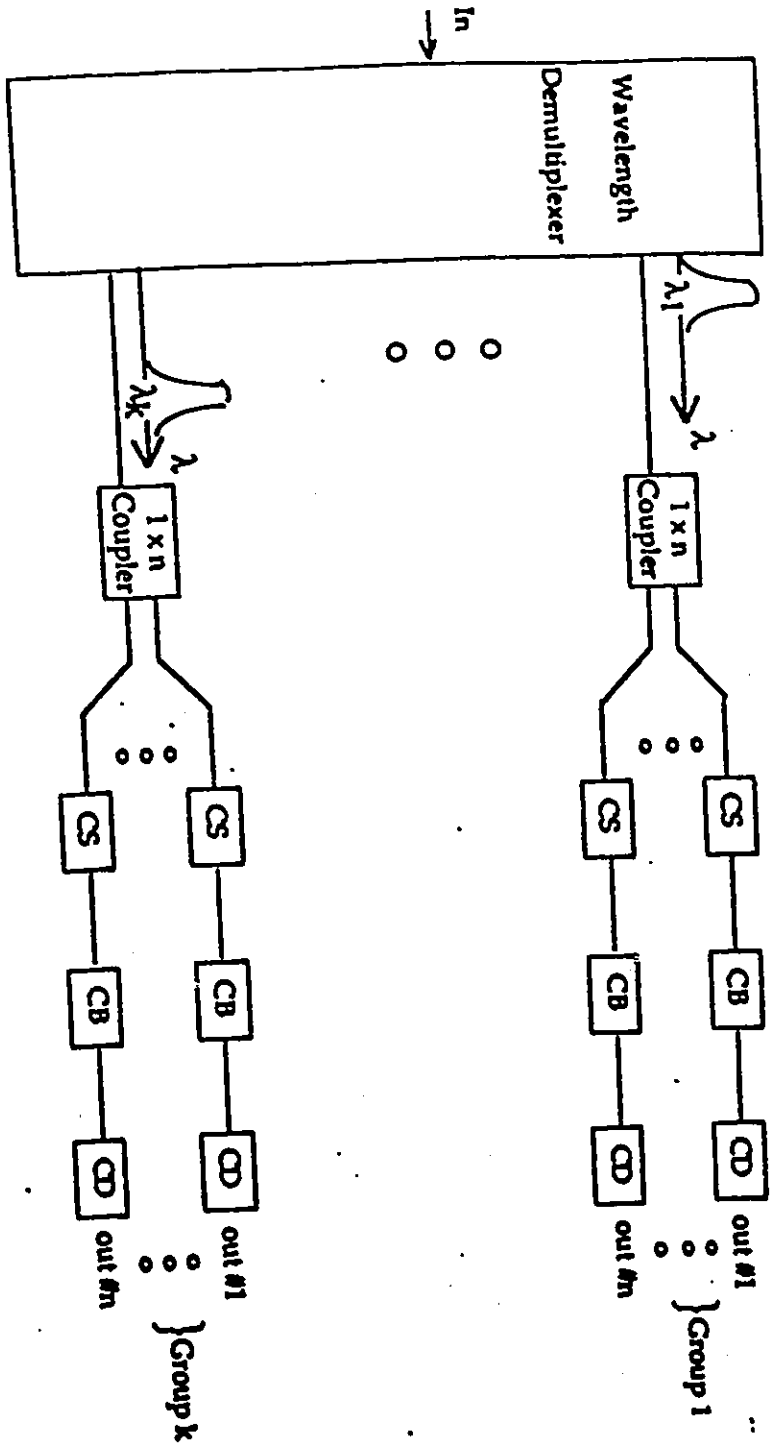

Fig. 4.15. Configuration of the Wavelength Demultiplexer on the Output Side

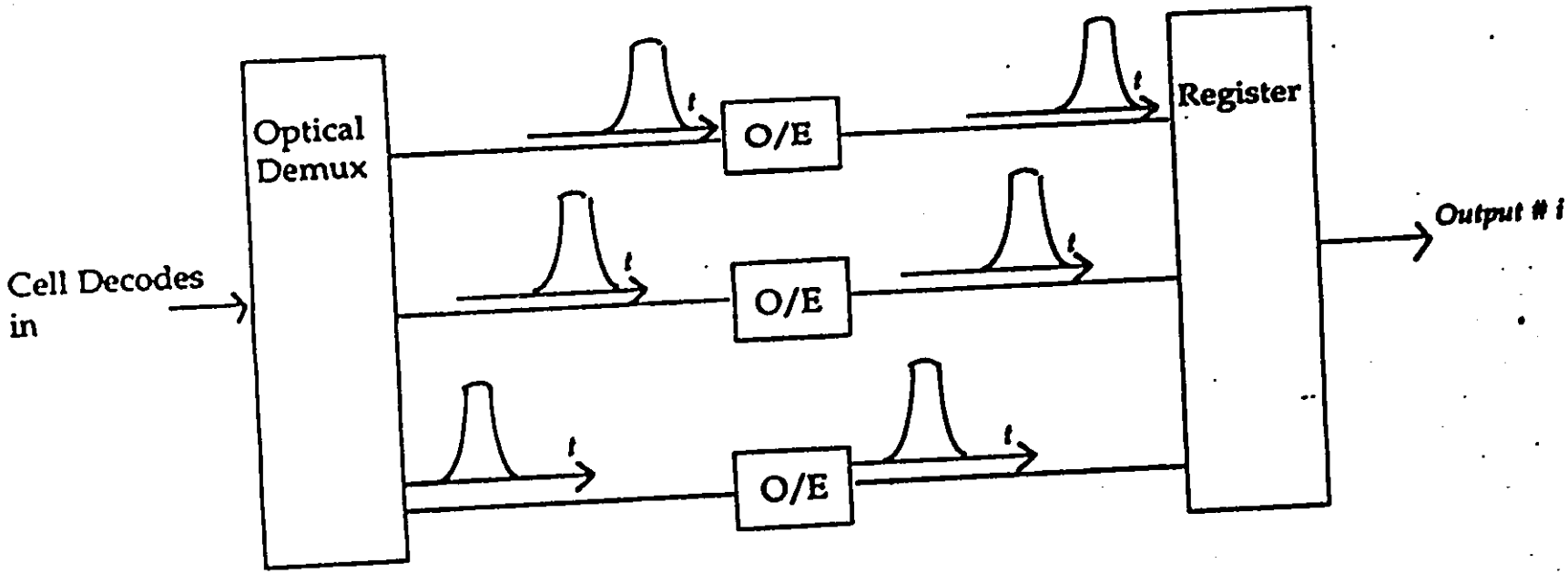

Fig. 4.16. Configuration of the Time Demultiplexing on the Output Side

produced by the de-multiplexer and converted to electrical pulses in parallel form; then these signals are stored in a register at every T seconds.

4.3.2.2. Switching Capacity with SONET Signal Rates

The advantage of this proposed ATM switch fabric is that it employs both time and wavelength division multiplexing, in order to obtain a higher capacity. For example, 40 input groups can be used in near future.

Because the tunable range of the grating is about 40 nm, and since the possible wavelength separation is $\equiv$ 1nm [43], 40 WDM channels can be multiplexed and de-multiplexed. Hence, 40 input groups are feasible.

Because the bandwidth around each wavelength can be 0.3nm in order to have a reasonable level of crosstalk [44], i.e., around 1.5 μm, the total available bandwidth on each wavelength can be as large as 40 GHz. If each channel has a bandwidth of about 1 $\equiv$ GHz, we can have 40 inputs per group. The total number of inputs ($N = n \times k$) can be 1600, and the optical bandwidth becomes 1600 GHz, which means, for an individual bandwidth of B GHz, $\frac{1600}{B}$ inputs can be obtained. That is, for example,

$\equiv$ 30864 SONET OC-1 (51.84 Mb/S) or
$\equiv$ 10288 SONET OC-3 (155.52 Mb/S) or
$\equiv$ 3429 SONET OC-9 (466.56 Mb/S) or
$\equiv$ 2572 SONET OC-12 (622.08 Mb/S) or
$\equiv$ 1714 SONET OC-18 (933.12 Mb/S) or
$\equiv$ 1286 SONET OC-24 (1244.16 Mb/S) or

≡ 857 SONET OC-36 (1866.24 Mb/S) or

≡ 643 SONET OC-48 (2488.32 Mb/S) lines can be switched.

4.3.3. Architecture II: Photonic ATM Switch Based on Optical Pulse FDM and WDM

4.3.3.1. Switching Architecture

The idea of designing an ultra high-capacity photonic ATM switch system, through multi-dimensional combinations among different domains of optical medium, implies an alternative solution, that is, to design ATM switching architecture based on an optical ultra-short pulse frequency-division and wavelength-division "multiplexing and de-multiplexing". Obviously, the key step involved in this approach is to design, for each specific wavelength λ_i (where $i = 1...k$), n "multiplexing" and "de-multiplexing" systems to perform ultra-short optical pulse frequency-division multiplexing and de-multiplexing. As discussed regarding Architecture I, ultra-short optical pulse time-division multiplexing and de-multiplexing is done with electronic logic control, such as a series of 1/2 frequency dividers for cell coding, and an up/down counter for buffering. The controllers are completely separated from the data channels. However, in the alternative approach of Architecture II, the proposed ultra-short optical pulse frequency-division multiplexing and de-multiplexing is performed through optical logic control. The control elements are integrated in the data transport network, which is all-optical. The detail functionality is described here.

Similar to Architecture I in structure, this alternative version of ATM switch fabric has an $N (= n \times k)$ inputs (k groups with n inputs per group, as shown in Figure 4.17), $N (= n \times k)$ outputs. On the input side, there are k groups each with n "multiplexing" systems to perform

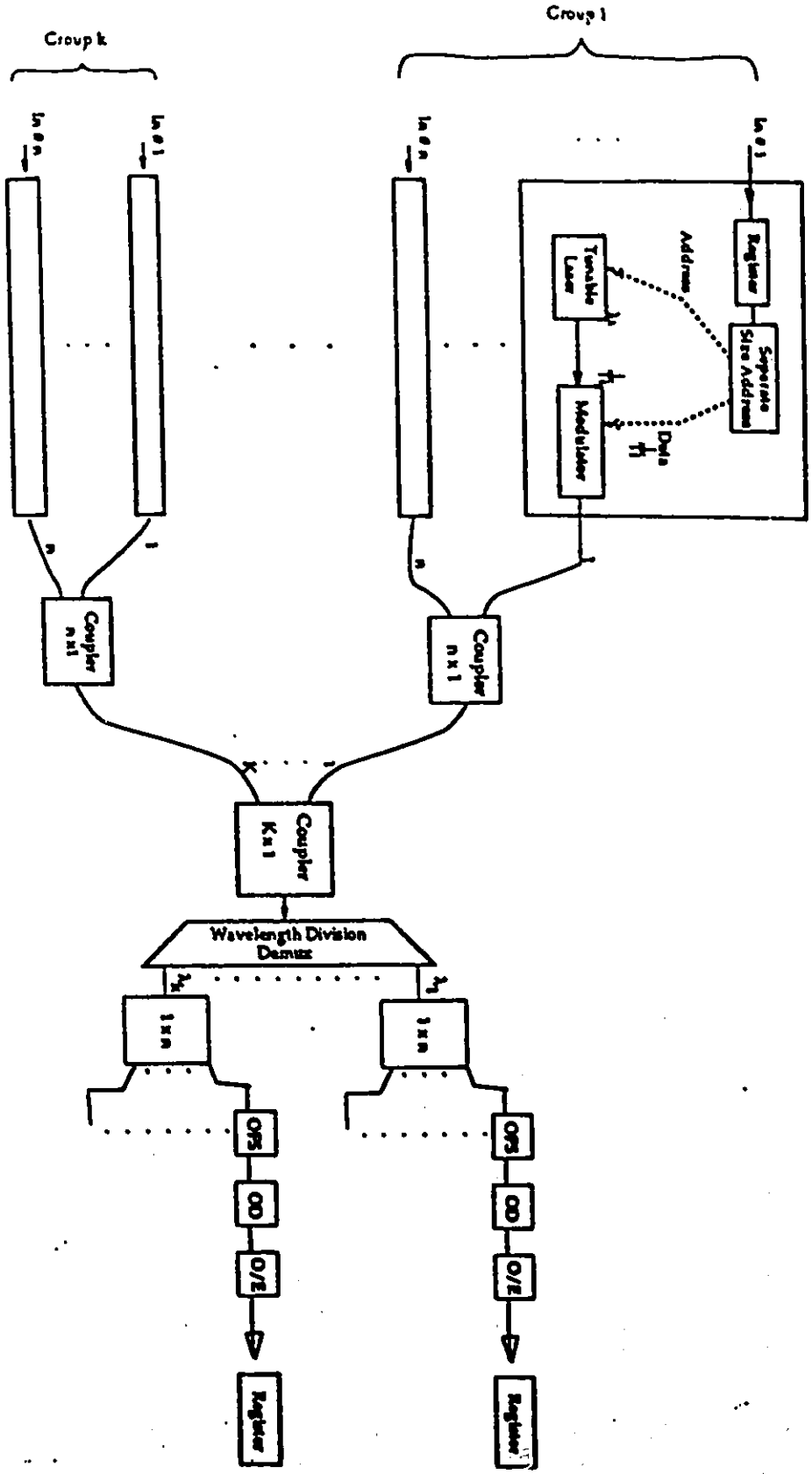

Fig. 4.17. Block Diagram of the Proposed Photonic ATM Switch #2

ultra-short optical pulse frequency-division multiplexing; therefore, n cells with different optical pulse frequencies are combined in the optical star coupler for each of the k groups. In addition, each cell consists of a series of binary optical pulses with wavelengths chosen from λ_1 to λ_k, depending on the receiver group address. On the output side, the wavelengths λ_1, ..., λ_k are ordered by wavelength de-multiplexer [43] in order to route the signal to its appropriate group on the output side; on each wavelength (output group) there are cells with n different optical pulse frequencies which will be split and directed into n different optical pulse frequency "de-multiplexing" systems. Each of them selects its unique optical pulse frequency by optical pulse frequency selector (OFS). The selected cells go through an Optical Decoder (OD), followed by the conventional O/E converter in order to complete the switching operation.

In this architecture, the optical pulse frequency of an optical signal refers to the repetition rate of the laser pulses, which is also the modulation rate of the input data to the external modulator. The particular pulse frequency can be controlled electrically. This unique "frequency" is used as a signature to identify a particular user from n different users on the same wavelength. As shown in Fig.4.18, on the same wavelength, User #1 sends a signal of pulse frequency $f_1=1/T_1$ with a duration τ, where T_1 is the time between pulses. User #2 sends a signal of pulse frequency $f_2=1/T_2$ and the same duration τ, so that each pulse is offset by the increasing multiples of δf in reference to f_1, and so on. The offset in time domain should be larger than the pulse duration τ but smaller than T_1/n. On a particular wavelength, optical ultra-short pulses generated by the lasers with different repetition rates are combined through an optical star coupler to complete the process of optical pulse frequency-division multiplexing. On the output side, the de-multiplexing is done by a splitter (a broadcast star coupler) to deliver the optical pulse frequency-multiplexed signals to n different paths so that on each path optical (pulse) frequency selector (OFS) works as a pulse frequency filter which

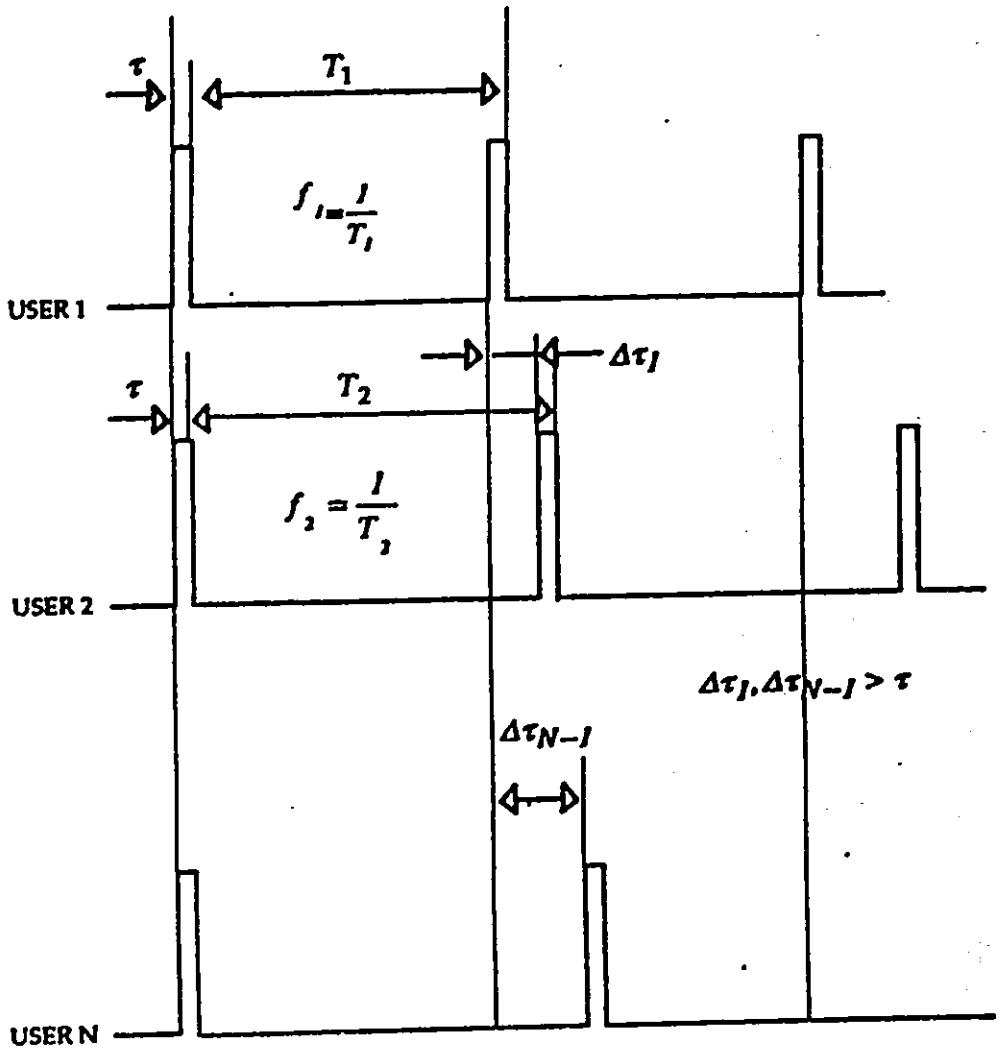

Fig. 4.18. Transmitting Signal from Different Optical Pulse Frequency Users

passes only cells with the unique selected pulse frequency and rejects the incoming cells from all other pulse frequencies.

In this switch architecture, each cell addresses a certain output by the following high and low addresses:

1. A "high" address (Virtual Path Identifier [VPI] in the cell header) specifies the order of the output group that the input cell will be going to. This address tunes the tunable source to λ_i. The selected wavelength will be one of the available wavelengths $\lambda_1 \ldots \lambda_k$, based on the wavelength allocation shown in Figure 4.12.

2. A "low" address (Virtual Channel Identifier [VCI] in the cell header) specifies the address of the input cell within the pre-specified group of the outputs. This address will be specified by the optical pulse frequency of the tunable laser and the data input rate to the external modulator.

As shown in Fig.4.17, electrical cells arrive at the inputs from various transmission links at different rates, asynchronously. They are first stored in a register, and their address fields in the cell header and data fields in the payload are read separately, according to the bit positions of VPI and VCI in the cell header and the bit location in the payload. The wavelength and optical pulse frequency of the tunable laser, as well as the input data rate to the external modulator, are specified by the address field. Then, with the repetition rate of fj on wavelength λ_i, the modulator modulates the optical pulses on the basis of the cell data fields, and sends them to an $n \times 1$ coupler for each group. An $n \times 1$ star coupler frequency-multiplexes each cell. Finally, the outputs of all input groups are coupled together by a $k \times 1$ star coupler, and the coupler distributes the cells over the optical highway (with signal multiplexed in optical pulse frequency and wavelength domain).

The optical pulse frequency and wavelength multiplexed signals arrive at the wavelength de-multiplexer as shown in Fig.4.14. In the de-multiplexer, each of the k Bragg Elements is tuned to one of the k wavelength λ_1 ... λ_k; therefore, if cells with wavelengths λ_1 ... λ_k arrive together, in the ith element, only λ_i will be deflected by 90^0 by the i-th element since it is tuned to λ_i, and $\lambda_1 ... \lambda_k$ will go through straight. Each deflected wavelength will go to the $1 \times n$ coupler and go through optical pulse frequency selector (OFS) and optical decoder (OD).

4.3.3.2. Design of Optical Pulse Frequency Selector

4.3.3.2.1. General Structure

Optical pulse frequency selector (OFS) is the optical logic control of the proposed photonic ATM switch, linked in the all-optical data transport network to make the ATM switch structure simple and all-optical in nature. In this paper, we propose a structure for the realization of this control function.

Each proposed OFS structure consists of two parts. One is an optical logic control signal generator (LCSG) and the other is an optical "ON -OFF Gate" controlled by the optical logic control signal originating from LCSG. As shown in Fig.4.19, the incoming cells to the proposed OFS are broadcast evenly by a 1 x (p +2) coupler, the $p+2$ outputs of this coupler are followed by delay lines of time interval of $0, Tk, 2Tk, ..., pTk, pTk + T'$. Accordingly, where $Tk = 1/fk$ is specified by the unique optical pulse frequency fk to be selected, and T' is the total processing time (or response time) of the optical logic control signal generator (LCSG) and "ON-OFF Gate". By counting upward, the outputs delayed by $0, Tk, 2Tk, ..., pTk$ are inputs of the optical logic control signal generator (LCSG), an "AND" gate in this case. The output delayed by $pTk + T'$ is the input to the optical "ON-OFF Gate", which is controlled by the

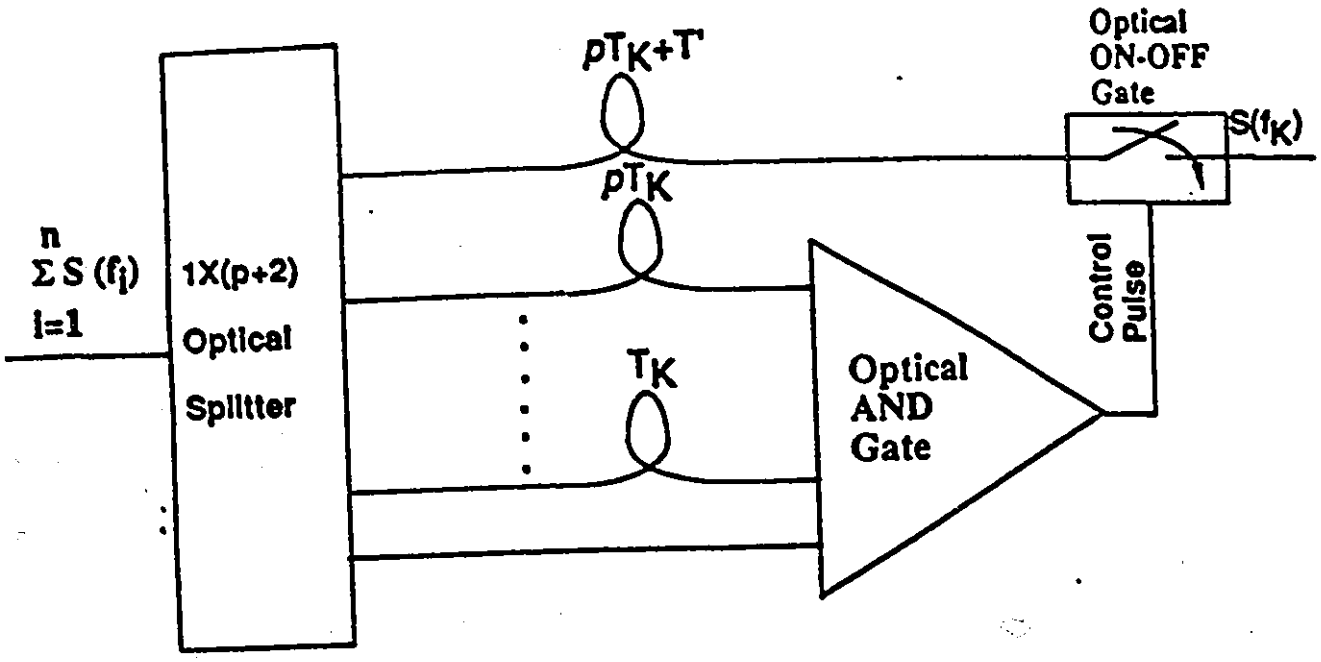

Fig.4.19. Block Diagram of OFS

optical logic control signal to retrieve the optical signal of frequency $f_k=1/T_k$ and reject the incoming signals from all others. By choosing the delay time T_k from T_1, T_2, ..., T_n corresponding to the reciprocals of the optical pulse frequencies $f_1, f_2, ..., f_n$, a signal with the specified optical pulse frequency f_k can be selected. This is done through the delay lines T_k, $2T_k$,..., pT_k so that only cells with the same repetition rate of laser pulses can produce logic "1" in the output of the "AND" gate. This in turn generates the optical control signal through the "AND" gate, to trigger the optical "ON-OFF Gate". When the "ON-OFF Gate" is triggered, it allows the cells to pass through. In other words, only the pulses that are one of the $p+1$ consecutive pulses equally spaced in time by the period of the desired signal T_k can propagate through. Obviously, the larger the number of the delay line p is, the more accurate the cell selection is. The number of delay lines p is determined by the required BER [42].

4.3.3.2.2. Design of Optical Control Signal Generator

In this structure, optical "AND" gate is proposed as optical control signal generator. Current technology provides several options for this component. One is to use bistable optical devices containing semiconductor non-linear refractive material [45][46][47] (i.e., non-linear semiconductor etalons, bi-stable semiconductor laser amplifiers). The other approach is to apply the quantum well self-electro-optic effect device (SEED) based on the quantum confined Stark effect (QCSE) [48]. Here, we describe briefly the mechanism of employing symmetric self-electro-optic effect devices (S-SEEDs) [49] [50] to implement an "AND" gate. Based on this, we propose a multi-stage "AND" gates approach, and the approach using a single-stage "AND" gate with a relatively higher preset pulse to implement the optical logic control signal generator (LCSG) in the pulse frequency selector (OFS) of this ATM switch fabric.

The S-SEED consists of two MQW pin diodes interconnected in series electrically as shown in Fig.4.20(a) below. Connected in this fashion, the diodes become complementary. When one of the diodes is "ON", the other is "OFF". Physically, one diode will be in an absorbing state while the other is in a transmissive state. The change of states is a function of the ratio of the two input powers. Thus, S-SEED can operate as an optical Set-Reset latch. The inputs are categorized into S (Set) input, R (Reset) input, and clock input. The S and R inputs are separated in time from clock inputs.

R input and S input are able to change the state of the device when the clock signal is not present. After the device has been put in its proper state, the clock signals are incident on both inputs. The clock has the same intensity for both inputs, making the device insensitive to optical power supply fluctuations. Its intensity is much higher than S input and R input. A larger differential optical gain can be achieved between output and input. This type of gain is referred to as time-sequential gain, in that the state of the device can be set with low-power beams and read out with subsequent high-power beams. The device also shows good input/output isolation because the large output does not coincide in time with the application of the input signals.

The power of signal on the S input relative to the power of the signal on the R input determines the logical level of the output, which is represented by the power of the signal coming from the Q output relative to the power of the signal coming from the Q' output. When the power of the signal incident on the S input is greater than the power of the signal on the R input, the power of the signal leaving the Q output will be greater than the power of the signal leaving Q' output, and a logical "1" will be represented on the output. On the other hand, when the power of the signal incident on the S input is less than the power of the signal on the R input, the opposite will occur.

To achieve "AND" operation, the device is initially set to its "OFF" or logic "0" state (i.e., Q low and Q' high), with preset pulse, *presetb*, incident on only one pin diode as shown in Fig.4.20 (a). The intensity of the preset pulse is equal to that of any input signal, assuming the intensities of the two input signals are equal, and attenuation in the fiber delay line is negligible. As an "AND" gate, S-SEED behaves like a three-terminal device. If both input signals have logic levels of "1" (i.e., set = 1, reset = 0), then the S-SEED "AND" gate is set to its "ON" state. For any other input combination, there is no change of state. The requirement of "AND" operation is fulfilled. After the signal beams determine the state of the device, the clock beams are then set high to read the state of the "AND" gate. The corresponding time diagram is shown in Fig.4.20 (b) below, and the optical logic table is shown in Fig.4.20 (c) below.

This S-SEED "AND" gate described above only works for two input signals. By connecting S-SEED "AND" gates in series with delay lines as shown in Fig.4.20 (d) below, implementation of OFS's optical control signal generator with $p+1$ inputs delayed by the time intervals of $0, Tk, 2Tk \ldots pTk$ can be completed. Except the first S-SEED "AND" gate, the preset pulse intensity of any other S-SEED "AND" gate is set to the larger intensity of the two inputs, which is also the output one from the proceeding S-SEED "AND" gate. The approach is categorized as the multi-stage "AND" gates method for the design of the optical control signal generator of the OFS in the proposed ATM switch fabric.

An alternative solution is to design the optical control signal generator of the OFS using only one S-SEED "AND" gate, with $p+1$ inputs delayed by the time intervals of $0, Tk, 2Tk \ldots pTk$, accordingly. To exercise a logic "AND" operation on $p+1$ inputs, the intensity of preset pulse *presetb* needs to be controlled to be exactly p times the intensity of the individual input signal. Here, the attenuation in fiber delay lines is assumed to be negligible. As shown in

Fig.4.20 (e) below, only when *p+1* inputs have a logical level of "1" (i.e., set = 1, reset = 0) is the total power of the signal incident on the S input is greater than the total power of the signal on the R input by an amount equal to the intensity of one input, and the S-SEED "AND" gate set to its "ON" state. For any other input combination, the total intensity on the reset input is always larger, because of the intensity of the preset pulse, and there is no change of state. The requirement of "AND" operation on *p+1* input is fulfilled.

4.3.3.2.3. Optical ON-OFF Gate

The operation of the optical "ON-OFF Gate" is described here. When the control light is not present, the signal light transmittance is zero; when the control light is present, the signal light transmittance is one. The operation can be realized by a semiconductor multiple quantum well (MQW) waveguide with a deep grating as the waveguide core [51]. Its mechanism is as follows: When the control light is injected into the MQW layer, the refractive index of the MQW layer is changed by a non-linear effect, namely, the carrier effect (band-filling or plasma effect). This leads to a shift of the Bragg wavelength to a shorter wavelength, and the transmittance at the signal light wavelength changes. As shown in Fig.4.21 below, by proper grating, the signal light transmittance is set to be zero around the specific "group wavelength" when the control light pulse is not present. This notch is shifted to a shorter wavelength and the signal light transmittance is changed to one around the specific "group wavelength" when the control light pulse is imposed. Hence the operation of "ON-OFF Gate" is fulfilled.

The switching speed of the optical "ON-OFF Gate" is dependent on the pulse width of the control light. System design issues such as the switching power level are also important. All these parameters define the requirement of optical logical elements in the proposed future photonic ATM switching system.

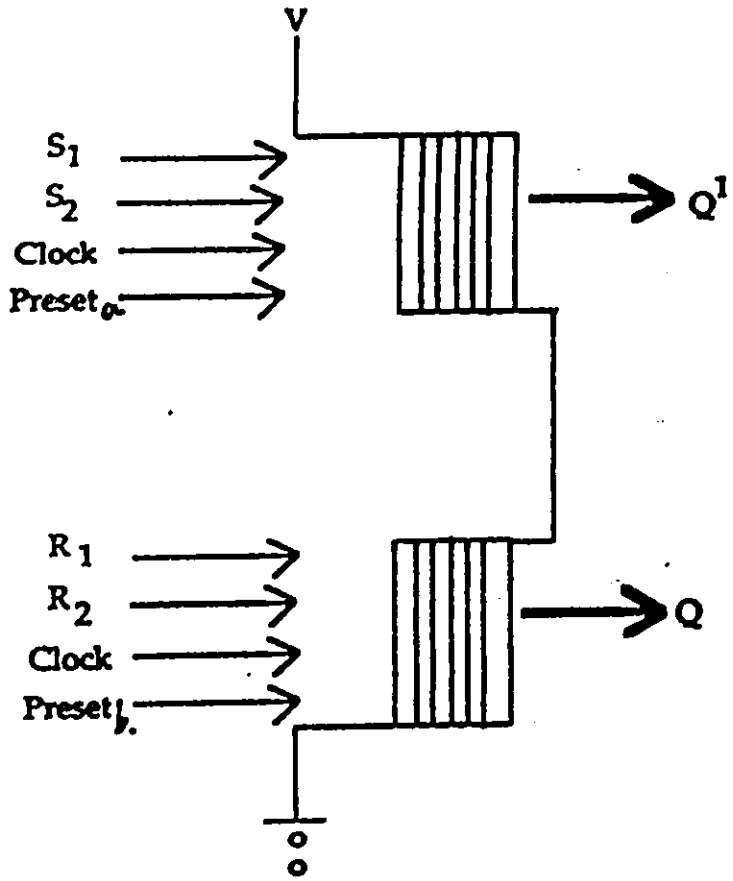

Preset a = 0. Preset b = I, I is the Intensity of individual Input signal.

Fig. 4.20 (a). Optical S-SEED and Gate in Multi-Stage Scheme

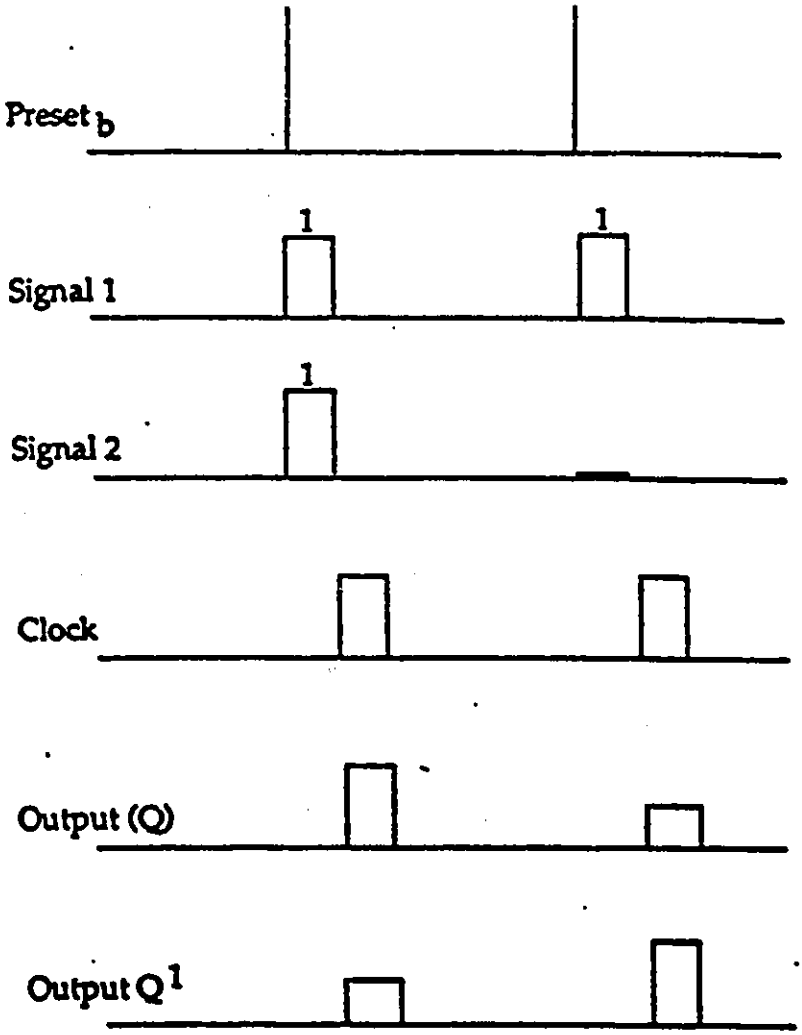

Fig. 4.20 (b). Time Diagram for Two Input Optical " AND " Gate

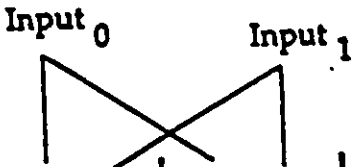

S_0	S_1	R_0	R_1	$Preset_a$	$Preset_b$	Q		Q^1
0	0	1	1	0	1	0		1
0	1	1	0	0	1	0	AND	1
1	0	0	1	0	1	0		1
1	1	0	0	0	1	1		0

Fig 4.20 (c). Optical Logic Based on S-SEED Devices

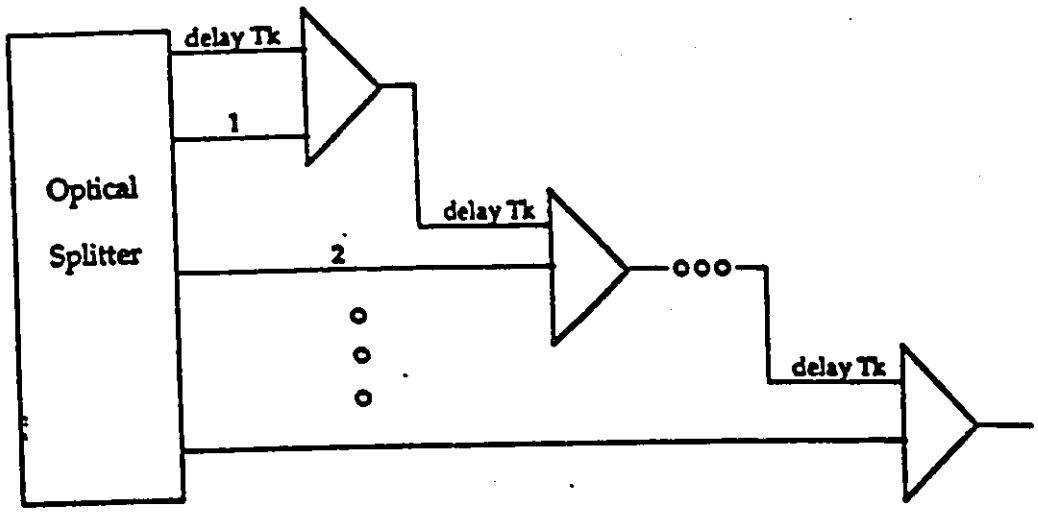

Fig. 4.20 (d). Block Diagram of Multistage Optical " AND " Gates

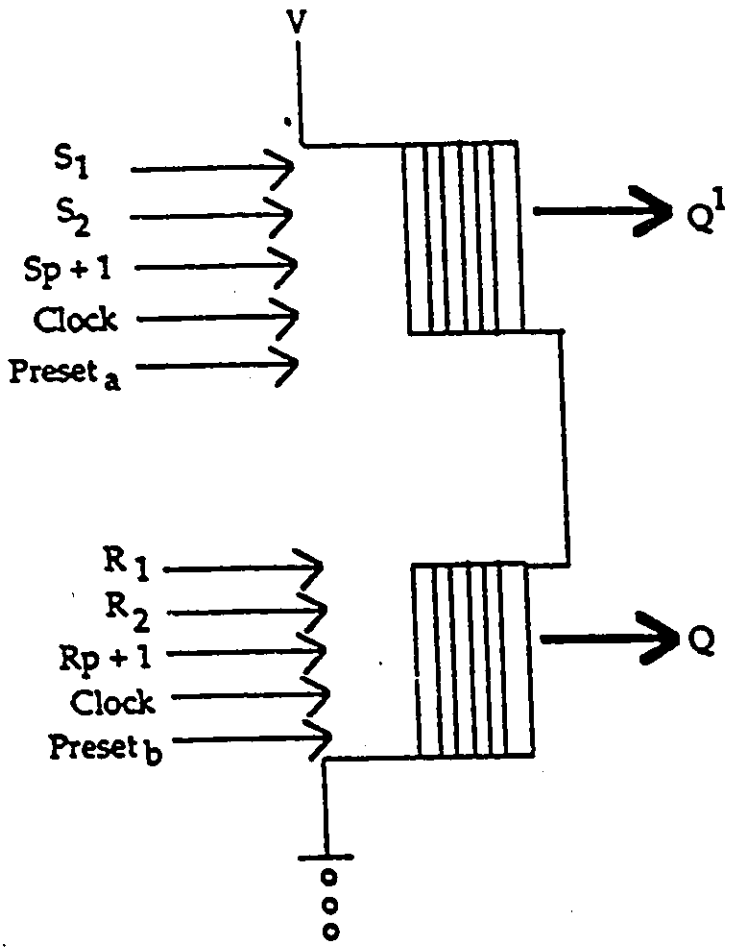

Preset a = 0, Preset b = pI, I is the intensity of individual input signal.

Fig. 4.20 (e). Optical S-SEED and Gate in Single-Stage Scheme

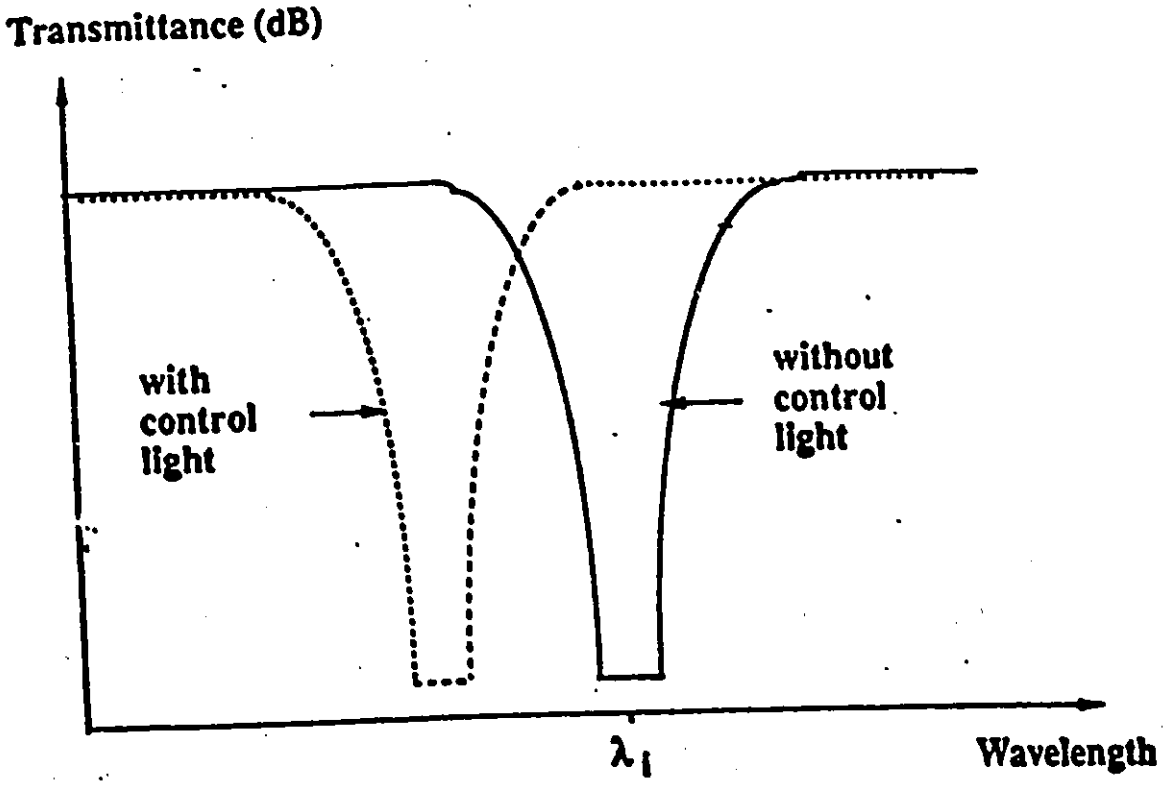

Fig. 4.21. Wavelength Transmittance Characteristics of ON-OFF Gate

4.3.3.3. Switching Capacity with SONET Signal Rates

The advantage of this proposed ATM switch fabric is that it employs both pulse frequency and wavelength division multiplexing, in order to obtain a higher capacity. For example, 40 input groups can be used in the near future. Because the tunable range of the grating is about 40 *nm*, and since the possible wavelength separation is $\cong$ 1*nm* [43], 40 WDM channels can be multiplexed and de-multiplexed. Up to 40 input groups are feasible.

- Number of inputs per group *(n)*: 160

Because the bandwidth around each wavelength can be 0.3*nm* in order to have a reasonable level of crosstalk [44], i.e., around 1.5 μm, the total available bandwidth on each wavelength can be as large as 40 GHz. As an example, the following parameters are taken for the optical pulse frequency multiplexing and demultiplexing system:

$\tau = 1\ ps,\ \delta\tau = 2\ ps,\ n = 160,\ f_{80} = 1\ Gb/S,$

then $f_1 = 1.188\ Gb/s,\ f_{160} = 0.862\ Gb/S$

$M = 4$, (M is the ratio of the bit-rate to the information rate)

the total information capacity is $(f_1+f_2+...+f_{160})/M = 160/4 = 40\ Gb/S$

The result matches the minimum crosstalk requirement.

- Total number of inputs *($N = n \times k$):* 6400

- Optical highway bandwidth: 6400 *GHz*

Thus if each input has a B GHz bandwidth, we could have $\frac{6400}{B}$ inputs,

that is,

≅ 123456 SONET OC-1 (51.84 Mb/S) or

≅ 41152 SONET OC-3 (155.52 Mb/S) or

≅ 13717 SONET OC-9 (466.56 Mb/S) or

≅ 10288 SONET OC-12 (622.08 Mb/S) or

≅ 6858 SONET OC-18 (933.12 Mb/S) or

≅ 5144 SONET OC-24 (1244.16 Mb/S) or

≅ 3429 SONET OC-36 (1866.24 Mb/S) or

≅ 2572 SONET OC-48 (2488.32 Mb/S) lines can be switched.

The generation of ultra-short optical pulse is important to realize this switch system. As seen in the above calculation, $\delta\tau$ is determined by τ such that $\tau < \delta\tau < T1/n$. If τ gets larger, the optical pulse frequency deviation from $f1$ to $f160$ will be increased. To satisfy the requirement range for $\delta\tau$, the number of input per group has to be reduced. This is illustrated by the examples shown in Table 4.4 and Table 4.5 below. When the number of input lines per group is less than the pre-designed one, 160, the maximum value taken is such that $\delta\tau = T1/n$, as shown in these tables. When $\delta\tau$ is chosen to be smaller for the same τ, the number of input lines gets larger, with the same optical pulse frequency deviation from $f1$ to fn. In practice, there is a certain bound on the deviation for setting optical pulse frequencies from the central optical pulse frequency, $fn/2$ (setting the central optical pulse frequency is also important for different signal rates). This is done in order that the bit rates of the switching system be relatively uniform and within the range of the transmission rates of the current DFB laser diodes. Thus, if the optical pulse width is broader, it is not possible to utilize the whole non-crosstalk bandwidth (-40 GHz) around each wavelength, and the number of inputs per group has to be decreased. Therefore, the ultra-short optical pulse is essential to the proposed ATM switch system based on optical pulse FDM and WDM. Its importance for the proposed ATM

switch fabric based on optical pulse TDM and WDM is even more obvious, since the cells are compressed in time in the switching system.

Table 4.4

Parameters used in this table: $\delta\tau = 2\tau$, $fn/2 = 0.62252$ Gb/s

τ (ps)	n	f1 (Gb /S)	f80 (Gb /S)	fn (Gb /S)
1	160	0.691	0.62252	0.566
2	160	0.775	0.62252	0.519
3	160	0.883	0.62252	0.479
4	134	0.928	0.62252	0.467
5	106	0.921	0.62252	0.468
6	88	0.917	0.62252	0.469
7	76	0.919	0.62252	0.468
8	66	0.914	0.62252	0.469
9	60	0.923	0.62252	0.466
10	54	0.921	0.62252	0.466

Table 4.5

Parameters used in this table: $\delta\tau = 1.5\tau$, $fn/2 = 0.62252$ Gb/s

τ (ps)	n	f1 (Gb /S)	f80 (Gb /S)	fn (Gb /S)
1	160	0.672	0.62252	0.566
2	160	0.730	0.62252	0.519
3	160	0.800	0.62252	0.479
4	160	0.883	0.62252	0.445
5	142	0.925	0.62252	0.468
6	118	0.923	0.62252	0.468
7	102	0.925	0.62252	0.467
8	88	0.917	0.62252	0.469
9	78	0.915	0.62252	0.469
10	72	0.925	0.62252	0.466

4.3.4. Comparison of Two Proposed Switching Architectures

We have proposed two large photonic ATM switch architectures based on combined optical pulse time/frequency and wavelength division multiplexing and de-multiplexing. Both have all-optical transport layers. Architecture I is electronically controlled, and incoming signals need to be at the same bit rate and be synchronized; Architecture II is optically controlled, and it can handle asynchronous incoming signals at different bit rates.

In general, the two proposed ATM switching architectures possess the following common features:

(1) In both architectures ultra-short optical pulses are used for cell signals, thereby minimizing the throughput losses associated with the device set-up time. Ultra-short light pulse can be obtained from a gain switched distributed feedback laser diode (DFB-LD) or mode-locked laser diode.

(2) Both architectures are two-dimensional. In Architecture I, optical pulses are time-division multiplexed on a pre-assigned wavelength by tunable lasers in each group, and then wavelength-division multiplexed between groups. In Architecture II, optical pulses are frequency-division multiplexed on a pre-assigned wavelength by tunable lasers in each group, and then wavelength-division multiplexed between groups. These multi-dimensional combinations among different domains of optical medium increase the switching throughput significantly, and fully exploit the transparency of the optical medium. With the feature of ultra-short optical pulse, these architectures can achieve an ultra-high throughput.

(3) From Architecture I to Architecture II, the evolution of photonic ATM switches is presented, namely from a hybrid opto-electronic approach to an all-optical approach. In Architecture I, the transport layer of the switching system is optical, and the control layer (a separate controller) of optical pulse TDMA uses electronic controllers. The control and data channels are completely separated. Architecture II presents a switch with control elements inseparable from the switch structure. Both layers are all-optical and physically merged into one, because the control and data channels are intimately linked. With the current device technologies, digital all-optical processing, i.e., optical logic, is not mature because of limits imposed by non-linear optical material and a high required optical power. On the other hand,

electronic technologies are currently more controllable and flexible. With software, the electronic devices can provide almost any function. Architecture I presents combinations of high bandwidth of photonics in the transport layer and high functionality of electronics in the control layer. The mixture of the processing capacity of electronics and communications capacity of optics allows a connection-intensive ATM switch architecture to be implemented with the current technology. Architecture II indicates the future direction: a photonic switch fabric with all-optical transport layer and control layer. Both layers are combined into one in the structure. As a different approach from the all-optical ATM switch architecture described in [41], which uses optical buffer memory and optical self-routing circuitry, the control function in Architecture II is performed by optical logical devices (i.e., optical "AND" gate) integrated into the data transport network. For such logical devices, data must have a very close relationship between the time for a logical operation (such as "AND" or "OR"); therefore, optical pulse frequency (repetition rate of laser pulse) divisioning is employed in Architecture II. Using optical pulse frequency-division multiplexing, this ATM switch fabric can handle asynchronous traffic at different bit rates. From a different point of view, Architecture I portrays how the limited capacity of photonic devices constrains the switching architecture, and Architecture II shows how the switching architecture defines the requirements on the optical devices.

Chapter 5
Conclusions and Suggestions

WDMA networks have been studied intensively in recent years. Typically, two approaches have been proposed, namely, single-hop broadcast-and-select scheme and multi-hop wavelength routing scheme. Each of them has certain advantage and drawback. In this thesis, a layered WDMA network architecture is proposed for the design of wide-area network. In this proposal, the network is considered to have three layers. The low layer is Local Area Network with broadcast and select scheme. The single-hop approach here is all-optical in nature. In this part, two WDMA LAN architectures with ring topology are proposed. Link performance is studied, and two-dimensional crosstalk issue is investigated for the optical amplifiers in the ring architecture. Regarding the limited available wavelength in this layer, network interconnection with wavelength routing scheme is proposed and studied in the intermediate layer. The emphasis here is on the wavelength reuse and network scalability. Throughput values are compared for different proposed topologies. In the top layer, centralized ultra-high-capacity photonic switch architecture based on optical pulse FDM and WDM is proposed and studied. The emphasis is on the implementation of optical control for the switch fabric. The approaches in the three layers benefit from the advantage of three different technologies and as a whole, the network provides great potential and is considered a good approach for the design of future optical network infrastructure.

As a method of approach, network architecture, system specification and device technology are integrated together in one study. For the device technology, the design of optical Add-Drop Multiplexer, optical Wavelength Selective Router and Optical Bridge are studied. In the system specification, link performance of optical ring LANs, closed-loop Markov chain for crosstalk of cascaded optical amplifiers in the ring network, and throughput

analysis for wavelength routing architecture are explored. For the network architecture, WDMA ring LAN with ADM, WDMA ring LAN with WSR, network interconnection architecture for wavelength reuse and optical switch architecture based on optical pulse FDM and WDM are proposed. This approach provides a clear picture for the connection between component and system.

With the state-of-the-art technology, the proposed network architecture offers significant advantages in network capacity and connectivity, and can be considered as a realistic approach for photonic Wide-Area Network architecture.

REFERENCES

[1]. J. W. Reedy, " *The TDM Ring-A Fiber Optic Transparent System for Campus or Metropolitan Networks,*" IEEE Jour. Selected Areas in Com., pp.1474-1483, Vol. SAC-4, No.9, Dec 1986.

[2]. M. I. Irshid, and M. Kavehrad, " *A Fully Transparent Fiber-Optic Ring Architecture For WDM Networks,* " IEEE Jour, Lightwave Tech., Vol.10, pp101 - 108, January 1992

[3]. W.I. Way, D.A. Smith, J.J.Johnson, and H.Izadpanah, " *A self-Routing WDM High-Capacity SONET Ring Network,*" IEEE Photonic Tech. Let., pp.402-405, Vol.4, April 1992.

[4]. A. Yariv, "*Optical Electronics*" , Saunders College Publishing, a division of Holt, Rinehart and Winston, Inc. 1991.

[5]. D. A. Smith, J.E. Baran,J.J. Johnson, and K.W. Cheung, " *Integrated-optic acoustooptic-tunable filters for WDM networks,*" IEEE J. Select Areas Commun., Vol. 8, no.6, pp.1151-1159, Aug.1990.

[6]. Y. Fujii, " *High-Isolation Polarization-Independent Optical Circulator Coupled with Single-Mode Fibers*", IEEE Jour, Lightwave Tech., Vol.9, pp.456 - 460, 1991.

[7]. M. Koga, and T. Matsumoto, " *High-Isolation Polarization-Insensitive Optical Circulator for Advanced Optical Communication Systems*", IEEE Jour, Lightwave Tech., Vol.10, pp.1210 - 1217, 1992.

[8]. C. W. Barnard, J. Chrostowski, and M. Kavehrad, " *Bidirectional Fiber Amplifiers*", IEEE Photon. Technol. Lett, Vol.4, Nov.8, pp.911-913, Aug. 1992.

[9]. Y. Sato and K. Aoyama, "*OTDR in optical transmission systems using Er-doped amplifiers containing optical circulators,*" IEEE Photon. Technol. Lett., vol. 3 no.11, pp.1001-1002,1991.

[10]. S. Nishi, K. Aida, and K. Makagawa, "*Highly efficient configuration of erbium-doped fiber amplifier,*" ECOC'90, MoG4.3 (Amsterdam, The Netherlands), 1990.

[11].Y . Fujii, " *High-Isolation Polarization-Independent Quasi-Optical Circulator*",IEEE Jour, Lightwave Tech., Vol.10, pp1226 - 1229, 1991.

[12]. H. Toba, K. Nakanishi, K Oda, K. Inoue, and T. Kominato, " *A 100-Channel Optical FDM Six-Stage In-Line Amplifier System Employing Tunable Gain Equalizers*" IEEE Photonic Technology Letters, Vol. 5 No. 2, February 1993.

[13]. J.L. Gimlett, M.Z. Iqbal, J. Young, L. Curtis, R. Spicer, N. K. Cheung, and S. Tsuji, "*11 Gbit/s Optical Transmission Experiment Using 1540 nm DFB Laser With Non-Return To-Zero Modulation and PIN/HEMT Receiver*". Electronics Letters Vol.25, No.9, 1989, p596-597.

[14]. M. J. Karol, " *Exploiting the Attenuation of Fiber-Optic Passive Taps to Create Large High-Capacity LAN's and MAN's.*" IEEE Journal of Lightwave Tech. Vol.9. No.3 1991. p400-408.

[15]. W. Liu, E. Strzelecki, F. Lin, T. Jannson, " *High Resolution Integrated Optic Holographic Wavelength Division Multiplexer*" SPIE 1990, San Jose, CA

[16]. V. Minier, A. Kevorkian, and J.M. Xu, " *Superimposed Phase Gratings in Planar Optical Waveguides for Wavelength Demultiplexing Applications,*" IEEE Photonic Technology Letters, Vol. 5 No. 3, March 1993.

[17]. Paul E. Green, Jr. " *Fiber Optic Networks*", Prentice Hall, 1993.

[18]. H. Toba, K. Nakanishi, K. Oda, K. Inoue, and T. Kominato, " *A 100-Channel Optical FDM Six-Stage In-Line Amplifier System Employing Tunable Gain Equalizers*", IEEE Photonic Technology Letters, Vol.5 No.2, February 1993.

[19]. T.E. Darcie, R.M.Jopson, and R.W.Tkach, " *Intermodulation Distortion in Optical Amplifiers from Carrier-Density Modulation,* " Electron. Lett., Vol.23, No.25, pp.1392-1394, Dec. 1987.

[20]. T. G. Hodgkinson and R.P. Webb, " *Application of Communication Theory to Analyze Carrier Density Modulation Effects in Traveling-Wave Semiconductor Laser Amplifiers,* " Electron. Lett., Vol.24, No.25, pp.1550-1552, Dec.1988.

[21]. K. Inoue, " *Observation of Crosstalk due to Four-Wave Mixing in a Laser Amplifier for FDM Transmission,* " Electron. Lett., Vol.23, pp.1293-1295, 1987.

[22]. R.M. Jopson, T.E. Darcie, K.T. Gayliard, R.T.Ku, R.E. Tench, T.C.Rice, and N.A. Olsson, " *Measurement of Carrier-Density Mediated Intermodulation Distortion in an Optical Amplifier,* " Electron. Lett., Vol.23, pp.1394-1395, 1987.

[23]. G. Grosskopf, R.Ludwig, R.G.Warts, and H.G. Weber, " *Four-Wave Mixing in a Semiconductor Laser Amplifier,* " Electron. Lett., Vol.24, pp.31-32, 1988.

[24]. R. Ramaswami, Private Communications.

[25]. Samuel Karlin and Howard M. Taylor, " *A First Course in Stochastic Processes*", Academic Press, Inc.

[26]. K. Inoue, " *Crosstalk and Its Power Penalty in Multichannel Transmission due to Gain Saturation in a Semiconductor Laser Amplifier*", Journal of Lightwave Tech. Vol.7, No.7, pp.1118-1124, July 1989.

[27]. R. Ramaswami, and P. A. Humblet, " *Amplifier Induced Crosstalk in Multichannel Optical Networks*", Journal of Lightwave Tech. Vol.8, No.12, pp.1882-1896, Dec.1990.

[28]. A. Takada, T. Sugie, and M. Saruwatari, " *High-Speed Picosecond Optical Pulse Compression from Gain-Switched 1.3 um DFB-LD through Highly Dispersive Single-Mode Fiber,* " Journal of Lightwave Tech., Vol.LT-5, No.10, pp.1525-1533, Oct.1987.

[29]. John P. Powers, " *An Introduction to Fiber Optic Systems*," Aksen Associates Incorporated Publishers, 1993.

[30]. Martin de Prycker, " *Asynchrous Transfer Mode*," Ellis Horwood, 1991.

[31]. Byeong Gi Lee, Minho Kang, and Jonghee Lee, " *Broadband Telecommunications Technology*," Artech House, 1993.

[32]. A. Yariv, "*Optical Electronics*" , Saunders College Publishing, a division of Holt, Rinehart and Winston, Inc. 1991.

[33]. Bahaa E.A. Saleh, and Malvin Carl Teich, " *Fundamentals of Photonics* ", John Wiley & Sons, Inc 1991.

[34]. S. Histon, " *Photonics in Switching*," IEEE Journal of Lightwave Telecommunication Systems, Vol. 3, No. 3, pp. 26-35, August 1992.

[35]. A. Jajszcyk and H. T. Mouftah, " *Photonic Fast Packet Switching*," IEEE Communications Magazine., Vol. 31, No. 2, pp. 58-67, February 1993.

[36]. Arturo Cisneros and Charles A. Brackett, " *A large ATM Switch Based on Memory Switches and Optical Star Couplers*," IEEE Journal of Select. Areas in Commun., Vol. 9, No. 8, pp. 1348-1360, October 1991.

[37]. Yoshihiro Shimazu and Masato Tsukada, " *Ultrafast Photonic ATM Switch with Optical Output Buffers*," IEEE/OSA Journal of Lightwave Tech., Vol. 10, No. 2, pp.265-272, February 1992.

[38]. M. Eisett, B. Grobkopf, R. Ludwig, W. Pieper and G. Weber, " *Photonic ATM Switching with Semiconductor Laser Amplifier Crates*," Electronics Letters, Vol.28, No. 15, pp. 1438-1439, July 1992.

[39]. T.Matsunaga, M.Yamaguchi, and M.Okuno, " *Photonic SD-Switching for Subscriber Networks in B-ISDN,*" Proceedings of the International Topical Meeting in Photonic Switching, Kobe, Japan, pp. 334-337, April 1990.

[40]. M.S. Goodman, *et al.*, " *Demonstration of Fast Wavelength Tuning for a High Performance Packet Switch,*" Proc. 14 Euro. Conf. on Opt. Commun.(ECOC'88), Brighton, U.K., pp. 255-258, Sept.11-15, 1988.

[41]. Makoto Nishio *et al.*, " *A New Architecture of Photonic ATM Switches,*" IEEE Communications Magazine, Vol. 31, No. 4, pp. 62-69, April 1993.

[42]. A. Frenkel, " *Pulse Frequency Division Multiplexing is a New Way to Increase the Capacity of a Local Fiber-Optic Communications Network,*" IEEE/OSA Journal of Lightwave Technology, Vol. 10, No. 11, pp. 1674-1679, November 1992.

[43]. M. Tabiani, M. Kavehrad, M. Irshid, "*A Novel Integrated-Optic WDM Cross-Connect for Wide-area All Optical Networks,*" IEEE/OSA Journal of Lightwave Technology, Vol. 11, No. 3, March 1993.

[44]. S. Fouchet, F.R. Landan, A. Carenco, F. Huet, " *Ti Implantation in LiNbO3: a New Tool to Realize Submicronic Gratings,*" 17th European Conference on Optical Communication ECOC'91 and 8th International Conference on Integrated Optics and Optical Fiber Communication ICOC'91, Paris, France, pp. 57-59, September 1991.

[45]. H. M. Gibbs, " *Optical Bistability-Controlling Light with Light,*" New York: Academic, 1985.

[46]. J. L. Jewell *et al*, " *Parallel Operation and Crosstalk Measurements in GaAs Etalon Optical Logic Devices,*" Appl. Phys. Lett., vol. 48, pp. 1342-1345, 1986.

[47]. T. Venkatesan, *et al*, " *Fabrication of Arrays of GaAS Optical Bistable Devices,*" Appl. Phys. Lett., vol. 48, pp. 145-147, 1986.

[48]. D. A. B. Miller, *et al*, " *Band-Edge Electroabsorption in Quantum Well Structures: The Quantum Confined Stark Effect,* " Phys. Rev. Lett.,vol. 53, pp. 2173-2175, 1984.

[49]. M. E. Prise *et al.*, "*A Module for Optical Logic Circuits Using Symmetric Self-Electrooptic Effect Devices,*" Apply Optics, vol. 29, May 1990.

[50]. A. L. Lentine *et al*, " *Symmetric Self-Electrooptic Effect Device: Optical Set-Reset Latch, Differential Logic Gate, and Differential Logic Gate, and Differential Modulator/Detector,*" IEEE Journal of Quantum Electronics, vol. 25, No. 8, pp. 1928-1936, August 1989.

[51]. Y. Shibata, M. Ikeda, K. Nakashima, T. Tamamura, and T. Nishida, " *All-Optical Multiple Quantum Well Grating Switch,*" Proceedings of the International Topical Meeting in Photonic Switching, Kobe, Japan, pp. 102-105, April 1990.